14:37:52 OCA PAD AMENDMENT - PROJECT HEADER INFORMATION 04/05/91

Active

Project #: E-16-656 Cost share #: E-16-336 Rev #: 5
Center # : R6633-0A0 Center shr #: F6633-0A0 OCA file #:
Work type : RES
Contract#: NAG-1-922 Mod #: ADMIN. Document : GRANT
Prime #: Contract entity: GTRC

Subprojects ? : N
Main project #:

Project unit: AERO ENGR Unit code: 02.010.110
Project director(s):
CALISE A J AERO ENGR (404)894-7145
FLANDRO G A AERO ENGR (404)-

Sponsor/division names: NASA / LANGLEY RESEARCH CTR, VA
Sponsor/division codes: 105 / 001

Award period: 881101 to 910831 (performance) 910831 (reports)

Sponsor amount	New this change	Total to date
Contract value	0.00	163,495.00
Funded	0.00	163,495.00
Cost sharing amount		20,349.00

Does subcontracting plan apply ?: N

Title: DEVELOPMENT OF ON-BOARD GUIDANCE ALGORITHMS FOR NASP APPLICATIONS

PROJECT ADMINISTRATION DATA

OCA contact: Ina R. Lashley 894-4820

Sponsor technical contact

DR DANIEL D MOERDER, GCD M/S 161
(804)865-4591

NASA LANGLEY RESEARCH CENTER
HAMPTON VA 23665-5225

Sponsor issuing office

ANNE S REED/BEVERLY R THOMAS
(804)865-3215

NASA LANGLEY RESEARCH CENTER
HAMPTON VA 23665-5225

Security class (U,C,S,TS) : U ONR resident rep. is ACO (Y/N): N
Defense priority rating : N/A N/A supplemental sheet
Equipment title vests with: Sponsor GIT
NONE PROPOSED.
Administrative comments -
> PER NASA PROVISIONS, WE ARE EXTENDING THIS GRANT FOR 3 MONTHS AS REQUESTED BY THE PI. NASA HAS BEEN NOTIFIED.

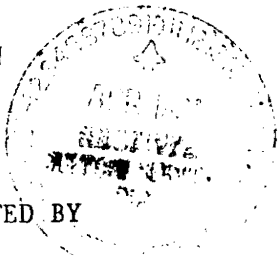

GEORGIA INSTITUTE OF TECHNOLOGY
OFFICE OF CONTRACT ADMINISTRATION

NOTICE OF PROJECT CLOSEOUT

Closeout Notice Date 01/09/92
Original Closeout Started 02/14/90

Project No. E-16-656 Center No. R6633-0A0

Project Director CALISE A J School/Lab AERO ENGR

Sponsor NASA/LANGLEY RESEARCH CTR, VA

Contract/Grant No. NAG-1-922 Contract Entity GTRC

Prime Contract No. _____

Title DEVELOPMENT OF ON-BOARD GUIDANCE ALGORITHMS FOR NASP APPLICATIONS

Effective Completion Date 910831 (Performance) 910831 (Reports)

Closeout Actions Required:	Y/N	Date Submitted
Final Invoice or Copy of Final Invoice	N	
Final Report of Inventions and/or Subcontracts	Y	
Government Property Inventory & Related Certificate	N	
Classified Material Certificate	N	
Release and Assignment	N	
Other _____	N	

Comments NO FORMAL INVOICE REQUIRED, PAYMEMT BY CASH DRAWDOWNS UNDER LETTER OF CREDIT.

Subproject Under Main Project No. _____

Continues Project No. _____

Distribution Required:

Project Director	Y
Administrative Network Representative	Y
GTRI Accounting/Grants and Contracts	Y
Procurement/Supply Services	Y
Research Property Managment	Y
Research Security Services	N
Reports Coordinator (OCA)	N
GTRC	Y
Project File	Y
Other _____	N
_____	N

Trajectory Optimization and Guidance Law Development for National Aerospace Plane Applications

Progress Report
December 1, 1988 to June 30, 1989

July 1989

Research Supported by
NASA Langley Research Center

NASA Contract Number NAG-1-922

Principal Investigators: A. J. Calise and G. A. Flandro
Graduate Research Assistant: J. E. Corban

School of Aerospace Engineering
Georgia Institute of Technology
Atlanta, GA 30332

NASA Contract Monitor: D. D. Moerder

Table of Contents

Summary of Work Completed

The work completed during the period December 1, 1988 to May 30, 1989 consists primarily of extensions to the analysis previously reported to include a number of important considerations. In particular, the vehicle model was extended to include angle of attack effects, the thrust vector component normal to the velocity vector, and flight in the subsonic and supersonic regimes. A multi-mode propulsion system consisting of turbojet, ramjet, SCRAMJET, and rocket engines was assumed and simple models for thrust generation and fuel consumption adopted for each engine cycle. The state space was further constrained by consideration of a maximum allowable aerodynamic heating rate. Singular perturbation methods were applied to this more realistic model and again yield a simple algorithm suitable for generating the fuel optimal altitude profile in real time. A simple iterative algorithm was derived that approximates the optimal engine transition points and the regions of cycle overlap. Feedback linearization was employed to derive an angle of attack controller which is used to guide the vehicle along the fuel-optimal altitude profile in simulations of flight within the atmosphere. A computer subroutine based on the space shuttle explicit guidance algorithm was written to handle the exoatmospheric phase of ascent guidance and allows for the simulation of insertion into orbit. The resulting software was employed to examine the influence of the added model complexity on the fuel-optimal ascent trajectories and the performance of the guidance algorithms.

I. Introduction

This is a report of the progress made in conducting research under contract to NASA (Contract Number NAG-1-922) during the period from December 1, 1988 to May 30, 1989. The research effort is directed at the problems of real-time trajectory optimization and guidance law development in National Aerospace Plane applications. In particular, singular perturbation methods are being applied to develop guidance algorithms suitable for on-board, real-time implementation. Sections II and III of this report provide a description of the vehicle model currently being employed and an overview of the analysis that has been completed. A detailed mathematical formulation of the optimization problem and the method of solution, along with a discussion of the numerical results that have been generated, is available in [1]. The results obtained prior to this reporting period are available in [2-4]. The guidance scheme employed for simulation of the exoatmospheric phase of insertion into orbit is briefly described in Section IV. A discussion of the problem areas that have been encountered is presented in Section V. Conclusions are stated in Section VI. Lastly, an overview of research planned for the next reporting period is presented in Section VII.

II. Vehicle Models

Two distinctly different vehicle models have been employed in the research conducted to date. The make-up of these two models, along with the advantages and limitations of each, is discussed below.

Model Number 1. The vehicle configuration detailed in the last progress report and the corresponding aerodynamic and propulsive models presented in that report are valid only at hypersonic speeds. This model was derived from a hypersonic research airplane concept studied by NASA in the mid 1970's. The concept's design, which employs a seventy degree swept delta wing, is based on a fixed geometry modularized SCRAMJET propulsion system that is closely integrated with the airframe. For modeling purposes, a full scale vehicle of 150 feet total length and 200,000 pounds take-off gross weight was assumed. The hypersonic aerodynamic characteristics assigned to the model are based on model wind tunnel data taken at Mach 6. The Mach number independence principle is used to extend these aerodynamic characteristics to higher Mach numbers. In particular, drag is assumed to have a conventional parabolic form, that is

$$D = qsC_{D_o} + KL^2/qs$$

where the symbol q represents dynamic pressure, s an aerodynamic reference area, and C_{D_o} the zero-lift drag coefficient. The coefficient of the induced drag component, K, is assumed independent of the Mach number, M, for $M > 5$ by means of the Mach number independence principle.

A simple conceptual model of a SCRAMJET engine, based on Billig's generic design guidelines, is employed to model SCRAMJET performance. A rocket, sized for orbital insertion, is assumed available to augment SCRAMJET thrust. To simplify the analysis it was assumed that the SCRAMJET would operate continuously at a stoichiometric fuel-to-air ratio, thus only the optimal rocket throttle control, h, need be determined. The total thrust, T, and total fuel consumption rate, f, are given by

$$T = T_s + hT_r \qquad h \in [0,1]$$

$$f = c_sT_s + hc_rT_r$$

where thrust specific fuel consumption is represented by c_s for the SCRAMJET and c_r for the rocket. The above model, detailed descriptions of which are available in [3] and [4], is referred to henceforth as Model Number 1.

Extension of Model Number 1 to include aerodynamic characteristics at subsonic and supersonic speeds requires that we recognize C_{D_o} and K as being Mach number dependent. Although model wind tunnel data was taken for this configuration at subsonic and supersonic speeds, it is not available at sufficiently low angles of attack. The desire for this data stems from the fact that the vehicle is expected to operate at very low angles of attack along the fuel-optimal trajectory. For this reason a new configuration, for which low angle of attack aerodynamic data is available, has been adopted and was used to construct the model described below.

Model Number 2. This model is based on the "Generic Hypersonic Aerodynamic Model Example," or GHAME, detailed in [5]. A nominal configuration of 233.4 feet total length and 300,000 pounds gross take-off weight is assumed. The assigned aerodynamic characteristics are taken directly from the GHAME documentation and extend from take-off to orbital velocities. Drag is again assumed parabolic in form but we now assume Mach number and angle of attack, a, dependencies as follows,

$$C_{D_o} = C_{D_o}(M) \qquad K = K(M,a)$$

A multi-mode propulsion system, assumed to consist of turbojet, ramjet, SCRAMJET, and rocket engine cycles, is stipulated for lack of more detailed information. The assumed propulsive characteristics for the air-breathing engines are adopted from [6]. This includes the SCRAMJET engine characteristics, i. e. the generic SCRAMJET model employed in Model Number 1 is not used in conjunction with the turbojet and ramjet data of [6], rather all three air-breathing engine types are modeled using the fuel specific impulse data given in [6] where

$$T = I_{sp}\,(0.029j)\,g\,r\,V\,C_a\,A$$

$$f = \tilde{T} / I_{sp}$$

and the undefined symbols represent:

I_{sp}	fuel specific impulse	V	velocity
j	the engine control	C_a	the capture area ratio
g	acceleration due to gravity	A	the engine inlet area
r	atmospheric density		

Note that, in general, C_a is a function of both angle of attack and Mach number. The rocket is modeled as for Model Number 1 and again sized for orbital insertion. This data set, referred to as Model Number 2, is valid over the entire flight regime from take-off to orbit.

The problem of vehicle trim, which applies to either Model and which is discussed in more detail in [1], is treated as a sub-system problem that can be ignored at this level of control law development.

III. Application of Singular Perturbation Theory

The work completed to date is restricted to considering the flight of a point mass in a vertical plane over a spherical, non-rotating Earth. The atmosphere is assumed stationary and the thrust vector is assumed to lie in the plane of symmetry. The equations of motion governing such flight can be reduced to a four state model in: radial distance from the center of the Earth, velocity, flight path angle, and vehicle mass. For convenience mass specific energy is introduced as a state variable in place the velocity. Given the performance index of maximum final mass, one can proceed to determine the optimal controls, i.e. to determine the optimal angle of attack and engine throttle control histories. In an attempt to avoid computationally intensive methods of solution, singular perturbation methods are applied by artificially introducing a small parameter in the dynamic equations to effect a time scaling. The solution to the full order problem is then investigated by examining the necessary conditions for optimality on differing time scales, that is, the solution to the full order problem is approximated by solving a series of low order problems. Ideally, the resulting low order problems will yield to analytic solution, but even if this is not the case one can often derive a simple algorithm that will yield a solution. This technique is especially attractive because the resulting solution is in feedback form.

For the particular application at hand, altitude and flight path angle dynamics are assumed fast in comparison to energy and mass dynamics. This assumption yields an optimal altitude

program as a function of energy and mass and a nonlinear feedback guidance law using angle of attack as a control. The necessary conditions for optimality also yield relations for evaluating the optimal engine controls as a function of state. The algorithm by which the optimal altitude program is generated and by which the optimal engine settings are determined is presented in detail in [1]. State variable inequality constraints on dynamic pressure and aerodynamic heating rate are easily enforced because altitude, an assumed "fast" variable, acts as a control in the "reduced solution," thus converting these two state variable inequality constraints into constraints of state and control.

Angle of attack control allows one to consider a realistic vehicle model that includes phenomenon such as the functional dependence of SCRAMJET thrust on angle of attack. This dependence has been shown to strongly influence the nature of the fuel-optimal ascent trajectories [1]. The use of angle of attack, rather than lift, as a control variable does not seriously degrade the performance (i.e. increase the run time) of the guidance algorithm previously reported. Several points are introduced, however, about which iteration is required.

Control of the multi-mode propulsion system consists of determining when to use each cycle type, the regions of overlap in cycle operation, and the optimal throttle settings for each when in operation. It is expected that all four cycle types will exhibit fuel flow variation in direct proportion to pilot command, that the air-breathing cycles will typically exhibit a nonlinear relation between fuel flow and thrust generation, and that it is reasonable to assume that the relation between fuel flow and thrust generation for the rocket is linear. For simplicity, one can ignore the nonlinearities cited above and examine the solution to the resulting bang-bang control problem. This leads to a set of analytic conditions (that must be iteratively satisfied) which determine the engine cycles to be employed along any segment of the ascent trajectory so as to minimize the fuel consumed in achieving orbit. This approximate approach, which is detailed in [1], proves very efficient. It does not, however, settle the question of whether or not intermediate values of throttle setting are optimal. In the particular case of rocket throttle control, intermediate values of throttle setting (i.e. singular arcs) were previously shown to be non-optimal for the given dynamic model. To reinforce this result, the rocket throttle singular surface was generated numerically and is plotted in the altitude-velocity plane in [1]. Singular arcs for rocket throttle could still be optimizing given a higher-order dynamic model. The methodology for determining the optimal throttle settings for the air-breathing engines is outlined in [1]. However, numerical investigation will require realistic nonlinear engine models.

The addition of a maximum aerodynamic heating rate constraint was completed using the procedure employed to handle a maximum dynamic pressure constraint in previously reported work. The model adopted for aerodynamic heating rate, as well as the influence of this constraint on the ascent trajectories, is discussed in detail in [1].

The boundary layer problem which is formulated to handle the altitude and flight path angle dynamics again results in a nonlinear feedback guidance law. This law is dependent on knowledge of the costates, which necessitates solution of the two-point boundary-value problem that results from the application of the necessary conditions for optimality. Previously developed methods for the approximate solution of this problem fail in the presence of state variable inequality constraints. This problem is discussed further in Section V. Feedback linearization is employed to overcome this hurdle (see [1] and [2]) and provides a near-optimal control law for tracking the reduced solution altitude profile. As illustrated in [2], little or no performance can be gained by further optimization of altitude and flight path dynamics beyond the feedback linearization approach cited above.

IV. Exoatmospheric Guidance

Flight beyond the Earth's atmosphere precludes the use of air-breathing engines. The solution to the minimum-fuel ascent-to-orbit problem for rocket powered vehicles has been studied for several decades. The solution in vacuum is well known to be in the form of a linear tangent steering law [7] and has been extensively employed for exoatmospheric guidance of rocket powered launch vehicles. A simple vector form of the linear tangent steering law based on the concept of velocity-to-be-gained handles all phases of space shuttle exoatmospheric powered flight and is detailed in [8]. This algorithm has been programmed for use in simulating rocket powered insertion into orbit once the computed fuel-optimal ascent trajectory exceeds a specified boundary for the sensible atmosphere. Note that the transition from angle of attack control and SCRAMJET thrust to control by the rocket thrust vector alone has not been optimized but approximated by this procedure. Optimization of this transition would consist of a terminal boundary layer analysis in the singular perturbation formulation.

V. Problem Areas

Vehicle Models. Model Number 1 as described in Section II is adequate for consideration of flight in the hypersonic regime but proves deficient at subsonic and supersonic speeds. Model Number 2 appears to overcome this difficulty by providing a continuous aerodynamic data set over the entire Mach range, including data at low angles of attack. However, this aerodynamic data set intentionally includes unrealistically high drag penalties. A realistic aerodynamic data set is desired to allow for proper engine sizing and to allow for the use of the developed software package to examine vehicle performance and the feasibility of the single-stage-to-orbit concept.

The air-breathing engine models employed thus far are not suitable for numerically investigating many nonlinear effects of interest. These include the question of whether or not intermediate values of air-breathing engine throttles are optimal and convexity of the hodograph. Assistance is needed in identifying and acquiring suitable engine models.

The State Constrained Boundary Layer Problem. Difficulty has been encountered in forming an approximate solution to boundary layer problems in which a state variable inequality constraint is to be enforced. In particular, the technique of linearizing the boundary layer necessary conditions about the reduced solution in order to pick the unknown initial conditions of the costates fails because purely imaginary eigenvalues are encountered. It has been shown that a discontinuity in the fast costate rates will occur at the juncture of an unconstrained arc (the boundary layer trajectory) and a constrained arc (the reduced solution). It is not clear at this time how to expand about such a point. For the same reasons, the technique for addressing altitude and flight path angle dynamics on differing time scales by penalizing flight path angle in the performance index also fails. Given purely imaginary eigenvalues, there is no mechanism to choose the weighting in the performance index so that the coupled system's behavior is emulated. This problem is of theoretical interest and an investigation is being initiated.

VI. Conclusions

The application of the minimum principle to a simple model of energy and mass dynamics results in an efficient algorithm for trajectory optimization that is suitable for on-board, real-time implementation. The use of angle of attack as a control variable, rather that lift, is easily incorporated into this algorithm, though some iteration is then required. Examination of the rocket throttle switching surface in the altitude/velocity plane confirms the previously reported result that intermediate values of rocket throttle setting are not optimal. Enforcing an aerodynamic heating constraint results in greater mass expenditure to achieve orbit and also increases the time of flight. Functional dependence of SCRAMJET thrust on vehicle angle of attack has a major impact on the nature of fuel-optimal ascent trajectories, in general dictating flight at a value of dynamic pressure lower than expected when Mach number is greater than 10. Finally, it has been shown that assumptions regarding propulsion system characteristics, namely that they enter into the optimization problem in a linear fashion, allow one to determine the optimal engine transition points as a function of state using a simple iterative test.

VII. Plans for the Next Reporting Period

The analysis of flight in a vertical plane using the aerodynamic, propulsive and dynamic models described in this report is complete in the sense that the algorithms and methodology are fully developed. Further investigation of points of interest require more detailed and realistic models that exhibit qualitatively correct nonlinear behavior. Given that such models can be developed or made available, additional points of interest include numerical investigation of the optimality of intermediate throttle settings and the convexity of the hodograph. Optimal control of a realistic propulsion system that includes variable geometry and shared hardware between cycles is also of interest but would require detailed knowledge of the system and its performance.

Theoretical investigation of the state variable inequality constrained boundary layer problem is of interest. A study of this problem in a general setting is being initiated. Note however, that solution of this problem is not required to implement the derived guidance algorithms.

The major effort to be undertaken during the next reporting period is to examine three-dimensional maneuvers as may be required for lift modulation, orbital plane change, and abort maneuvers. The approach will again center around singular perturbation methods, treating out-of-plane dynamics as an additional boundary layer. Once this effort is complete and a three dimensional simulation code is available, it will be of interest to estimate the errors introduced by the rotational velocity of the Earth, winds, the perturbing effects of gravity, density holes in the upper atmosphere, etc. Possible abort maneuvers, initiated in response to engine-out conditions or heat shield failure, will also be studied.

Tasks planned for the next reporting period are detailed below.

- Further develop the vehicle model as follows.
  - Acquire the aerodynamic characteristics of NASP vehicle configurations that become available and compare with Models 1 and 2.

- Acquire suitable turbojet and ramjet engines models which exhibit realistic nonlinear behavior.

- If possible, acquire models of other engine concepts, the air-turbo-ramjet for instance, and incorporate them into the software package as optional devices.

- Further investigate SCRAMJET modeling issues including variation of engine performance with angle of attack, additional thrust derived from fuel preheat, additional fuel flow required for engine cooling at the higher Mach numbers, additional thrust due to unburned fuel ejection, variable geometry, dual-mode (ramjet-SCRAMJET) operation, and the magnitude of the normal component of thrust.

- Acquire or develop more accurate means for estimating the aerodynamic heating rates encountered and for identifying the transition from turbulent to laminar flow.

- Adopt a suitable model for winds in the upper atmosphere.

• Extend the analysis to include consideration of:

  - The optimality of intermediate values of throttle setting given suitable nonlinear models of the air-breathing engine cycles are available.

  - The convexity of the hodograph.

  - The further optimization of orbital insertion by treating it as a terminal boundary layer.

  - Three-dimensional dynamics as may be required for lift modulation, orbital plane change, or abort maneuvers.

  - A rotating, oblate Earth

  - A nonstationary atmosphere

• Continue the derivation of a suitable guidance algorithm:

  - Address the theoretical issues associated with the inclusion of a state variable constraint in the boundary layer analysis. If possible devise a method for synthesizing an approximate boundary layer angle of attack control solution for the constrained case.

  - Extend the Singular Perturbation formulation to include out-of-vertical plane dynamics as an additional layer.

  - Consider the possibility of an exact nonlinear transformation of the boundary layer necessary conditions to a linear optimal control problem with a quadratic index of performance.

- Evaluate the resulting real-time guidance algorithms in non-real-time simulation studies.
  - Compare the guided solutions with exact numerical solutions obtained using the Program to Optimize Simulated Trajectories (POST).
  - Examine the robustness of the guided solutions to variations in atmospheric conditions (gusts, density holes, etc.), off-nominal engine performance, and other modeling uncertainties.
- Conduct sensitivity studies to examine the impact of vehicle sizing parameters on the nature of the optimal trajectories.
- Compute the CPU time required to cycle through the guidance algorithm in order to evaluate its suitability for real-time control and for comparison to other approaches to real-time trajectory optimization.

References

[1] Corban, J. E., A. J. Calise, and G. A. Flandro, "A Real-Time Guidance Algorithm for Aerospace Plane Ascent to Low Earth Orbit," Proceedings of the 1989 ACC, Pittsburgh, PA, June.

[2] Corban, J. E., A. J. Calise, and G. A. Flandro, "Trajectory Optimization and Guidance Law Development for Transatmospheric Vehicles," Proceedings of the 1989 International Conference on Control and Applications (ICCON), April 3-6, Jerusalem, Israel.

[3] Calise, A. J., G. A. Flandro, and J. E. Corban, "Trajectory Optimization and Guidance Law Development for National Aerospace Plane Applications, Final Report for Period July 1, 1987 to November 30, 1988, NASA Contract Number NAG-1-784, December, 1988.

[4] Calise, A. J., J. E. Corban, and G. A. Flandro, "Trajectory Optimization and Guidance Law Development for National Aerospace Plane Applications, Proceedings of the 1988 ACC, Vol 2, pp. 1406-1411, Atlanta, GA, June 15-17.

[5] Bowers, A. H., and K. W. Iliff, "A Generic Hypersonic Aerodynamic Model Example (GHAME) for Computer Simulation," A proposed NASA Technical Note, Ames Research Center, June 16, 1988.

[6] Waltrup, P. J., G. Y. Anderson, and F. D. Stull, "Supersonic Combustion Ramjet (SCRAMJET) Engine Development in the United States," Preprint 76-042, The 3rd International Symposium on Air Breathing Engines, The Johns Hopkins University Applied Physics Laboratory, March, 1976.

[7] Bryson, A. E., Jr., and Yu-Chi Ho, Applied Optimal Control, Hemisphere Publishing Corporation, New York, NY, 1975.

[8] McHenry, R. L., T. J. Brand, A. D. Long, B. F. Cockrell, and J. R. Thibodeau III, "Space Shuttle Ascent Guidance, Navigation, and Control," *The Journal of the Astronautical Sciences*, Vol. XXVII, No. 1, pp. 1-38, January-March, 1979.

Rapid Near-Optimal Trajectory Generation and Guidance Law Development for Single-Stage-to-Orbit Airbreathing Vehicles

January 1990

Research Supported by
NASA Langley Research Center

NASA Contract Number NAG-1-922

Principal Investigators: A. J. Calise and G. A. Flandro
Research Assistant: J. E. Corban
NASA Contract Monitor: D. D. Moerder

School of Aerospace Engineering
Georgia Institute of Technology
Atlanta, Georgia 30332

Rapid Near-Optimal Trajectory Generation and Guidance Law Development for Single-Stage-to-Orbit Airbreathing Vehicles

January 1990

Research Supported by
NASA Langley Research Center

NASA Contract Number NAG-1-922

Principal Investigators: A. J. Calise and G. A. Flandro
Research Assistant: J. E. Corban
NASA Contract Monitor: D. D. Moerder

School of Aerospace Engineering
Georgia Institute of Technology
Atlanta, Georgia 30332

Summary

During the current reporting period, January 1 to December 31, 1989, general problems associated with on-board trajectory optimization, propulsion system cycle selection, and with the synthesis of guidance laws were addressed for ascent to low-Earth-orbit of an air-breathing, single-stage-to-orbit vehicle. This report follows a previous one entitled "Trajectory Optimization and Guidance Law Development for National Aerospace Plane Applications" and dated December 1988. The work reported herein builds directly upon the analytical results presented in that document. A good portion of this work focused on making improvements to the vehicle models employed. The NASA "Generic Hypersonic Aerodynamic Model Example" and the "Langley Accelerator" aerodynamic data sets were acquired and implemented. Work pertaining to the development of purely analytic aerodynamic models also continued at a low level. A generic model of a multi-mode propulsion system was developed that includes turbojet, ramjet, scramjet, and rocket engine cycles. Provisions were made in the dynamic model for a component of thrust normal to the flight path. Computational results, which characterize the nonlinear sensitivity of scramjet performance to changes in vehicle angle of attack, were obtained and incorporated into the engine model. Additional trajectory constraints were also introduced. The constraints now treated are: maximum dynamic pressure, maximum aerodynamic heating rate per unit area, angle of attack and lift limits, and limits on acceleration both along and normal to the flight path.

The remainder of the research effort focused, for the most part, on required modifications to the previously derived algorithm when the model complexity cited above was added. In particular, analytic switching conditions were derived which, under appropriate assumptions, govern optimal transition from one propulsion mode to another for two cases: the case in which engine cycle operations can overlap, and the case in which engine cycle operations are mutually exclusive. The resulting guidance algorithm was implemented in software and exercised extensively. It was found that the approximations associated with the assumed time scale separation employed in this work are reasonable except over the Mach range from roughly 5 to 8. This phenomenon is due to the very large thrust capability of scramjets in this Mach regime when sized to meet the requirement for ascent to orbit. Very little mass penalty is induced by the resulting inaccuracies in the trajectory over this region because it is traversed rapidly. However, the reduced solution climb paths prove to be unfeasible within this Mach range when subject to the full model dynamics and active trajectory constraints. These difficulties were successfully overcome by accounting for flight path angle and flight path angle rate in construction of the flight path over this Mach range. The resulting algorithm provides the means for rapid near-optimal trajectory generation and propulsion cycle

selection over the entire Mach range from take-off to orbit given a realistic nonlinear vehicle model and all pertinent trajectory constraints.

The only significant problem area encountered to date relates to the lack of a general theory for singularly perturbed systems that are subject to state-variable inequality constraints. Such constraints are common to a wide class of flight vehicles but have received little attention in the literature when the dynamic system is singularly perturbed. A study was initiated in this area and it was found that, when the reduced solution lies on a state-variable inequality constraint boundary, the boundary layer trajectories are of finite time in the stretched time scale. The possibility of costate discontinuites at the juncture between constrained and unconstrained arcs makes direct application of existing theory difficult at best. A transformation technique was identified that eliminates some of these difficulties, but at the cost of possibly increased system order and the introduction of singular arcs. Much work remains to be done in this area.

Work on development of simple, efficient algorithms for prediction of vehicle aerodynamic and propulsive performance have continued during the present phase of the program. Improvements in modeling of the hypersonic lifting body module have eliminated previous discrepancies between measured and predicted aerodynamic behavior. Several modes of data entry are now implemented making assessment of a given vehicle configuration very simple. An interactive program mode has been devised that makes possible direct and immediate assessment of configuration changes on selected vehicle performance paramaters. The algorithms developed in this program are of potential use in applications beyond those originally envisioned.

Four conference papers have now been published which discuss most of the results of this research effort. A Ph.D. Dissertation that details the entire effort to date was published in Decemeber of 1989. A full-length paper entitled "Rapid Near-Optimal Trajectory Generation for Single-Stage-to-Orbit Airbreathing Vehicles" has been submitted for publication in the AIAA Journal of Guidance, Control and Dynamics and a new paper is now being prepared for the 1990 AIAA GN&C Conference on the issue of state contraints in singularly perturbed systems.

Table of Contents

List of Figures

List of Symbols

c_j = thrust specific fuel consumption for engine type j
C_1 = inequality constraint, dynamic pressure
C_2 = inequality constraint, aerodynamic heating
C_3 = inequality constraint, tangential acceleration
C_4 = inequality constraint, normal acceleration
C_{D_o} = zero-lift drag coefficient
C_{L_α} = lift curve slope
D = aerodynamic drag
E = mass specific energy
F_C = thrust component aligned with the velocity vector
F_S = thrust component normal to the velocity vector
f = total fuel flow rate
f_{max_i} = combined fuel flow rate for any number of independent engines of type i when operating at a stoichiometric fuel-to-air ratio
g = acceleration due to gravity at mean sea level
h = altitude, given by $r - r_E$
H = Hamiltonian function
J = performance index
K = coefficient of the lift induced drag component
L = aerodynamic lift
m = vehicle mass
M = Mach number
n = total number of different engine cycles employed
n-p = number of engine types employed for which fuel flow rate varies in direct proportion to φ but thrust varies in a nonlinear fashion with φ
n_1 = component of acceleration aligned with the velocity vector
n_2 = component of acceleration normal to the velocity vector
p = number of engine types employed that exhibit linear dependence of both fuel flow rate and thrust on η
q = dynamic pressure
Q = aerodynamic heating rate per unit area
r = radial distance from the center of the Earth
r_E = mean sea level
s = aerodynamic reference area
S_j = switching function for bang-bang control of η_j
t = time
t_f = final time
T = net thrust
T_k = combined thrust of any number of independent engines of type k, k=1 to p
U = pseudo control variable
V = velocity
W = Vehicle weight, taken at mean sea level (W = mg)
α = angle of attack
α_{ZL} = angle of attack for zero lift
γ = flight path angle
δ_e = elevon deflection

ε = perturbation parameter, 0 or 1

ε_{Tk} = angle between T_k and the body longitudinal axis

η_j = throttle control, engine type j

λ_x = costate, subscript denotes related state

μ = gravitational constant for the Earth

ρ = atmospheric density

σ = bank angle

τ = transformed time variable, $\tau = t/\varepsilon$

φ_i = fuel equivalence ratio, engine type i

π = vector containing control for each engine type

SECTION 1
Introduction

Emerging technology in many engineering fields, including hypersonic air-breathing propulsion, computational fluid dynamics, and high temperature materials, may soon make possible a vehicle configuration that has been the subject of study for over four decades[1]. This vehicle concept is commonly referred to as an aerospace plane. Its development, in one version or another, is being pursued by a number of industrialized nations. The current U.S. concept consists of a single-stage vehicle propelled, for the most part, by airbreathing engines. Most notable among the airbreathing cycles to be employed is that of the supersonic combustion ramjet or "scramjet." This aircraft is to be fueled by liquid hydrogen and will take-off and land horizontally on conventional runways. Operational objectives include hypersonic cruise in the upper atmosphere for long durations and the ability to accelerate to orbital velocity. Potential missions for such a vehicle include transportation to low-Earth-orbit, intercontinental passenger transportation, and a wide range of defense missions. This research effort is focused upon the particular mission of single-stage-to-orbit which promises, by the use of air-breathing hypersonic propulsion and greatly reduced launch operations, an order of magnitude reduction in the cost of placing payloads in low Earth orbit [2,3].

Even with the greatly improved fuel efficiency of airbreathing propulsion over current rocket engine technology, the ability to attain orbit in a single-stage vehicle will be marginal at best[4]. Trajectory optimization will play an important role in mission success for this reason. In fact, because the airbreathing propulsion system characteristics are sensitive to vehicle attitude and atmospheric conditions, precise trajectory control will be required. State-of-the-art launch vehicle guidance technology is heavily reliant on pre-mission, ground-based trajectory generation/optimization. In order to be cost effective, aerospace plane operations will have to approach those of modern commercial airlines. Technology dependent upon pre-mission, ground-based trajectory optimization is inadequate for this task; real-time, on-board trajectory optimization will be required[5].

The state of the art in trajectory optimization for complex nonlinear systems consists of a number of well developed numerical methods of solution. Unfortunately, these algorithms are poorly suited for on-board, real-time implementation. They are, in general, computationally intense, require an initial guess of the solution, and are lacking in global convergence characteristics. While some success in designing a reliable algorithm to numerically solve a two

point boundary value problem in an on-board computer has been achieved for orbit transfer[6], the diverse mission requirements and complex control structure of a general purpose aerospace plane will likely require that structured methods for order reduction be employed.

Energy state approximations and singular perturbation methods have been successfully employed to derive near-analytic trajectory optimization algorithms in the past. Near-optimal feedback guidance laws have also been obtained. These methods also contribute considerable insight into the nature of the optimal profiles and their relation to vehicle aerodynamic and propulsion characteristics. Early studies were devoted to fighter aircraft performance optimization[7-9]. However, many of the modeling approximations employed for analysis of subsonic and supersonic aircraft optimal trajectories are not valid for a vehicle with hypersonic cruise and orbital capabilities.

This research report presents an analysis of the problem of fuel-optimal ascent to low-Earth-orbit of an airbreathing, single-stage-to-orbit vehicle. Section II presents the problem formulation. A generic multi-mode propulsion system is defined which incorporates turbojet, ramjet, scramjet, and rocket engines. Inequality constraints on dynamic pressure, aerodynamic heating rate, and vehicle acceleration are also introduced. In Section III an algorithm for generating fuel-optimal climb profiles is derived employing an energy state approximation. This algorithm results from application of the minimum principle to a low order dynamic model that includes general functional dependence on angle of attack and a normal component of thrust. Switching conditions are derived which, under appropriate assumptions, govern optimal transition from one propulsion mode to another. The use of bank angle to modulate the magnitude of the vertical component of lift is also investigated. A nonlinear transformation technique is employed to derive a feedback controller for tracking the computed trajectory. Section IV provides an overview of the vehicles models employed in this work. Section V provides a presentation and discussion of representative numerical results, and Section VI states conclusions drawn from this work. The main body of the report is followed by two appendices. Appendix A details an initial investigation into the characteristics of boundary layer systems when the reduced solution lies on a state-variable inequality constraint boundary. Appendix B details work performed in analytical vehicle model development.

SECTION 2
General Problem Formulation

Consider atmospheric flight of a point mass over a spherical non-rotating Earth. The equations governing such flight can be reduced to a four state model as follows,

$$\dot{E} = \frac{V(F_C - D)}{m} \tag{1}$$

$$\dot{m} = -f(r,E,\pi,\alpha) \tag{2}$$

$$\varepsilon\dot{\gamma} = \frac{(F_S + L)\cos\sigma}{mV} - \frac{\mu\cos\gamma}{Vr^2} + \frac{V\cos\gamma}{r} \tag{3}$$

$$\varepsilon\dot{r} = V\sin\gamma \tag{4}$$

The perturbation parameter, ε, which has been artificially inserted, is nominally one. It is assumed that the atmosphere is stationary and that the thrust vector lies in the vehicle's plane of symmetry. In (1), mass specific energy, E, is employed as a state variable in place of velocity, V, where

$$E = V^2/2 - \mu/r \tag{5}$$

The reference point for zero gravitational potential is taken at a radial distance approaching infinity. The symbol V is to be taken as

$$V = [2(E + \mu/r)]^{1/2} \tag{6}$$

everywhere it appears in this analysis. Position and heading dynamics are decoupled from (1–4) by the assumption of a non-rotating Earth and are not of interest at present.

Drag is assumed to have a conventional parabolic form

$$D = qsC_{D_o} + KL^2/qs \qquad \text{where} \qquad q = \rho V^2/2 \tag{7}$$

The assumed functional dependence for C_{D_o} , the zero lift drag coefficient, and K, the coefficient of the induced drag component, are:

$$C_{D_o} = C_{D_o}(M) \qquad K = K(M,\alpha) \tag{8}$$

Lift is given by

$$L = qsC_L(r,E,\alpha,\delta_e) = qsC_{L\alpha}(\alpha - \alpha_{ZL}) \tag{9}$$

The lift curve slope, $C_{L\alpha}$, and the angle of attack for zero lift, α_{ZL} , are assumed to be Mach number dependent.

A multi-mode propulsion system composed of n different engine types (i.e. cycles) is assumed. Net thrust is given by

$$T = [\, F_C^{\,2} + F_S^{\,2} \,]^{1/2} \tag{10}$$

where F_C represents the component of net thrust along the velocity vector and F_S represents the component of net thrust normal to the velocity vector, i.e. in the lift direction. These components are depicted in Figure 1 and given by:

$$F_C = \sum_{j=1}^{p} \eta_j T_j \cos(\alpha + \varepsilon_{T_j}) + \sum_{i=p+1}^{n} T_i \cos(\alpha + \varepsilon_{T_i}) \tag{11}$$

$$F_S = \sum_{j=1}^{p} \eta_j T_j \sin(\alpha + \varepsilon_{T_j}) + \sum_{i=p+1}^{n} T_i \sin(\alpha + \varepsilon_{T_i}) \tag{12}$$

Each of the n engine cycles (i.e. turbojet, ramjet, scramjet, rocket, etc.) is controlled by variation of the fuel flow rate in direct proportion to command. Of the total number of engine types to be considered, p are assumed to exhibit a linear relation between fuel flow rate and thrust generation. Each engine of this type shall be controlled by varying its throttle setting, η_j. This assumption is typically employed for rocket engines. For the remaining n–p engine cycles, the relation between fuel flow rate and thrust generation is assumed nonlinear. Control of each engine of this type shall be effected by variation in its fuel equivalence ratio, φ_i. This behavior is typical of air-breathing cycles. The subscripted symbol T_k (k = 1 to n) in (11) and (12) represents the net thrust generated

by any number of independent engines employing a particular cycle k. The symbol ε_{T_k} denotes the angle between T_k and the body longitudinal axis (see Figure 1). Note that in general,

$$T_j = T_j(r,E,\alpha) \qquad \eta_j \in [0,1] \qquad j = 1 \text{ to } p \tag{13}$$

$$T_i = T_i\,(r,E,\varphi_i,\alpha) \qquad \varphi_i \in [0,1] \qquad i = p+1 \text{ to } n \tag{14}$$

$$\varepsilon_{T_k} = \varepsilon_{T_k}(r,E,\alpha) \qquad k = 1 \text{ to } n \tag{15}$$

The total fuel flow rate, f, is given by

$$f = \sum_{j=1}^{p} \eta_j\, c_j(r,E,\alpha)\, T_j(r,E,\alpha) + \sum_{i=p+1}^{n} \varphi_i\, f_{max_i}(r,E,\alpha) \tag{16}$$

where c_j represents the thrust specific fuel consumption for engine type j and f_{max_i} represents the product of thrust specific fuel consumption and thrust at a stoichiometric fuel-to-air ratio for engine type i. For convenience all of the engine throttle controls are collected into a single vector as follows,

$$\pi^T = [\eta_1, \eta_2, \ldots, \eta_p, \varphi_{p+1}, \ldots, \varphi_n] \tag{17}$$

The control variables are angle of attack, α, bank angle, σ, the fuel equivalence ratios, φ_i, for engine types 1 through n, and engine throttle settings, η_j, for engine types n+1 through p. The objective is to minimize the fuel consumed in gaining energy, with the performance index given by,

$$J = -\,m(t_f) \tag{18}$$

The final time, t_f, is free. Minimization of (18) is to be carried out subject to maximum dynamic pressure and maximum aerodynamic heating rate inequality constraints and acceleration limits defined by

$$C_1\,(r, E) = q - q_{max} \leq 0 \tag{19}$$

$$C_2 (r, E, \alpha) = Q - Q_{max} \leq 0 \tag{20}$$

$$C_3 (r, E, m, \alpha, \pi) = n_1 - n_{1max} \leq 0 \tag{21}$$

$$C_4 (r, E, m, \alpha, \pi) = n_2 - n_{2max} \leq 0 \tag{22}$$

The symbols n_1 and n_2 represent the accelerations in g's along and normal to the velocity vector (i.e. in the lift direction), respectively.

SECTION 3

Singular Perturbation Analysis

3.1 Reduced Solution.

Lift as a Control. We first consider a simplified problem in which flight is constrained to a vertical plane, the thrust vector is aligned with the velocity vector, and thrust production is assumed independent of vehicle angle of attack:

$$\sigma = 0, \qquad F_S = 0, \qquad F_C = T \tag{23}$$

Furthermore, we consider only that portion of the trajectory in the hypersonic regime. In this regime we need only consider a dual-mode propulsion system (i.e. n = 2). The system consists of a bank of scramjet engine modules assumed to operate continuously and a rocket engine that can be throttled as desired. The constraint (21), which can lead to the requirement for intermediate values of throttle setting, will be ignored. In this simplified setting the total fuel flow rate and net thrust can be represented as

$$T = T_s(r,E) + \eta\, T_r(r) \quad ; \quad \eta \in [0,1] \tag{24}$$

$$f = c_s(r,E)\, T_s + \eta\, c_r(r)\, T_r \tag{25}$$

where thrust specific fuel consumption is represented by c_s for the scramjet and c_r for the rocket. Under these assumptions the governing equations of motion can be written as,

$$\dot{E} = \frac{V(T - D)}{m} \tag{26}$$

$$\dot{m} = -f\,(r,E,\eta) \tag{27}$$

$$\dot{\varepsilon\gamma} = \frac{L}{mV} - \frac{\mu \cos\gamma}{Vr^2} + \frac{V \cos\gamma}{r} \tag{28}$$

$$\dot{\varepsilon r} = V \sin\gamma \tag{29}$$

The control variables are now rocket engine throttle, η, and vehicle lift, L. The objective remains to minimize the fuel consumed in gaining energy.

Setting $\varepsilon = 0$ in (26-29) reduces the order of the dynamic system to two and results in what is conventionally referred to as the energy state approximation. That is, altitude and flight path angle dynamics are assumed fast in comparison to energy and mass dynamics, and altitude now takes on the role of a control variable[9]. The differential equations (28) and (29) are reduced to algebraic equations which yield the following relations:

$$\gamma_o = 0 \tag{30}$$

$$L_o = m[(\mu/r^2) - (V^2/r)] \tag{31}$$

The subscript zero denotes reduced solution values and is omitted below where not deemed necessary for clarity. The reduced solution Hamiltonian is given by

$$H_o = \lambda_E \dot{E} + \lambda_m \dot{m} + \text{constraints} = 0 \tag{32}$$

where

$$\lambda_m (t_f) = -1.0 \tag{33}$$

Satisfaction of the minimum principle with respect to altitude, h, is equivalent to the following operation (see Appendix B of reference 10),

$$h_o^* = \arg\max_h [V(T-D)/f] \Big|_{\substack{E = \text{constant} \\ T > D \quad q \le q_{max} \\ \eta = \eta^* \quad Q \le Q_{max}}} \tag{34}$$

Consideration of the constraints (19, 20) simply limits the search space over which the maximization of (34) takes place. The superscript asterisk denotes an optimal value of control. This operation yields an optimal altitude program as a function of vehicle energy and mass. Note that η appears linearly in the Hamiltonian resulting in a bang-bang control solution for rocket throttle setting. A switching condition, S, results from the evaluation of $\partial H_o/\partial \eta$ and is given by,

$$S = \lambda_E(V/m) - \lambda_m c_r \tag{35}$$

Using (32) to eliminate λ_E in (35) and taking into account the sign of λ_m† yields the following analytic switching condition:

$$\eta = 0 \quad \text{if} \quad [(c_r - c_s)/c_r]T_s > D$$
$$\eta = 1 \quad \text{if} \quad [(c_r - c_s)/c_r]T_s < D \tag{36}$$

Intermediate values of rocket throttle setting are not optimal. This fact is revealed by examination of the matrix H_{uu}, which is required to be at least positive semidefinite along an optimizing singular arc. For convenience, V, rather than h is taken as the control-like variable so that $u^T = [\, V,\eta \,]$. The determinant of H_{uu}, which is symmetric, must be greater than or equal to zero for positive semidefiniteness. However, it can be shown that

$$\det H_{uu} = -\left\{H_{V\eta}\right\}^2 \tag{37}$$

which is negative for $H_{V\eta} \neq 0$, which is generally the case.

It can happen that the velocity set is not convex in a region of interest, and, in the absence of convexity, one can not guarantee that an optimal control exists. Thus the possibility of a chattering control solution should be examined. Conclusions regarding this matter are model dependent and are discussed in reference 16. It is sufficient to say here that no chattering solutions for rocket throttle setting were found for the vehicle models examined.

The reduced solution costates are determined as[12]:

$$\lambda_{r_o} = 0 \qquad \lambda_{m_o} \cong -\, m(t_f)/m \tag{38}$$

$$\lambda_{\gamma_o} = \lambda_{E_o}\,[2KV^2L_o/(qs)] \qquad \lambda_{E_o} = \lambda_{m_o}\,\{fm/[V(T-D)]\} \tag{39}$$

---

† The "influence function", λ_m, represents the variation in the performance index, J, with respect to mass[11]. Since $J = -\, m(t_f)$, λ_m cannot change sign (i.e. it is not possible for a reduction in vehicle mass as fuel is expended along the climb path to increase the final mass of the vehicle).

Angle of Attack as a Control. Consider now the full model complexity formulated in Section II with the exception that flight remains constrained to a vertical plane. That is, consider flight over the entire Mach range, including the subsonic and supersonic regimes. Assume a multi-mode propulsion system consisting of turbojet, ramjet, scramjet, and rocket cycles (i.e. n = 4). Allow for a component of net thrust normal to the velocity vector and consider the possibility that the performance of one or more of the air-breathing engine cycles is dependent on vehicle angle of attack. Consider also the constraint on axial acceleration given by (21). The method of solution proceeds as before.

Setting $\varepsilon = 0$ in (1-4) reduces the differential equations (3) and (4) to algebraic relations:

$$\gamma_o = 0 \tag{40}$$

$$L_o = m(\mu/r^2 - V^2/r) - F_S \tag{41}$$

The control α_O is eliminated via (41). That is, given values of r and E, α_o is iteratively determined using (41) while enforcing trim through elevon deflection, δ_e. More concisely,

$$\alpha_o(r,E) = \{\alpha_o: L(r,E,\alpha,\delta_e) - L_o(r,E,\pi,\alpha) = 0\} \tag{42}$$

The reduced solution Hamiltonian is again given by (32). But since drag, given by (7), is dependent on L_o^2, which in turn depends on engine controls through F_S, as given in (12), the φ_i and the η_j both enter nonlinearly in the Hamiltonian. Satisfaction of the minimum principle with respect to h and π is equivalent to the following operation,

$$h_o^*, \pi^* = \arg\max_{h,\pi} [V(F_C - D)/f] \Big|_{\substack{E = \text{constant} \quad Fc > D \\ q \le q\max \quad Q \le Q\max \\ n_1 \le n_{1\max} \quad n_2 \le n_{2\max}}} \tag{43}$$

This operation yields both an optimal altitude program as a function of vehicle energy and mass and the corresponding optimal engine controls.

If we neglect the dependence of reduced solution drag on the sine component of net thrust, F_S, then the η_j enter linearly in H_o. In such case we have bang-bang solutions for the η_j with possible

singular arcs along which intermediate throttle settings may be optimal. The switching functions are determined as before from $\partial H_o/\partial \eta_j$,

$$S_j = [f(\pi)\cos(\alpha + \varepsilon_{T_j})/(F_C(\pi) - D)] - c_j \qquad j = 1+n \text{ to } p \tag{44}$$

Throttle settings are then governed by the following relations:

$$\begin{aligned} &\eta_j = \eta_{min} \quad \text{if} \quad S_j < 0 \\ &\eta_j \text{ singular} \quad \text{if} \quad S_j = 0 \text{ for finite time} \\ &\eta_j = \eta_{max} \quad \text{if} \quad S_j > 0 \end{aligned} \tag{45}$$

The S_j are dependent on the η_k, $k \neq j$. Thus an iterative scheme is required to arrive at the optimal combination of throttle settings if $j > 1$.

Thus far in the analysis it has been assumed that each engine cycle can be independently controlled. Since much of the captured mass flow and some or all of the engine hardware will be shared by the various engine cycles employed, it is perhaps more useful to consider operation of the various air-breathing cycles as mutually exclusive. In reality, dual combustion over a finite range of Mach number will be required to smoothly transition from subsonic to supersonic combustion[13]. One can view the case of mutually exclusive engine cycles as a problem in which the system equations are discontinuous at cycle transition points along the trajectory. Following the terminology of reference 11, suppose that one set of system equations,

$$\dot{x} = f^{(1)}(x,u,t) \tag{46}$$

applies for $t < t_1$, where t_1 is free, and another set of system equations applies for $t > t_1$, namely,

$$\dot{x} = f^{(2)}(x,u,t) \tag{47}$$

Here x and u denote general state and control vectors, respectively. It is necessary for optimality that

$$H^{(1)}(t_1-) = H^{(2)}(t_1+) \tag{48}$$

The condition (48) can be used to determine the optimal point of transition from one set of system equations to another. In this case $f^{(1)}$ and $f^{(2)}$ differ only by the thrust produced by the particular engine cycle being employed and by the associated difference in fuel consumption. Satisfaction of

(48) can be reduced to the following equality where the condition $H_o = 0$ has been employed to eliminate costate dependence

$$(T_i \cos(\alpha + \varepsilon_{T_i}) - D)/c_i T_i = (T_j \cos(\alpha + \varepsilon_{T_j}) - D)/c_j T_j \tag{49}$$

This result is, in fact, obvious from examination of (43). That is to say, points at which a change in engine cycle can occur require that the function to be maximized be equal for either choice of the propulsion cycle. When the functional evaluations are not equivalent, one or the other is greater and dictates the optimal choice of cycle.

Bank Angle as a Control. It is reasonable to assume that the performance of the proposed scramjet engines will be sensitive to vehicle angle of attack. Furthermore, it is quite likely that thrust production will depend on angle of attack in a nonlinear way. Given that this is true, any particular engine installation will exhibit an angle of attack for which engine performance is best. This angle of attack for best engine performance, call it the design angle of attack, may in turn vary with Mach number[14]. If such nonlinear behavior is assumed and the optimal flight path is constructed using (43), one finds that, since fuel optimization is very sensitive to engine performance, the optimal trajectory tends to remain on a contour along which the design angle of attack is maintained. It can happen, however, that overall performance is improved if the design angle of attack is maintained while flying at lower altitudes, and hence at higher values of dynamic pressure. Of course, maintaining the design angle of attack at a higher dynamic pressure generates additional lift which causes the vehicle to immediately climb above the desired flight path. Thus, in order to fly along the optimal path, the extra lift associated with maintaining the design angle of attack must be "dumped." One procedure for accomplishing this task is to roll back and forth in such a way that, on average, the component of lift in the vertical direction is reduced to that required to maintain the optimal climb rate. It may in fact be more practical to appropriately offset the initial vehicle heading and to then execute a single coordinated turn that accomplishes the same objective. With bank angle thus introduced as an additional control, satisfaction of the minimum principle with respect to h, π, and α is equivalent to the following operation,

$$h_o^*, \pi^*, \alpha_o^* = \arg\max_{h,\pi,\alpha} [V(F_C - D)/f] \Big|_{\substack{E = \text{constant} \quad Fc > D \\ q \le q_{max} \quad Q \le Q_{max} \\ n_1 \le n_{1max} \quad n_2 \le n_{2max}}} \tag{50}$$

where bank angle, σ, is determined so that

$$L \cos \sigma = L_o \tag{51}$$

3.2 Boundary Layer Analysis.

The unconstrained boundary layer solution associated with (1–4) is obtained by introducing the time transformation $\tau = t/\varepsilon$ and again setting $\varepsilon = 0$. That is, energy and mass are held constant while altitude and flight path angle dynamics are examined on a stretched time scale. The resulting necessary conditions for optimality yield an optimal feedback guidance law for lift control which depends on the unknown costate λ_γ (see Section 5.2.2 of reference 10). In the absence of a state inequality constraint such as (19), a suitable approximation to λ_γ can be obtained by linearizing the boundary layer necessary conditions about the reduced solution[10,15]. However, this procedure is not applicable when the reduced solution lies on a state constraint boundary. This problem is discussed in detail in Appendix A. The boundary layer control solutions for engine throttle settings are similar to those of the reduced solution. The η_j enter the Hamiltonian linearly, but the switching conditions that govern their behavior are also dependent on the unknown costate λ_γ. This dependence drops out of the switching conditions if the sine component of thrust, F_S, is neglected.

Feedback Linearization - Lift as a Control.. As an alternative approach to handling the control of altitude and flight path dynamics, a nonlinear transformation technique is employed as follows[10]. Consider the boundary layer altitude and flight path angle dynamics given in (32) and (33) on a transformed time scale $\tau = t/\varepsilon$. Note that we have system equations in block triangular form. To proceed we take successive total time derivatives of r until explicit dependence on the control appears. The prime notation denotes differentiation with respect to τ.

$$r'' = (L\cos\gamma)/m + (V^2 \cos^2\gamma)/r - (\mu/r^2) \tag{46}$$

The control, L, appears in the second time derivative and we define U, the pseudo control, as

$$U = r'' \tag{47}$$

It is desired that U be determined as follows

$$U = K_p\left(r_o - r\right) + K_d\left(\dot{r_o} - r'\right) \tag{48}$$

where r_o denotes the reduced solution radius at the current energy level and the time derivative of r_o denotes the climb rate required to stay on the reduced solution as energy is gained. This climb rate can be estimated by defining an appropriate increment in energy, evaluating the reduced solution at this higher energy level, and then estimating the required climb rate using a forwards difference.

The inverse transformation is defined by solving for L in (47) using (46) and (48),

$$L = \{U + (\mu/r^2) - [(V^2/r)\cos^2\gamma]\}(m/\cos\gamma) \tag{49}$$

This lift control solution is constrained directly by (21). Note that as r and γ approach their reduced solution values, (49) approaches the reduced solution value of lift given by (35). A block diagram depicting the conceptual implementation of the nonlinear transformation technique to yield the controller defined by (49) is presented in references 10, 15 and 16. The corresponding closed loop transfer function is

$$G(s) = (K_d s + K_p)/(s^2 + K_d s + K_p) \tag{50}$$

where the gains K_p and K_d for the second order system can be written in terms of the damping ratio, ζ, and natural frequency, ω_n, as

$$K_p = \omega_n^2 \qquad K_d = 2\zeta\omega_n \tag{51}$$

The performance of this controller can be dictated by selecting the values of K_p and K_d to yield the desired dynamic response. This lift control solution applies equally well to the unconstrained or the inequality constrained case.

Feedback Linearization - Angle of Attack as a Control. Direct extension of the lift control solution presented above to include the angle of attack effects included in (1-4) results in the following feedback control law,

$$\alpha^* = \left\{ \alpha: \left[U + \frac{\mu}{r^2} - \frac{V^2 \cos^2 \gamma}{r} \right] \frac{m}{\cos \gamma} - (F_S + L) = 0 \right\} \tag{63}$$

The pseudo-control, U, is defined as before where again K_p, proportional gain, and K_d, rate gain, are selected to yield the desired controller performance. Optimal lift, which is directly constrained by (21), is then determined by,

$$L^* = qsC_{l_\alpha} (\alpha^* - \alpha_{ZL}) \tag{64}$$

SECTION 4
Vehicle Models

Four different vehicle models were employed to generate the numerical results presented in the next section. The first, referred to as Model 1, is based on a hypersonic research vehicle concept studied by NASA in the 1970's and is powered by a combination of scramjet and rocket propulsion[10]. This model is useful only in the hypersonic regime. Models 2 and 3 are based on a "Generic Hypersonic Aerodynamic Model Example," or GHAME, developed more recently by NASA[17]. A nominal configuration of 233.4 feet total length and 300,000 pounds gross take-off weight was assumed. The trimmed aerodynamic characteristics were taken directly from the GHAME documentation. For Model 2 the largely empirical GHAME I aerodynamic data set was employed. For Model 3 the numerically generated GHAME II aerodynamic data set was employed. Both sets extend from take-off to orbital velocities. Thrust for both Models 2 and 3 is provided by a multi-mode propulsion system composed of turbojet, ramjet, scramjet, and rocket engines. The airbreathing propulsive characteristics for this model were adopted from reference 18. A rocket, sized for orbital insertion (roughly 15,000 lbs. of thrust in vacuum), is assumed available over the entire Mach range[10]. This system corresponds to the case $p = n = 4$ in (11), (12), and (16). As a result, the switching conditions given by (45) can be used to determine all of the cycle transition points. Figure 2 presents the adopted variation in fuel specific impulse with Mach number for the various engine cycles. The various engines where sized by trial and error and do not represent an optimal configuration. The generation of scramjet thrust due to mass ejection when operating above a stoichiometric fuel-to-air ratio is not modeled. Thrust induced pitching moments, which can be significant[16], were not considered when trimming the aircraft. A fourth model was constructed by combining an aerodynamic data set provided by the NASA Langley Research Center (referred to as the "Langley Accelerator") with the propulsive data described above. Additional details regarding these models are available in references 10 and 19.

A simple model for convective heating rate per unit area, Q, was adopted from reference 20,

$$Q = (4.919\ \text{E-}08)\ \rho^{0.5}\ V^{3.0} \tag{52}$$

Equation (52) gives Q in Watts/cm^2 given density in kg/m^3 and velocity in m/sec and corresponds to equilibrium conditions on the surface of a sphere or wing leading edge 10 cm in radius and cooled by reradiation alone. For reference, a contour of $Q = 800$ in the altitude-velocity plane corresponds roughly to a contour along which skin temperature remains at approximately 2000° F three feet aft of the leading edge assuming laminar flow[21].

SECTION 5
Numerical Results

Reduced solution trajectories were generated by carrying out the maximization process indicated in (34), (43), and (50) over the energy range from take-off to orbit. Numerous results are available in reference 19. Only a few representative plots are presented here. Figure 3 depicts reduced solution trajectories for Model 1 in the altitude/velocity plane. Dynamic pressure is limited to 2000 psf while maximum allowable heating rate is varied. The trajectories follow the dynamic pressure constraint boundary until the specified contour of maximum heating rate is encountered. The path then follows the constant heating rate contour until reaching the trajectory for which no heating rate constraint was enforced. At this point the heating constraint becomes inactive and the trajectory rejoins the unconstrained climb path. The mechanism causing the altitude discontinuity at a velocity of 22,000 ft./sec. is similar to that which has been noted in the transonic region for supersonic fighter aircraft[15]. Included in Figure 3 is the rocket switching surface, i.e. the contour along which the switching function (39) remains zero. At altitudes below this contour the optimal rocket throttle setting is zero whereas above the contour the optimal throttle setting is one. The performance penalty paid in enforcing the heating constraint is presented in Figure 3 as time required and percent gross weight consumed to achieve an orbital energy level. This performance penalty must be weighed against the complications of using active cooling, the weight of heat shielding, and various other factors in the vehicle design process.

Figure 4 presents the reduced solution climb path in the altitude-velocity plane for Vehicle Model 4. The dynamic pressure constraint is again enforced, an aerodynamic heating constraint is not, and a limit on axial acceleration is introduced. The trajectories vary predictably as the magnitude of the acceleration constraint is changed. Some throttling of the engines is employed but in general the vehicle prefers instead to climb to reduce the excess thrust available. Note that the altitude discontinuity present in Figure 3 does not occur for this vehicle, but is in fact implicit in matching a terminal altitude condition at orbital velocity. The horizontal bars at the top of the figure indicate the velocity range over which the operation of each engine cycle was deemed optimal, including regions of cycle overlap. The rocket operation was not optimal during atmospheric flight for this case.

Computational investigations of the sensitivity of scramjet performance to changes in angle of attack predict highly nonlinear behavior[14]. Figure 5 presents a scramjet thrust scaling factor employed to model this effect. This figure is based on a liberal interpretation of the computational

results presented in reference 14. This curve is shifted with respect to the horizontal axis in order to represent inlet designs which favor maximum engine performance at an angle of attack other than zero.

Figure 6 presents variations in the dynamic pressure constrained reduced solution trajectories for Model 3 when thrust variation with angle of attack for both the ramjets and scramjets, as depicted in Figure 5, is included. The angle of attack for best engine performance is varied over the range from 0.5 to 3.0 degrees. When only scramjets are operating, the vehicle tends to prefer a path along which the "design" angle of attack is strictly maintained. The performance penalty paid for a change in the design angle of attack is modest however, since in this Mach region, the acceleration capability of the vehicle is high. When the thrust scaling factor of Figure 5 is assumed Mach dependent in accordance with the results of reference 14, a much greater variation in the trajectory is experienced[19].

The peak in the trajectories at approximately 3000 ft./sec. in Figure 6 is due to turbojet shut down. This peak is significantly reduced when the turbojet inlet area is increased, indicating that the climb away from the dynamic pressure constraint boundary is due to the decreasing level of thrust available from the turbojet as the Mach number increases. With an increase in altitude comes a reduction in vehicle drag, but the turbojet switching surface is encountered at an altitude of approximately 75,000 ft. and the turbojet shut down. The SCRAMJET almost immediately switches on, and with a much greater magnitude of thrust, can sufficiently overcome vehicle drag, even at a higher dynamic pressure. Thus the trajectory returns to the dynamic pressure constraint boundary. Note that the ramjet is turned on at a very low Mach number (i.e. M = 0.81) even though it is extremely inefficient in this speed range (see Figure 2). This behavior has been noted by past researchers and is due to the presence of a "pinch point" (i.e. a point of minimum thrust minus drag) in the transonic region. The size of the ramjet was selected without regard to its weight. However, optimization of the vehicle configuration must take into account the mass of each engine and the mass of the required engine cowling. Results obtained indicate that the optimal trajectory for such an optimized configuration may prefer the use of rocket (rather than ramjet) thrust to augment turbojet thrust at the transonic pinch point.

As stated above, cycle operations are represented in Figure 6 by horizontal bars. The transition points were very nearly the same for thrust independent of or dependent on angle of attack. The overlap in air-breathing cycles is desirable to provide smooth cycle transitions. For Model 3, turbojet sizing requires about 25 sq. ft. of inlet area, whereas the total number of ramjet modules selected require 200 sq. ft. of inlet area. Thus it should be possible to start the majority of the

ramjet engines in a sequence that avoids excessive accelerations while maintaining turbojet thrust. Once the velocity for turbojet shut-down is reached, turbojet airflow can be diverted to the remaining ramjet modules. The number of required scramjet modules is likewise larger than the number of required ramjet modules, and a similar argument for cycle overlap can be made. Of course, the actual system will no doubt share much of the engine hardware amongst the various cycles employed in addition to sharing the captured mass flow. Thus the actual optimization of engine transitions will be more complex.

Modulation of the vertical component of lift via bank angle variation was also evaluated for Model 3. Carrying out the maximization process indicated in (50) alters the trajectories presented in Figure 6 only slightly. The changes correspond to those portions of the trajectory where $\alpha_o < \alpha_{design}$. As such, only a very modest gain in performance was achieved. However, if design constraints force the scramjet design angle of attack to differ significantly from the angle of attack for zero lift, much greater savings can be obtained.

Figure 7 depicts the reduced solution trajectory for Vehicle Model 2 in the altitude-velocity plane. A maximum allowable dynamic pressure of 2000 psf is the only constraint enforced. The dashed line labeled 1 represents the fuel-optimal climb path when scramjet performance is assumed independent of vehicle angle of attack. The percent of take-off gross weight consumed in attaining orbital energy is 61. The solid line label 2 represents the fuel-optimal climb path when scramjet performance is assumed to vary with angle of attack according to Figure 5, with optimum engine performance assumed to occur at an angle of attack of 3 degrees across the Mach range. In this case the trajectory tends to remain on the dynamic pressure constraint boundary for the majority of the flight. The percent of take-off gross weight consumed in attaining orbital energy in this case is 68.2. The weight penalty of 7.2 percent of the take-off gross weight most likely exceeds the payload capability of the vehicle. This comparison indicates the critical need to accurately model the many interactions present among disciplines.

Figure 8 depicts the altitude time history for simulated flight of Model 3 using the lift control law derived via feedback linearization to track the corresponding reduced solution. The ramjet cycle was eliminated and the trajectory is subjected to the following constraints: dynamic pressure $\leq$ 2000 psf, reference heating rate $\leq$ 400 Watts/cm^2, and axial acceleration $\leq$ 3.0 g's. In general this vehicle preferred to climb in order to satisfy an axial acceleration limit rather than to throttle back the engines. The rapid climb at roughly 400 seconds is due to scramjet turn-on and this preferred behavior. The large overshoot just before 500 seconds is due to the inability of the vehicle to pull down as the altitude for which $n_1 \leq 3$ at full throttle is approached. This overshoot

can be reduced somewhat by careful gain scheduling and having the controller look ahead in energy. However, the requirement to fine tune the controller for each trajectory generated is *not* desirable for the intended applications of this algorithm. The problem has less to do with the controller than with the generation of the trajectory itself.

Over the vast majority of the trajectory the flight path angle is small and the flight path angle rate very modest so that (41) provides a good approximation to the actual lift required to follow the flight trajectory. However, when the scramjet is initially turned on at a relatively high value of dynamic pressure, the energy rate of the vehicle is greatly increased. The necessity of simultaneously climbing to avoid violating the dynamic pressure constraint boundary results in a large flight path angle rate. The time scale separation assumed in (1-4) is simply not appropriate over this small portion of the trajectory. A simple way to overcome this difficulty consists of estimating the flight path angle and time interval between energy levels, combining them to form an estimate of the flight path angle rate, and then inverting relation (3) to obtain the required lift. By restricting the accelerations normal to the flight path when constructing the reduced solution in this region, a feasible trajectory can always be obtained.

Figure 9 depicts the reduced solution climb path for Model 3 again with a maximum dynamic pressure of 2000 psf, a maximum aerodynamic heating rate of 400 Watts/cm^2, but with a maximum axial acceleration of 1g to amplify the problem ($\gamma = 0$ in the lift calculations). Also depicted is the modified trajectory when the method described above is implemented (γ and $d\gamma/dt \neq 0$). The results in the altitude/velocity plane are quite dramatic over the speed range from 3,000 to 12,000 ft./sec. The near vertical altitude transition at a velocity of approximately 3,000 ft./sec. is eliminated, as is the dive that followed. The arc which follows in the velocity range from 5,000 to 13,000 ft./sec. corresponds to the region over which the axial acceleration limit is active. Less altitude change is commanded in this region; more throttle is used to reduce the axial acceleration instead. The remainder of the trajectory, the same for either case, constitutes flight along the heating constraint boundary. Despite the significant change in trajectory, only 200 additional pounds of fuel are consumed and the difference in time of flight is only about 60 seconds. These small differences are due to the fact that the velocity interval from 3,000 to 12,000 ft./sec. is traversed very rapidly in time, corresponding to only a small fraction of the total time of flight.

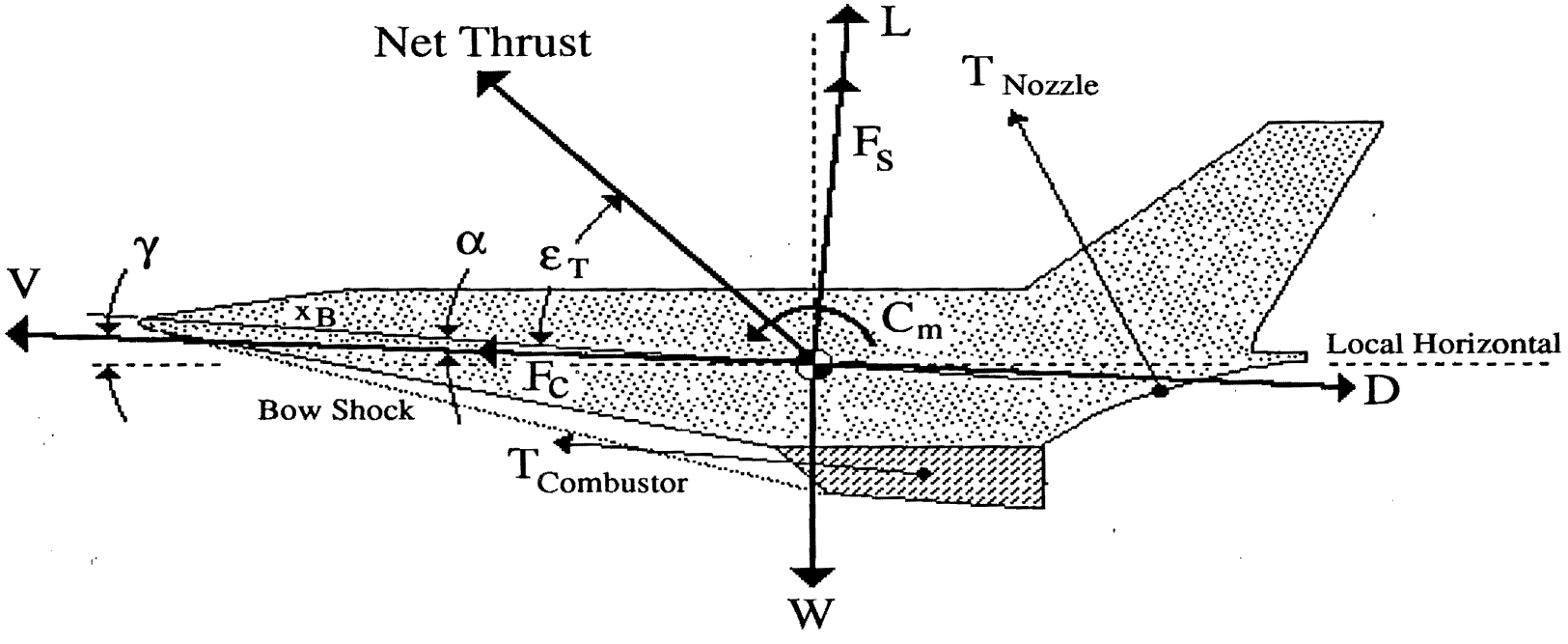

Figure 1 Partial Force and Moment Diagram

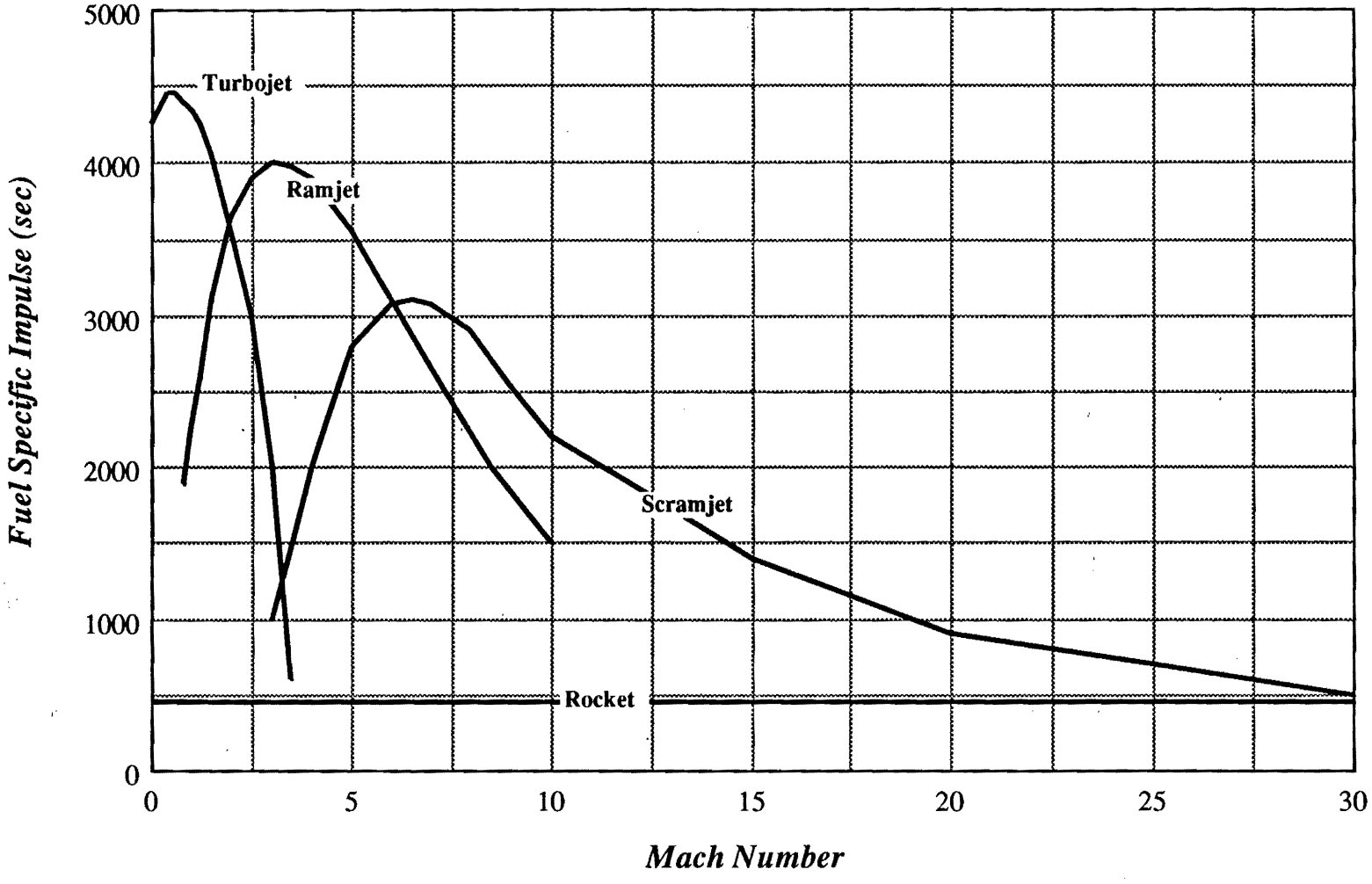

Figure 2 Fuel specific impulse versus Mach number for the various propulsion cycles available to Vehicle Models 2 through 4.

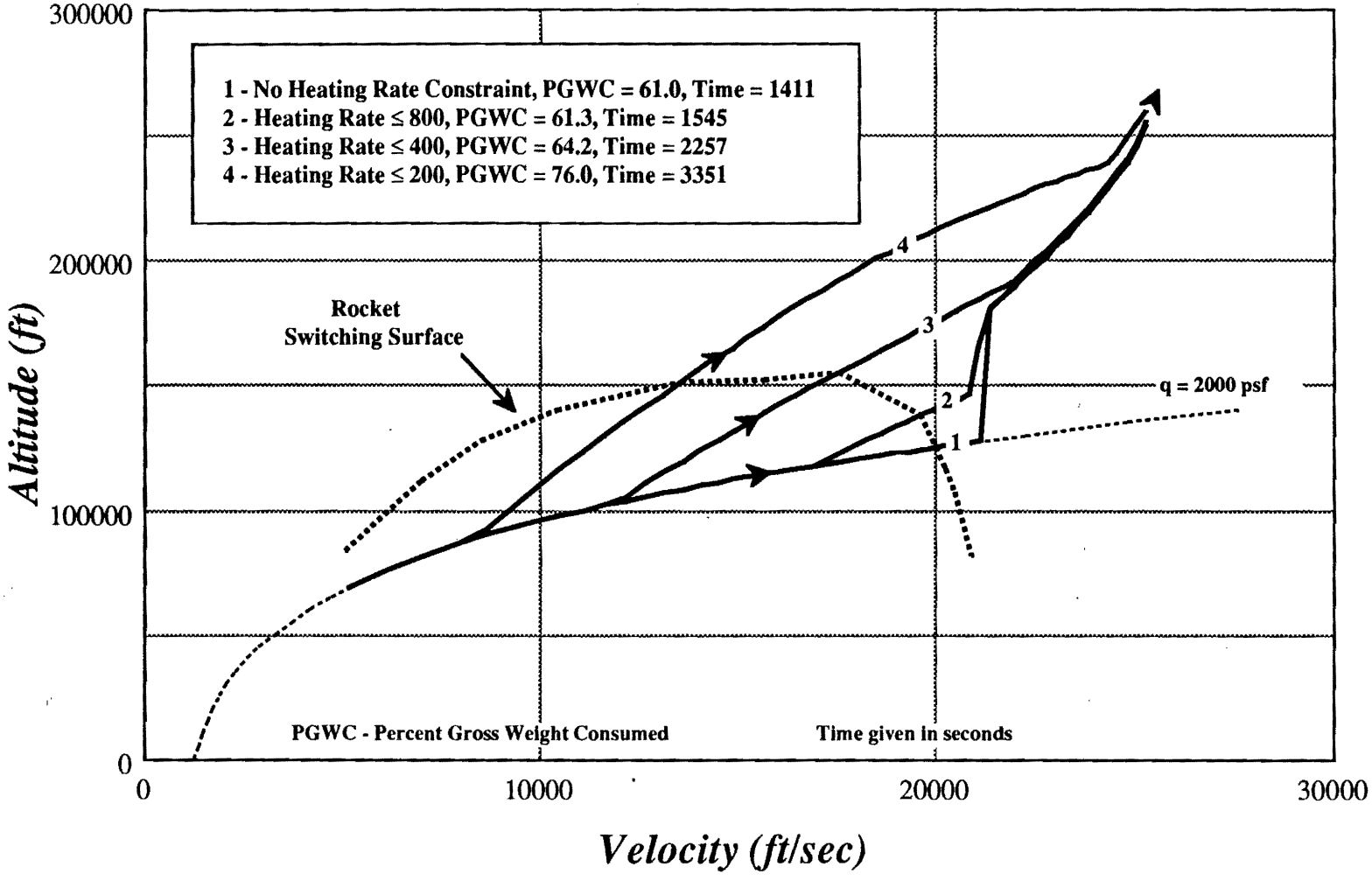

Figure 3 Reduced Solution for Vehicle Model Number 1 as the maximum aerodynamic heating rate constraint (shown in Watts/cm²) is varied.

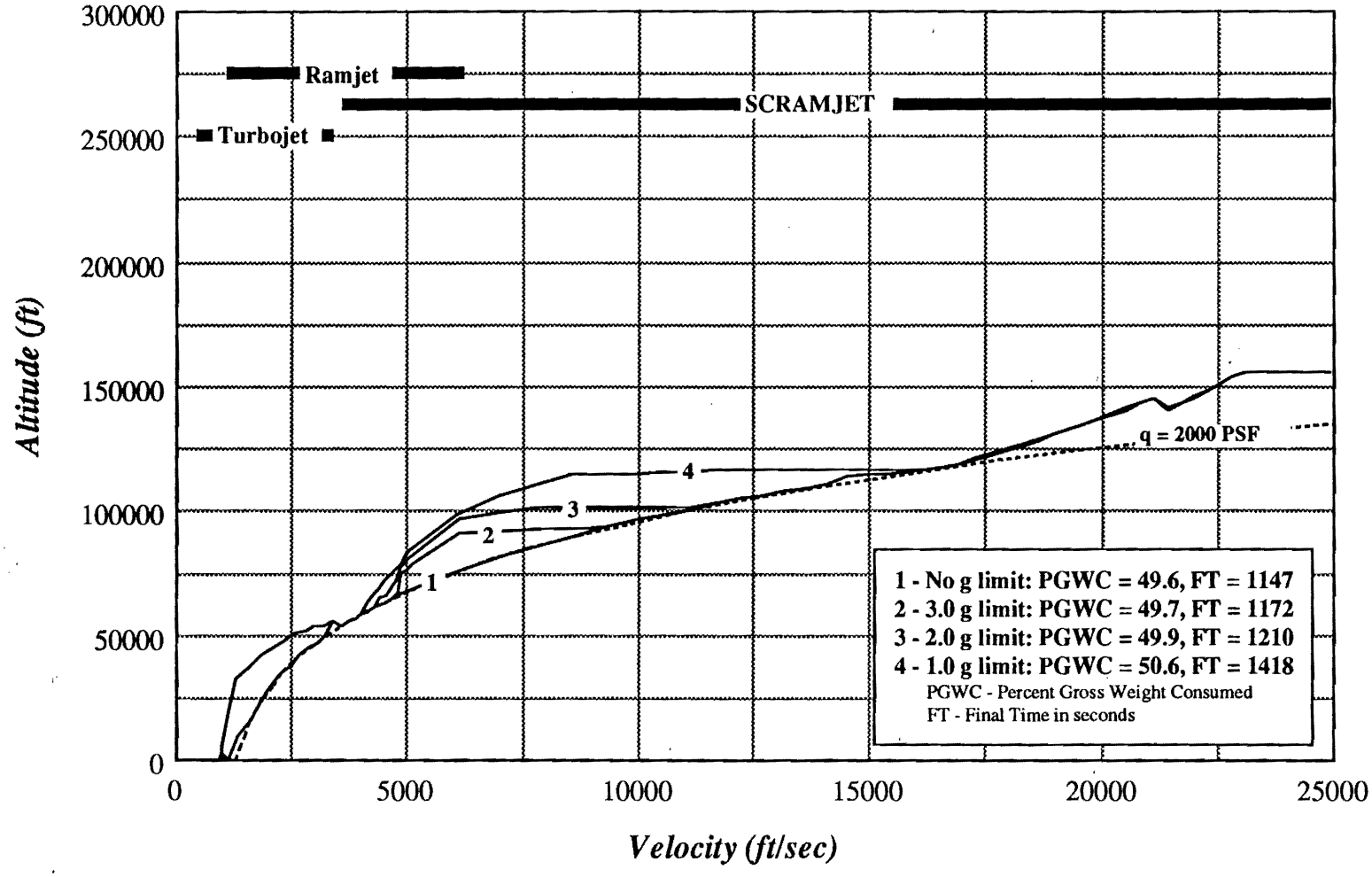

Figure 4 Reduced Solution for Vehicle Model Number 4; variation in the magnitude of the axial acceleration constraint is shown.

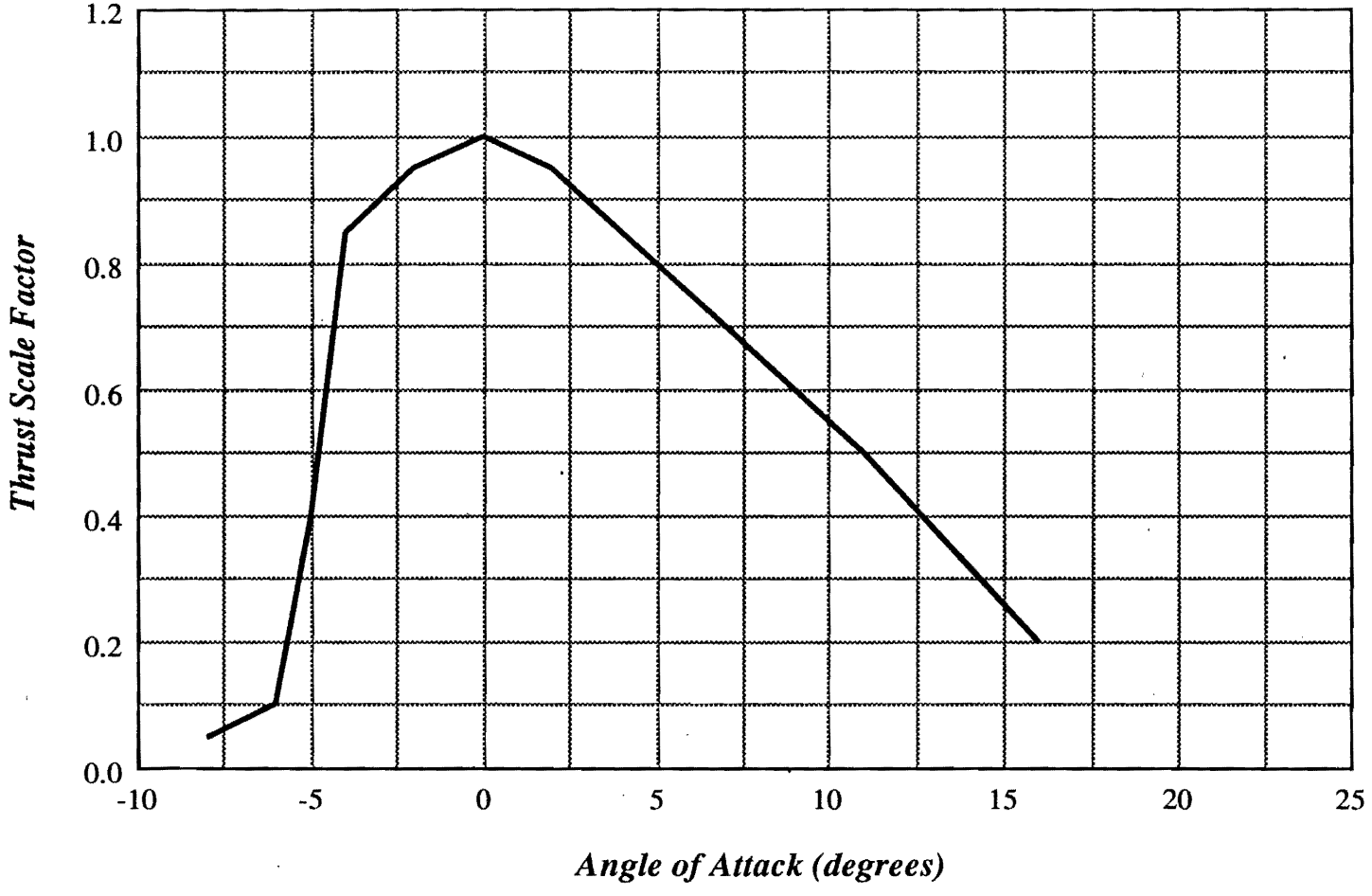

Figure 5 Assumed variation in scramjet thrust with angle of attack.

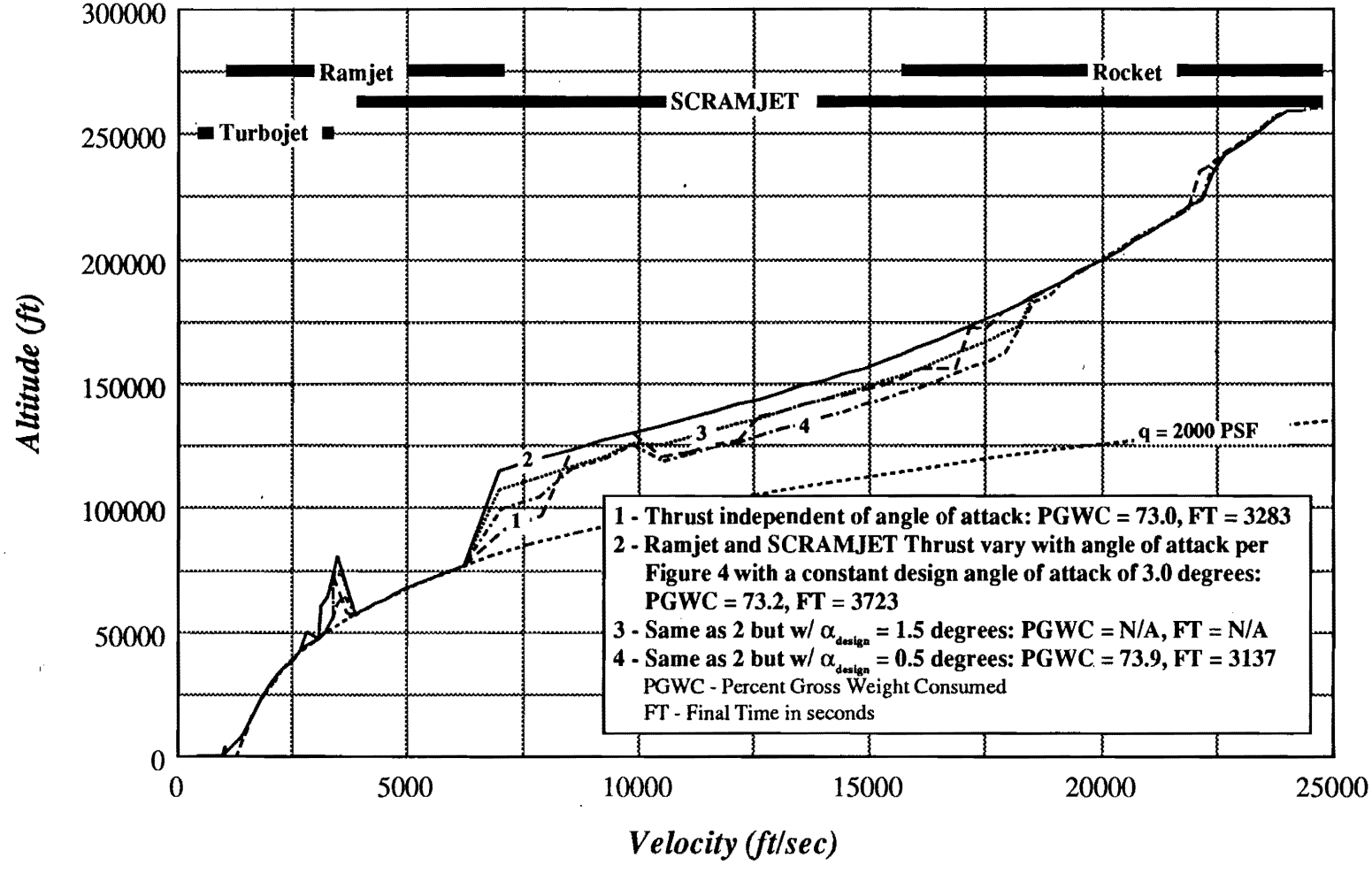

Figure 6 Reduced Solution for Vehicle Model Number 3; the effect of thrust variation with angle of attack is shown as the design angle of attack is varied.

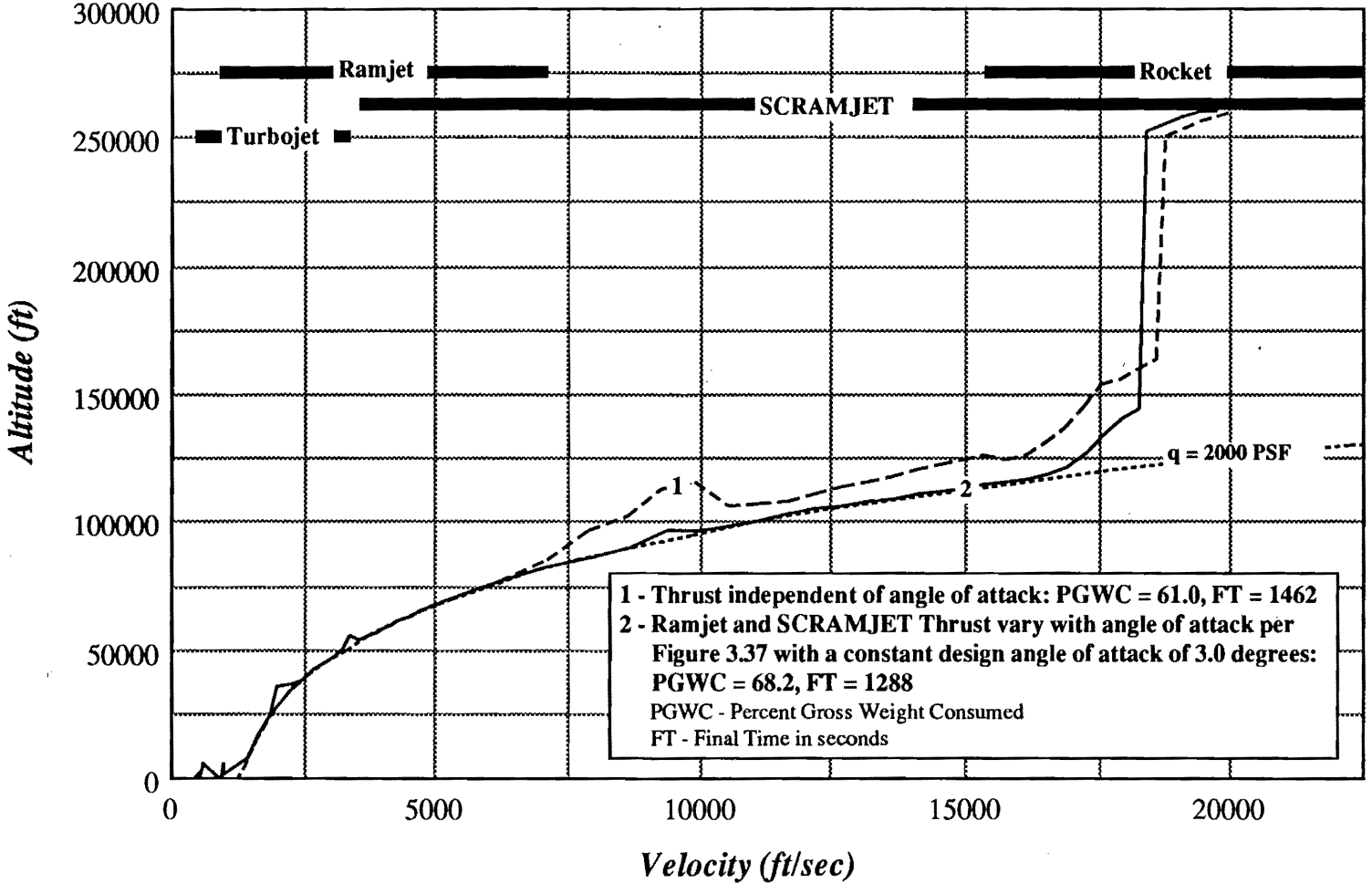

Figure 7 Reduced Solution for Vehicle Model Number 2; the effect of thrust variation with angle of attack is shown.

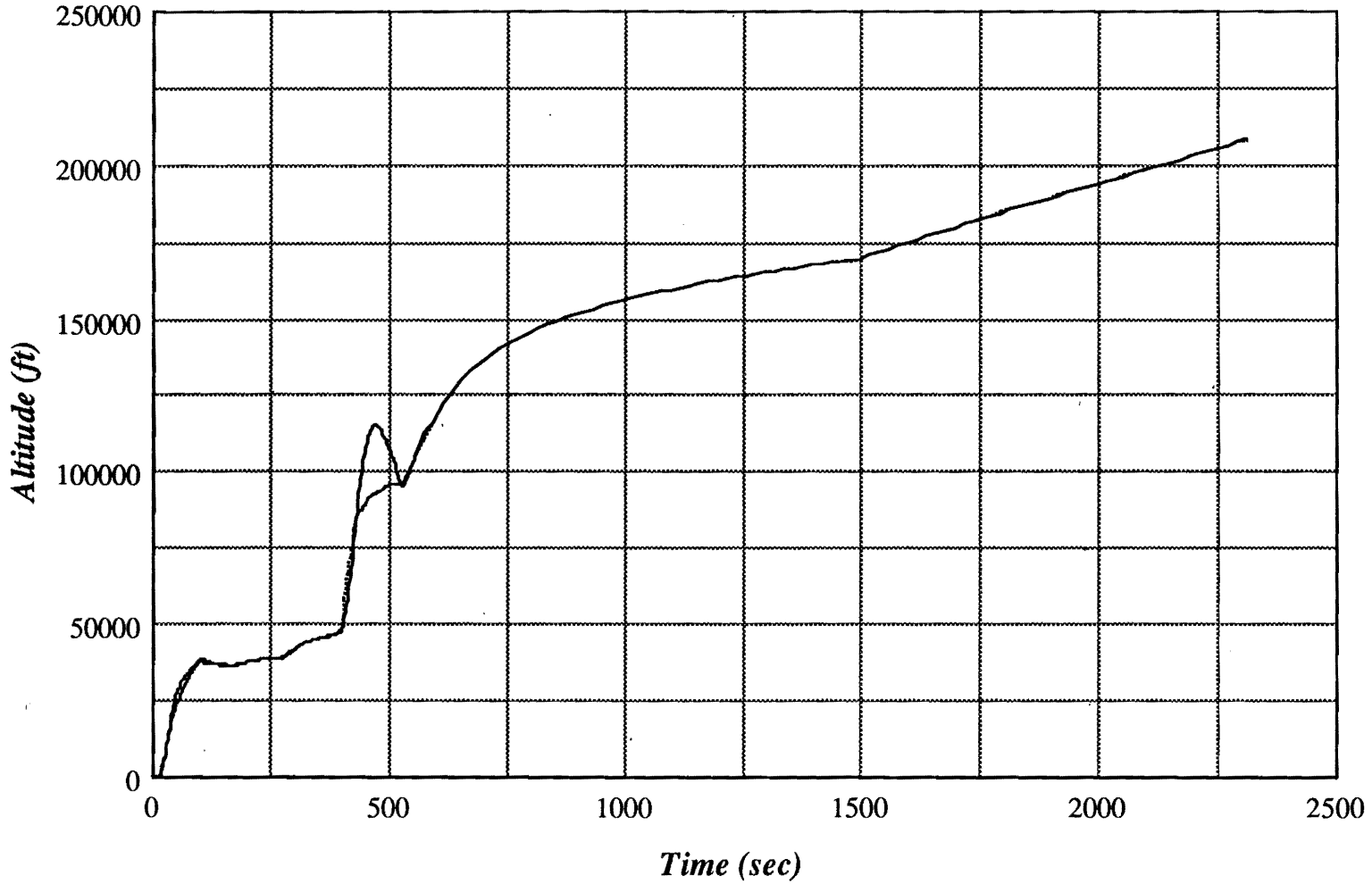

Figure 8 Guided solution for Model 4; altitude time history.

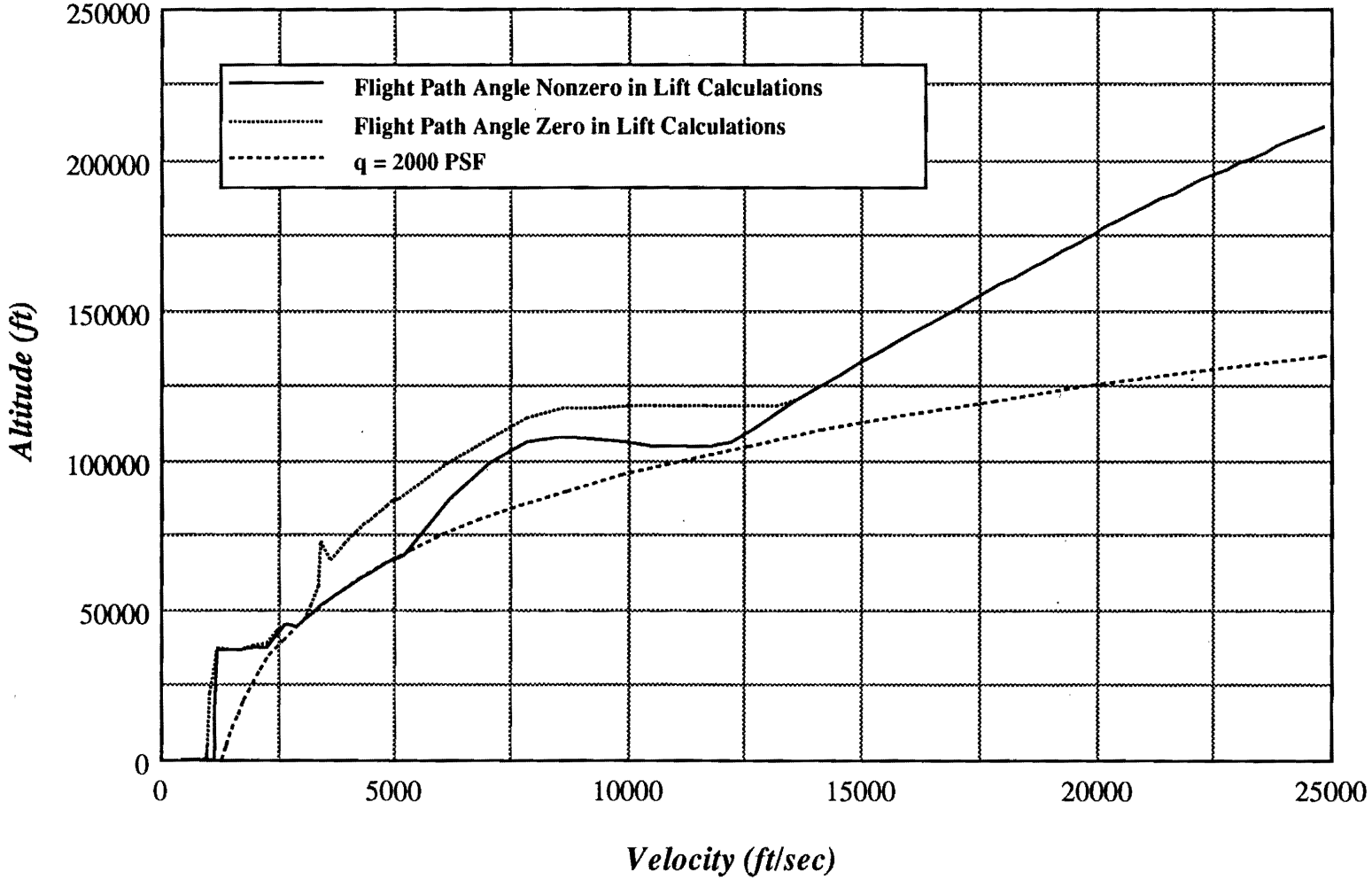

Figure 9 Reduced Solution for Model 4; comparison of the trajectory when flight path angle and flight path angle rate are included in the calculation of lift with the trajectory when they are not included.

SECTION 6
Conclusions and Recommendations

6.1 Conclusions

This research effort has demonstrated the utility of singular perturbation methods in the study of single-stage-to-orbit airbreathing vehicles and, in particular, in the derivation of efficient algorithms for ascent trajectory optimization and optimization of engine cycle transitions. The analysis extends over the entire Mach range from take-off to orbit and accomodates a realistic nonlinear vehicle model and all pertinent trajectory constraints. A number of important modeling and analysis issues not treated in the early stages of this effort were identified and addressed during this reporting period. Reasonable assumptions regarding propulsion system characteristics were introduced that allow the optimal engine cycle transition points to be determined as a function of state using a simple iterative test. These switching conditions lead to significant computational savings during the optimization process. Functional dependence of scramjet thrust on vehicle angle of attack was shown to have a major impact on the nature of fuel-optimal ascent trajectories. Also, depending on the actual vehicle configuration and the characteristics of the engine inlets, roll maneuvers used to modulate the vertical component of lift were shown to sometimes improve the index of performance during ascent. Over those limited regions of flight where the energy state approximation was found to be poor, simple lift corrections that account for non zero flight path angle and flight path angle rate were introduced that significantly improve the trajectory generation methodology.

6.2 Recommendations

Future efforts should be directed towards enhancing the performance and applicability of the derived algorithm. Such efforts should include the development of detailed multi-disciplinary vehicle models, the incorporation of additional controls such as thrust vectoring, reaction jets, and variable geometry, optimal control of the total heat load on the vehicle, the study of three-dimensional maneuvers, including abort, an examination of robustness issues, and improvements in speed of operation.

The demonstrated capability for rapid near-optimal trajectory generation has yet to be exploited in the development of efficient tools for fully integrated hypersonic vehicle design. Efforts to move in this direction should include tieing a parameter optimization algorithm around the trajectory optimization code that has been developed and the incorporation of this algorithm into a fully integrated control system design methodology.

Work of more general theoretical interest was also initiated during this reporting period. It was found that state-variable inequality constrained boundary layer systems are not well understood. Many of the characteristic features of such systems were identified. For instance, it was found that, when the reduced solution lies on a state-variable inequality constraint boundary, the boundary layer trajectories are of finite time in the stretched time scale. The possibility of costate discontinuites at the juncture between constrained and unconstrained arcs makes direct application of existing theory difficult. A transformation technique was identified that eliminates some of these difficulties, but at the cost of possibly increased system order and the introduction of singular arcs. Further research in this area is recommended.

Continued work with the integrated aerodynamic/propulsion performance prediction program has resulted in a highly accurate and useful means both for providing the needed vehicle parameters in the present program and for more general transatmospheric flight performance calculations. The program is evolving into a completely interactive performance estimation package, which will make it possible to view effects of small configuration changes on any performance parameters. The user can view in animated graphical form the effect of desired vehicle configuration changes. These modifications can be entered graphically by moving defining points on the vehicle outlines or by means of shifting simulated "levers" built in to the computer program. For example wing incidence angle, twist, wing area, fin cant angle, etc. can be changed continuously with simultaneous graphical output showing the effect on selected performance parameters. We anticipate many applications for this analytical capability and will continue to improve upon it.

6.3 Publications

Four conference papers have now been published which discuss most of the results of this research effort[12,15,16,49]. A Ph.D. Dissertation that details the entire effort to date was published in Decemeber of 1989[19]. A full-length paper entitled "Rapid Near-Optimal Trajectory Generation for Single-Stage-to-Orbit Airbreathing Vehicles" has been submitted for publication in the AIAA Journal of Guidance, Control and Dynamics and a new paper is now being prepared for the 1990 AIAA GN&C Conference on the issue of state contraints in singularly perturbed systems.

References

[1]Heppenhiemer, T. A., "Keepers of the Flame," *AIR & SPACE/Smithsonian*, Vol.4, No. 5, Dec. 89/Jan. 90, pp. 88-95.

[2]*National Aero-Space Plane, A Technology Development and Demonstration Program to Build the X-30*, United States General Accounting Office Report to Congressional Committees, GAO/NSIAD-88-122, April 1988.

[3]Williams, R. M., "National Aero-space Plane: Technology for America's Future," *Aerospace America*, Vol. 24, No. 11, Nov. 1986, pp. 18-22.

[4]Gregory, T. J., "Credibility of NASP," *Aerospace America*, Vol. 27, No. 9, Sept. 1989, pp. 42-46.

[5]Hardtla, J. W., Piehler, M. J., and Bradt, J. E., "Guidance Requirements for Future Launch Vehicles," AIAA Paper 87-2462, Aug. 1985.

[6]Bradt, J. E., Hardtla, J. W., and Cramer, E. J., "An Adaptive Guidance Algorithm for Aerospace Vehicles, AIAA Paper 85-1917, Aug. 1985.

[7]Bryson, A. E., Jr., "Energy-State Approximation in Performance Optimization of Supersonic Aircraft," *Journal of Aircraft*, Vol. 6, Nov.-Dec. 1969, pp. 481-488.

[8]Kelley, H. J., "Flight Path Optimization with Multiple Time Scales," *Journal of Aircraft*, Vol. 8, April 1971, pp. 238-240.

[9]Calise, A. J., "Extended Energy Management Methods for Flight Performance Optimization," *AIAA Journal*, Vol. 15, March 1977, pp. 314-321.

[10]Calise, A. J., Corban, J. E., and Flandro, G. A., "Trajectory Optimization and Guidance Law Development for National Aerospace Plane Applications," Final Report for Period July 1, 1987 to November 30, 1988, NASA Contract Number NAG-1-784, December 1988.

[11]Bryson, A. E., Jr., and Ho, Yu-Chi, *Applied Optimal Control*, Hemisphere Publishing Corp., New York, 1975.

[12]Calise, A. J., Corban, J. E., and Flandro, G. A., "Trajectory Optimization and Guidance Law Development for National Aerospace Plane Applications," Proceedings of the 1988 ACC, Vol. 2, June 15-17, Atlanta, GA, pp. 1406-1411.

[13]Kandebo, S. W., "Pratt Demonstrates Low-Speed Propulsion Concept for National Aero-Space Plane," *Aviation Week & Space Technology*, p. 79, June 26, 1989.

[14]Walton, J., "Performance Sensitivity of Hypersonic Vehicles to Changes in Angle of Attack and Dynamic Pressure," AIAA Paper No. 89-2463.

[15]Corban, J. E., Calise, A. J., and Flandro, G. A., "Trajectory Optimization and Guidance Law Development for Transatmospheric Vehicles," Proceeding of the 1989 IEEE International Conference on Control and Applications (ICCON), April 3-6, Jerusalem, Israel.

[16]Corban, J. E., A. J. Calise, and G. A. Flandro, "Optimal Guidance and Propulsion Control for Transatmospheric Vehicles," AIAA Paper 89-3617, Aug. 1989.

[17]Bowers, A. H. and Iliff, K. W., "A Generic Hypersonic Aerodynamic Model Example (GHAME) for Computer Simulation," A proposed NASA Technical Note, Ames Research Center, June, 1988.

[18]Waltrup, P. J., Anderson, G. Y., and Stull, F. D., "Supersonic Combustion Ramjet (SCRAMJET) Engine Development in the United States," Preprint 76-042, The 3rd International Symposium on Air Breathing Engines, The Johns Hopkins University Applied Physics Laboratory, March, 1976.

[19]Corban, J. E., "Real-Time Guidance and Propulsion Control for Single-Stage-to-Orbit Airbreathing Vehicles," Ph.D. Dissertation, The Georgia Institute of Technology, December 1989.

[20]Tauber, M. E., G. P. Menees, and H. G Adelman, "Aerothermodynamics of Transatmospheric Vehicles," AIAA-86-1257, AIAA/ASME 4th Joint Thermophysics and Heat Transfer Conference, Boston, Mass., June 2-4, 1986.

[21]Johnston, P. J., A. H. Whitehead, Jr., and G. T. Chapman, "Fitting Aerodynamics and Propulsion into the Puzzle," *Aerospace America*, September 1987, pp 32-37 and 42.

[22]Jacobson, D. H., M. M. Lele, and J. L. Speyer, "New Necessary Conditions of Optimality for Control Problems with State-Variable Inequality Constraints," Journal of Mathematical Analysis and Applications, 35, pp. 255-284, 1971.

[23]Kreindler, E., "Additional Necessary Conditions for Optimal Control with State-Variable Inequality Constraints," Journal of Optimization Theory and Applications," Vol. 30, No. 2, Oct. 1982, pp. 241-251.

[24]Boykin, W. H., Jr., and T. E. Bullock, "State Constraints and Singular Solutions to Penalty Function Optimization Problems," AIAA Journal, Vol. 10, No. 2, Feb. 1972, pp. 137-141.

[25]Calise, A. J., "On the Use of Singular Perturbation Methods in the Solution of Variational Problems," Proceedings of the Joint Automatic Controls Conference, Columbus, Ohio, 1973, pp. 184-192.

[26]Calise, A.J., Moerder, D.D., "Singular Perturbation Techniques for Real Time Aircraft Trajectory Optimization and Control," NASA Contractor Report 3597, August, 1982.

[27]Falco, M. and H. J. Kelly, "Aircraft Symmetric Flight Optimization," Control and Dynamic Systems, Advances in Theory and Applications, Vol. 10, Academic Press, New York, NY, 1973. (see Figure 14 on page 114)

[28]McHenry, R. L., T. J. Brand, A. D. Long, B. F. Cockrell, and J. R. Thibodeau III, "Space Shuttle Ascent Guidance, Navigation, and Control," *The Journal of the Astronautical Sciences*, Vol. XXVII, No. 1, pp. 1-38, January-March, 1979.

[29]Hargraves, C. R., and S. W. Paris, "Direct Trajectory Optimization Using Nonlinear Programming and Collocation," *Journal of Guidance*, Vol. 10, No. 4, July-August 1987, pp. 338-342.

[30]Jacobson, D. H. and M. M. Lele, "A Transformation Technique for Optimal Control Problems with a State Variable Inequality Constraint," *IEEE Transactions on Automatic Control*, Vol. AC-14, No. 5, Oct. 1969, pp. 457-464.

[31]Calise, A. J. and J. E. Corban, "Optimal Control of Singularly Perturbed Nonlinear Systems with State Variable Inequalty Constraints," presented at the IFAC Workshop on Singular Perturbations and Asymptotic Methods in Systems and Control, Boston, MA, August 17-18, 1989.

[32]McIntyre, J. and B. Paiewonsky, "On Optimal Control with Bounded State Variables," Advances in Control Systems, Theory and Applications, Vol. 5, Academic Press, New York, NY, 1967.

[33]Bryson, A. E., Jr., W. F. Denham, and S. E. Dreyfus, "Optimal Programming Problems Problems with Inequality Constraints I: Necessary Conditions for Extremal Solutions," *AIAA Journal*, Vol. 1, No. 11, Nov. 1963, pp. 2544-5550.

[34]Denham, W. F. and A. E. Bryson, Jr., "Optimal Programming Problems Problems with Inequality Constraints II: Solution by Steepest Ascent," *AIAA Journal*, Vol. 2, No. 1, Jan. 1964, pp. 25-34.

[35]Speyer, J. L., "Nonlinear Feedback Solution to a Bounded Brachistchrone Problem in a Reduced State Space," IEEE Transactions on Automatic Control, Feb. 1967, pp. 90-94.

[36]Speyer, J. L. and A. E. Bryson, Jr., "Optimal Programming Problems with a Bounded State Space, " AIAA Journal, Vol. 6, No. 8, pp. 1488-1491, Aug. 1968.

[37]Taylor, J. G., "Comments on a Multiplier Condition for Problems with State Variable Inequality Constraints," IEEE Transactions on Automatic Control, Oct. 1972, pp. 743-744.

[38]Hamilton, W. E., Jr., "On Nonexistence of Boundary Arcs in Control Problems with Bounded State Variables," IEEE Transactions on Automatic Control, Vol. AC-17, No. 3, June 1972, pp. 338-343.

[39]Russak, I. B., "Second Order Necessary Conditions for Problems with State Inequality Constraints," SIAM Journal of Control, Vol. 13, No. 2, Feb. 1975, pp. 372-388.

[40]Maurer, H., "On Optimal Control Problems with Bounded State Variables and Control Appearing Linearly," SIAM Journal of Control and Optimization, Vol. 15, No. 3, May 1977, pp. 345-362.

[41]Lowen, P. D., "State Constraints in Optimal Control"

[42]Ardema, M. D., "Singular Perturbations in Flight Mechanics," NASA TM X-62, 380, Aug. 1974; Revised July 1977.

[43]Ardema, M. D., "Linearization of the Boundary Layer Equations of the Minimum Time to Climb Problem," Journal Guidance and Control, Vol. 2, No. 5, pp. 434-436.

[44]Shankar, U. J., E. M. Cliff, and H. J. Kelly, "Singular Perturbation Analysis of Optimal Climb-Cruise-Dash," AIAA Guidance and Control Conference, Monterey, CA, August 17-19, 1987.

[45]Weston, A. R., Cliff, E. M., and H. J. Kelly, "Altitude Transitions in Energy Climbs," *Automatica*, Vol. 19, No. 2, pp. 199-202, 1983.

[46]Ardema, M. D., "Nonlinearly Singularly Perturbed Optimal Control Problems with Singular Arcs."

[47]Heck, B. S., and A. H. Haddad, "Singular Perturbation Analysis for Linear Systems with Vector Quantized Control," Proceedings of the 1989 American Control Conference, Pittsburgh, PA, June 21-23, pp. 2178-2183.

[48]Conversation with A. J. Calise and Eyad H. Abed of the University of Maryland at the 1989 AIAA GN&C Conference, Boston, MA, Aug. 14-16, 1989.

[49]Corban, J. E., Calise, A. J., and Flandro, G. A., "A Real-Time Guidance Algorithm for Aerospace Plane Optimal Ascent to Low Earth Orbit," Proceeding of the 1989 American Control Conference (ACC), June 21-23, Pittsburgh, Pa.

Appendix A

State Inequality Constrained Boundary Layers

Abstract

The established necessary conditions for optimality in nonlinear control problems that involve state-variable inequality constraints are applied to a class of singularly perturbed systems. The distinguishing feature of this class of systems is a transformation of the state-variable inequality constraint, present in the full order problem, to a constraint involving states and controls in the reduced problem. It is of particular interest to construct the zeroth order boundary layer solution when the reduced solution lies on the constraint boundary. It is shown that, in general, the boundary layer problem is of finite time in the stretched time variable. A special case is identified in which the boundary layer time scale transformation results in an increase in state inequality constraint order. In this case, required smoothness properties possessed by the full order system may be lost, and the application of existing necessary conditions for singularly perturbed systems then becomes invalid. A Valentine transformation can be used to regain required smoothness, but at the price of introducing singular arcs and an increase in system order. Finally, the various system properties and characteristics described in the body of the appendix are illustrated with several simple examples.

I. Introduction

State inequality constraints are commonly encountered in the study of dynamical systems. The study of rigid body aircraft dynamics and control is certainly no exception. For instance, a maximum allowable value of dynamic pressure is usually prescribed for aircraft with supersonic capability. This limit is required to ensure that the vehicle's structural integrity is maintained and constitutes an inequality constraint on vehicle state. State inequality constraints have been studied extensively by researchers in the field of optimal control, and necessary conditions for optimality when functions of state are constrained have been obtained[1-3]. However, the construction of solutions via this set of conditions proves very difficult, and most practitioners rely on direct

approaches to optimization that employ penalty functions for satisfaction of state inequality constraints[4].

As discussed in the literature, the use of singular perturbation techniques in the study of aircraft trajectory optimization can, through order reduction, lead to both open and closed loop solutions that are computationally efficient. These methods can also be used to circumvent difficulties associated with enforcing a state inequality constraint in the reduced solution[5]. As an example consider the minimum time intercept problem of[6]. A near optimal feedback solution is obtained via singular perturbation theory that includes consideration of an inequality constraint on dynamic pressure. In the zeroth-order reduced solution, algebraic constraints are obtained when the perturbation parameter, ε, which premultiplies the so called "fast" dynamic equations, is set to zero. These constraints can be used to eliminate the fast states (in this case altitude and flight path angle) from the reduced problem. One can choose, however, to retain one or more of the fast states and to eliminate instead some of the original control variables. The retained fast state variables are treated as new controls, and the original state constraint becomes a constraint involving both state and control in the reduced problem. In subsequent analysis of boundary layers, altitude resumes its status as a state variable, and dynamic pressure once again becomes a function of state alone. However, because the reduced solution for the example F-8 aircraft does not lie on the dynamic constraint boundary during ascent, the inequality constraint on dynamic pressure was not considered. Of note is the fact that modern supersonic fighter aircraft (such as the F-15) do ride the dynamic pressure constraint boundary during the ascent leg of the minimum time to intercept path.

In addition to the example cited above, dynamic pressure bounds are encountered during fuel-optimal climb for supersonic transports[7] for rocket powered launch vehicles such as the U.S. space shuttle[8] , and for single-stage-to-orbit air-breathing launch vehicles[9]. If, as in applying singular perturbation methods in seeking a solution to any of these problems, the reduced solution climb path lies directly on the dynamic pressure constraint boundary for a portion of the flight, then it is necessary to consider boundary layer transitions onto the constrained arc. This problem, which proves quite perplexing, has received almost no attention in the literature.

This appendix documents an initial investigation of the features of boundary layer transitions to state constrained arcs. Section II provides a brief review of first order necessary conditions derived for state-variable inequality constrained problems in optimal control. Section III discusses the optimal control of singularly perturbed systems subject to state-variable inequality constraints in general, and in particular examines the features of state inequality constrained boundary layers when the reduced solution lies on the constraint boundary. Section IV provides several simple

examples which illustrate the problem features discussed in earlier sections. Section V completes the appendix by providing some concluding remarks.

II. Constrained Problems in Optimal Control

The introduction of a state inequality constraint of the form

$$S(x,t) \leq 0 \tag{A.1}$$

can lead to considerable difficulty when attempting to obtain an optimal control solution. One approach to incorporating state inequality constraints into necessary conditions for optimality consists of constructing successive total time derivatives of S until explicit dependence on the control appears[11]. If p time derivatives are required then (1) is referred to as a p^{th} order state variable inequality constraint. The function $S^p(z,u,t)=0$ is then adjoined to the Hamiltonian as a constraint to be enforced when S=0. This approach introduces the following additional tangency conditions at the point of entry to a constrained arc

$$N(z,t) = \begin{bmatrix} S(z,t) \\ S^1(z,t) \\ \vdots \\ S^{p-1}(z,t) \end{bmatrix} = 0 \tag{A.2}$$

These same tangency conditions also apply at a point where the path leaves the constraint boundary. The equations (2) constitute a set of interior boundary conditions that must be met at each juncture between a constrained and unconstrained arc. Unfortunately, in order to satisfy these interior boundary conditions one must allow for the possibility of discontinuities in the costate variables at the junctures. An alternative set of necessary conditions can be obtained by adjoining the constraint function, rather than its p^{th} derivative, to the Hamiltonian and then employing a separating hyperplane theorem[22]. These conditions prove simpler and "sharper" than those of reference 11 however the possibility of discontinuous costates is still present. The gap between the necessary conditions of references 11 and 22 is defined in reference 23. A third alternative involves enploying a transformation technique in which a slack variable is used to transform the state inequality constrained problem into an unconstrained problem of higher dimension[30,31]. The work associated with the derivation of these first order necessary conditions is detailed in

references 32-38. Second order necessary conditions for optimality in the presence of state constraints have also been derived[39] as have conditions for various special cases[40]. Work continues in the area of state constrained optimization as evidenced by the approach of Lowen[41].

III. Optimization of Singularly Perturbed Systems Subject to State Inequality Constraints

Consider the system of singularly perturbed nonlinear differential equations:

$$dx/dt = f(x,y,u,t) \tag{A.3}$$

$$\varepsilon\, dy/dt = g(x,y,u,t) \tag{A.4}$$

with an index of performance of the form

$$J = \varphi[z(t_f), t_f] + \int_{t_o}^{t_f} L[z(t), u(t), t]\,dt \tag{A.5}$$

where x and f are of dimension n, y and g are of dimension m, $x(t_o)$ and $y(t_o)$ are given, ε is a small parameter, $t_o \le t \le t_f$, and the control u(t) is of dimension p. Zero order necessary conditions for optimality of the associated reduced and boundary layer problems in the absence of state constraints are readily available[42]. However, the following restrictions apply: f, g, $\partial f/\partial x$, $\partial f/\partial y$, $\partial g/\partial x$, and $\partial g/\partial y$ must be continuous and u must be piecewise continuous. Because of these restrictions on smoothness a direct extension of the necessary conditions of for state constrained problems to include singularly perturbed systems is not possible. This is due to the previously mentioned fact that discontinuities in the costates can occur at the junctures between constrained and unconstrained arcs. Alternately, the state inequality constrained singularly perturbed problem of interest can be converted into an unconstrained singularly perturbed problem of higher dimension by introduction of a slack variable[30]. This approach does eliminate the problem of discontinuous costates. However, the state constrained arc is replaced by a singular arc and the prospect of increased system dimension is unwelcome given the basic tenet of seeking order reduction.

Consider the flight dynamics problem detailed in the main body of this report. An inequality constraint on dynamic pressure of the form

$$S(h,V) = q - q_{max} \leq 0 \tag{A.6}$$

is to be enforced where

$$q = \rho V^2/2 \tag{A.7}$$

The symbol ρ represents atmospheric density and V represents the flight velocity. Given the equations of motion (1-4) expressed in the main body of this report, the first time derivative of (A.6) can be expressed as,

$$dS/dt = dq/dt = [V^3(\partial\rho/\partial r)/2 - \rho\mu V/r^2] \sin\gamma + \rho V(T - D)/m \tag{A.8}$$

Recall that the symbol T represents thrust, D, aerodynamic drag, m, vehicle mass, r, radial distance from the center of the Earth, γ, flight path angle, and μ, the gravitational constant for the Earth. Assume, as is typically done, that atmospheric drag can be represented as follows,

$$D = qsC_{Do} + KL^2/qs \tag{A.9}$$

where s represents an aerodynamic reference area, C_{Do},the zero lift drag coefficient, and K, the coefficient of the induced drag component. Note that the drag is explicitly dependent on the lift, L, which is treated as a control. In addition, the relation for thrust, T, is usually explicitly dependent on the engine throttle control. These controls appear explicitly in the first time derivative of the constraint function, (A.8), and it is thus classified as a first order state inequality constraint (i.e. p = 1). It is shown in reference 22 that when the constraint function is adjoined directly to the Hamiltonian and p = 1, no jumps in the costates will occur at the entry of an unconstrained arc onto a constrained arc. In this case the smoothness properties required by general singular perturbation theory are not violated and we may proceed with the application of singular perturbation methods with confidence.

The state inequality constraint on dynamic pressure is conveniently reduced to a state and control constraint function in construction of the reduced solution (i.e p becomes zero). This occurs because altitude, a state variable in the full order problem, becomes a control variable in the

reduced solution. Enforcing this state/control constraint in the reduced solution is a trivial matter. Now consider the construction of the zeroth order initial boundary layer. Assuming that energy is characterized as a slow state, application of the time stretching transformation $\tau = t/\varepsilon$ and again setting ε to zero yields an energy rate of zero. As such, the last term in (A.8) is no longer present. Instead, the first time derivative of the constraint function is given by,

$$dS/d\tau = dq/d\tau = [V^3(\partial\rho/\partial r)/2 - \rho\mu V/r^2] \sin\gamma \qquad (A.10)$$

With the last term of (A.8) absent, control dependence does not explicitly appear in (A.10). That is, the classification of the constraint function is altered following the time scale transformation when ε is set to zero. Taking the time τ derivative of (A.10), (i.e. forming the 2nd time τ derivative of S), yields a term containing the time derivative of the flight path angle, γ. The expression for flight path angle rate is as follows,

$$\gamma' = \frac{L}{mV} - \frac{\mu \cos\gamma}{Vr^2} + \frac{V \cos\gamma}{r} \qquad (A.11)$$

which is explicitly dependent on the lift control. Thus, in the boundary layer, the inequality constraint on dynamic pressure is 2nd order. Unfortunately, there is no guarantee that the costates are continuous for this case as there was for the case p = 1. Note that this type of behavior, in which the inequality constraint function order varies, is not present in all singularly perturbed problems with state inequality constraints, just for a certain class of them. For instance, if the constraint function is dependent on fast states alone, this variation does not occur.

If jumps in the costates are in fact present at the juncture between an unconstrained and a constrained arc, the smoothness properties required are violated and the available necessary conditions for optimal control of a singularly perturbed system cannot be applied directly. In some cases it is not possible for the boundary layer dynamic system to "ride" the constraint boundary before reaching the reduced solution. In such case the boundary layer costates can, at most, be discontinuous at the juncture between the initial boundary layer and the reduced solution and only if the reduced solution at that point is on the constraint boundary. It is also possible that no such jumps will occur.

If we proceed assuming that such jumps do not occur, then in most cases of interest the functional form of the boundary layer control solution in the presence of a state-variable inequality

constraint can be obtained. If this functional form involves an unknown costate, then use of the derived control solution is prevented unless the associated two point boundary value problem (TPBVP) is solved. To avoid solution of the TPBVP, as is desired in seeking a solution suitable for on-board, real-time implementation, an approximation for the unknown costate can be formed. If the costate history is continuous, the linearization technique of reference 43 can be applied to form the estimate. Unfortunately, for the case described above in which the reduced solution lies on the constraint boundary and the inequality constraint order is elevated to 2 by the boundary layer time scale transformation, purely imaginary roots result when the linearization technique is applied. Thus it is not possible to find a stablizing costate approximation given arbitrary initial states. In an unconstrained problem, the lack of an appropriate eigen-structure indicates that the problem does not exhibit the time scale properties assumed. Boundary layer transients do not exist for such cases; in fact there are fast oscillations that do not die out. The addition of an artificial cost term in formulation of the problem is suggested as an ad-hoc way to circumvent this difficulty. By proper choice of the weighting on can guarantee the proper structure of the linearized boundary layer system[44].

An interesting feature of the constrained boundary layer system described above is the presence of a finite costate rate at the juncture with the reduced solution. This behavior is illustrated in the sketch presented as Figure 1. In the figure, t_1 denotes the time at which an unconstrained arc joins a constrained arc (i.e. a juncture point).

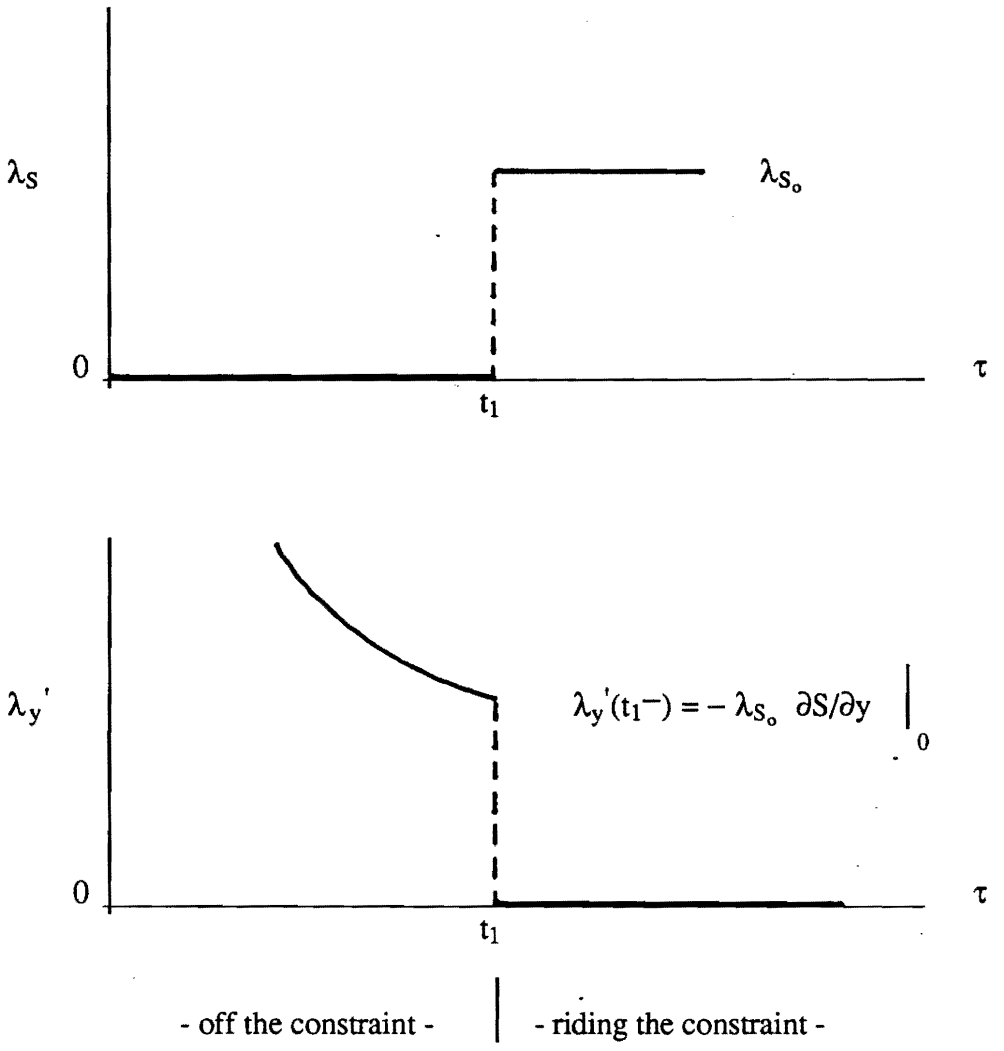

Figure 1 Illustration of finite costate rate at juncture between boundary layer and reduced solution trajectories.

Identification of the behavior illustrated in Figure 1 is based on the following construction.

$$\left.\frac{\partial H_{BL}}{\partial y}\right|_{\substack{u=u^* \\ S\le 0}} = \left.\frac{\partial H_{BL}}{\partial y}\right|_{\substack{u=\text{constant} \\ S\le 0}} + \cancel{\frac{\partial H_{BL}}{\partial u^*}}^{0}\frac{\partial u^*}{\partial y} \equiv -\lambda_y' \qquad \text{(A.12)}$$

Note that, since the last term in (A.12) is zero, this relation is equal to the negative of the costate rate. The following relation can also be constructed.

$$\left.\frac{\partial H_{BL}}{\partial y}\right|_{\substack{u=u^* \\ S\le 0}} = \left.\frac{\partial H_{BL}}{\partial y}\right|_{\substack{u=u^* \\ \text{unconstrained}}} + \lambda_S \frac{\partial S}{\partial y} \tag{A.13}$$

Now as τ tends to t_1^- we find that,

$$-\lambda_y'(t_1-) = \underbrace{\left.\frac{\partial H_{BL}}{\partial y}\right|_{\substack{u=\text{constant} \\ \text{unconstrained}}}}_{0} + \underbrace{\lambda_S \left.\frac{\partial S}{\partial y}\right|_{t_1^-}}_{0} \tag{A.14}$$

($\lambda_S = 0$ for $\tau < t_1$)

$$= -\lambda_{S_o} \left.\partial S/\partial y\right|_0 \quad \text{at } t_1^+ \text{ this becomes } \lambda_{S_o}$$

Thus the fast costate rate, λ_y', has a finite value at t_1^- and then jumps to zero at t_1^+. The boundary layer system no longer approaches the reduced solution asymptotically as in the unconstrained case. Instead, a ***finite time*** boundary layer is implied. Similar finite time boundary layer phenomenon have been discovered by the investigators of interior boundary layers and boundary layers that approach singular arcs[45,46]. Using this terminal value for the costate rate it is possible to show analytically for problems of interest that the linearized boundary layer system will always have purely imaginary roots when the reduced solution lies on the state-variable inequality constraint boundary.

Consider the possibility of integrating the boundary system backwards in time from the reduced solution using the finite terminal value of costate rate to get started. Note that only a single extremal will be generated unless an additional free parameter is introduced into the problem. Since it should be possible to reach any set of initial conditions that do not violate the constraint, such a parameter surely exists. The only available parameter appears to be the magnitude of the possible costate jump at the juncture. This would imply that the costate history will be discontinuous at the juncture for all initial conditions that do not lie on the single extremal generated when it is assumed no jump occurs.

Assuming that first order necessary conditions for optimality can be obtained for which the requirement for smoothness can be relaxed (see for instance reference 47), one would again require a scheme for obtaining a stabilizing estimate of the unknown costates that appear in the optimal control law. However, to the author's knowledge, no directly applicable stability theory for finite time phenomenon is available for completing this task[48]. Alternately, one can consider transforming the constrained problem into an unconstrained problem, generally of higher order. The optimal trajectory of the transformed problem exhibits singular arcs which correspond, in the original constrained problem, to arcs which lie on the constraint boundary[30]. Because of this, the technique for costate approximation using the linearized boundary layer system, will fail. The reader is referred to the literature for a description of the work that has been done with regard to understanding control of singularly perturbed systems that include singular arcs[46].

IV. Examples

Several simple examples are now presented which illustrates the application of the Valentine transformation technique described in reference 46 *without* the penalty of increased system order[31]. The phenomena of a finite time boundary layer is illustrated in example 2.

Example 1

Consider the following singularly perturbed dynamical system with initial conditions at zero.

$$\dot{x}_1 = x_2 - u^2 \qquad x_1(0) = 0 \qquad \text{(A.15)}$$

$$\varepsilon \dot{x}_2 = x_3 \qquad x_2(0) = 0 \qquad \text{(A.16)}$$

$$\varepsilon \dot{x}_3 = u \qquad x_3(0) = 0 \qquad \text{(A.17)}$$

The following 2nd order (i.e. p = 2) state inequality constraint is to be enforced,

$$S = x_2 - 1 \leq 0 \qquad \text{(A.18)}$$

The final value of x_1 is specified, the final time is free, and the performance index is given by,

$$J = \int_0^{t_f} dt \tag{A.19}$$

Using Valentine's device, the inequality constraint (A.18) is converted into an equality by the introduction of a "slack variable," α^{30}.

$$S + \alpha^2/2 = 0 \tag{A.20}$$

Differentiating (A.18) p times (p = 2) with respect to time, the following set of equations is obtained,

$$x_3/\varepsilon + \alpha\alpha_1/\varepsilon = 0 \qquad \text{where } \varepsilon\, d\alpha/dt \equiv \alpha_1 \tag{A.21}$$

$$u/\varepsilon^2 + \alpha_1{}^2/\varepsilon^2 + \alpha\alpha_2/\varepsilon^2 = 0 \quad \text{where } \varepsilon\, d\alpha_1/dt \equiv \alpha_2 \tag{A.22}$$

Using the transformations $x_2 = 1 - \alpha^2/2$, $x_3 = \alpha\alpha_1$, and $u = -\alpha_1{}^2 - \alpha\alpha_2$, (A.15-17) become,

$$\dot{x}_1 = 1 - \frac{\alpha^2}{2} - \left(\alpha_1^2 + \alpha\alpha_2\right)^2 \tag{A.23}$$

$$\varepsilon\dot{\alpha} = \alpha_1 \tag{A.24}$$

$$\varepsilon\dot{\alpha}_1 = \alpha_2 \tag{A.25}$$

Reduced solution. By setting ε to zero, (A.24) and (A.25) are reduced to the following,

$$\overset{o}{\alpha}_1 = 0 \tag{A.26}$$

$$\overset{o}{\alpha}_2 = 0 \tag{A.27}$$

The reduced solution Hamiltonian is given by,

$$H = \lambda_x \left[1 - \frac{\alpha^2}{2} - \left(\alpha_1^2 + \alpha\alpha_2 \right)^2 \right] + \lambda_\alpha \alpha_1 + \lambda_{\alpha_1} \alpha_2 + 1 = 0 \qquad \text{(A.28)}$$

Evaluation of first order necessary conditions for optimality results in the following,

$$H = 0 \;\; \& \;\; H_\alpha = 0 \quad \Rightarrow \quad \lambda_x^o = -1 , \quad \alpha^o = 0 \qquad \text{(A.29)}$$

$$H_{\alpha_1} = 0 \quad \Rightarrow \quad \lambda_\alpha^o = -1 \qquad \text{(A.30)}$$

$$H_{\alpha_2} = 0 \quad \Rightarrow \quad \lambda_{\alpha_1}^o = -1 \qquad \text{(A.31)}$$

Boundary Layer Problem. Introducing the time scale transformation $\tau = t/\varepsilon$ and again setting ε to zero, the boundary layer dynamics are given by

$$\alpha' = \alpha_1 \qquad \text{(A.32)}$$

$$\alpha_1' = \alpha_2 \qquad \text{(A.33)}$$

where the prime notation denotes differentiation with respect to the stretched time τ. The boundary layer Hamiltonian is given by,

$$H_{BL} = \frac{\alpha^2}{2} + \left(\alpha_1^2 + \alpha\alpha_2 \right)^2 + \lambda_\alpha \alpha_1 + \lambda_{\alpha_1} \alpha_2 = 0 \qquad \text{(A.34)}$$

The costate dynamics are given by

$$\lambda_\alpha' = -\alpha - 2\left(\alpha_1^2 + \alpha\alpha_2 \right)\alpha_2 \qquad \text{(A.35)}$$

$$\dot{\lambda}_{\alpha_1} = -4\left(\alpha_1^2 + \alpha\alpha_2\right)\alpha_1 - \lambda_\alpha \tag{A.36}$$

And when the constraint is inactive, the control, α_2, is determined by the necessary condition,

$$\frac{\partial H_{BL}}{\partial \alpha_2} = 2\left(\alpha_1^2 + \alpha\alpha_2\right)^2\alpha + \lambda_{\alpha_1} = 0 \tag{A.37}$$

Note that when the constraint is active, α is zero and the condition (A.37) yields no direct control solution. Riding the constraint boundary corresponds to a singular arc in the transformed problem.

Example 2

Consider a simplification of Example 1, namely the singularly perturbed dynamical system,

$$\dot{x}_1 = x_2 - u^2 \tag{A.38}$$

$$\varepsilon \dot{x}_2 = u \tag{A.39}$$

The inequality constraint (A.18) becomes a 1st order (i.e. p = 1) state inequality constraint,

$$S = x_2 - 1 \leq 0 \tag{A.40}$$

The final value of x_1 is again specified, the final time is free, and the performance index is again given by,

$$J = \int_0^{t_f} dt \tag{A.41}$$

Using Valentine's device, the inequality constraint (A.40) is converted into an equality by the introduction of a "slack variable," α[30].

$$S + \alpha^2/2 = 0 \tag{A.42}$$

Differentiating (A.42) p times (p = 1) with respect to time, the following equation is obtained,

$$u/\varepsilon + \alpha\alpha_1/\varepsilon = 0 \qquad \text{where } \varepsilon\, d\alpha/dt \equiv \alpha_1 \tag{A.43}$$

Using the transformations $x_2 = 1 - \alpha^2/2$ and $u = -\alpha\alpha_1$, (A.38-39) become,

$$\dot{x}_1 = 1 - \frac{\alpha^2}{2} - (\alpha\alpha_1)^2 \tag{A.44}$$

$$\varepsilon\dot{\alpha} = \alpha_1 \tag{A.45}$$

Reduced solution. By setting ε to zero, (A.45) is reduced to the following,

$$\alpha_1^o = 0 \tag{A.46}$$

The reduced solution Hamiltonian is given by,

$$H = \lambda_{x_1}\left[1 - \frac{\alpha^2}{2} - (\alpha\alpha_1)^2\right] + \lambda_\alpha\alpha_1 + 1 = 0 \tag{A.47}$$

Evaluation of first order necessary conditions for optimality results in the following,

$$H = 0 \;\; \& \;\; H_\alpha = 0 \quad \Rightarrow \quad \lambda_x^o = -1, \quad \alpha^o = 0 \tag{A.48}$$

$$H_{\alpha_2} = 0 \quad \Rightarrow \quad \lambda_\alpha^o = 0 \tag{A.49}$$

from which it is evident that

$$x_1^o(t) = t \tag{A.50}$$

$$x_2^{\circ}(t) = 1 \tag{A.51}$$

Boundary Layer Problem. Introducing the time scale transformation $\tau = t/\varepsilon$ and again setting ε to zero, the boundary layer dynamics are given by

$$\alpha' = \alpha_1 \tag{A.52}$$

where the prime notation denotes differentiation with respect to the stretched time τ. The boundary layer Hamiltonian is given by,

$$H_{BL} = \frac{\alpha^2}{2} + (\alpha\alpha_1)^2 + \lambda_\alpha \alpha_1 = 0 \tag{A.53}$$

The costate dynamics are given by

$$\lambda_\alpha' = -\alpha\left(1 + 2\alpha_1^2\right) \tag{A.54}$$

The condition that the partial derivative of the Hamiltonian with respect to the control be zero yields the following result,

$$H_{\alpha_1} = 0 \quad \Rightarrow \quad \alpha_1 = -\frac{\lambda_\alpha}{2\alpha^2} \tag{A.55}$$

Substituting this result back into the condition that the Hamiltonian be zero, the following result is obtained.

$$H = 0 \quad \Rightarrow \quad \lambda_\alpha = \pm\sqrt{2}\,\alpha^2 \tag{A.56}$$

Substituting (64) into (63) we find that the optimal value of the control, α_1, is constant; namely,

$$\alpha_1^* = \pm\frac{1}{\sqrt{2}} \tag{A.57}$$

With this result it is possible to integrate equation (A.52) to obtain,

$$\alpha(\tau) = \sqrt{2} \pm \frac{\tau}{\sqrt{2}} \tag{A.58}$$

When the boundary layer trajectory reaches the constraint boundary (i.e. $x_2 = 1$), $\alpha = 0$ and the expression (A.58) yields a finite final time of 2 units of boundary layer time. Transforming back, we obtain an expression for u in terms of x_2,

$$u^* = \sqrt{1 - x_2} \tag{A.59}$$

where integration of the original differential equation (A.39) yields,

$$x_2 = 1 - \left(1 - \frac{\tau}{2}\right)^2 \tag{A.58}$$

V. Conclusions

In conclusion, state-variable inequality constrained singularly perturbed problems can exhibit complex boundary layer phenomenon that are not well understood. The order of the state constraint can increase when going from the full order problem to a boundary layer analysis. Because discontinuous costate histories can be introduced by the presence of state inequality constraints, a direct application of available singular perturbation theory, which requires the state and costate histories to be smooth, is not possible. The boundary layer phenomenon associated with such problems appear to be finite time. A stability theory for finite time phenomenon, as required to construct a suitable approximation for costates appearing in derived feedback control laws, is not available at this time. Valentine's transformation can be used to overcome some of these difficulties, but at the expense of introducing singular arcs and possibly increased system order.

Appendix B

Permormance Modeling of Hypersonic Vehicles

I. Introduction

In order to carry out useful performance studies, trajectory optimization and guidance law development for hypersonic transatmospheric vehicles, it is necessary to utilize an accurate model of the aerodynamics and propulsion system characteristics. Since actual vehicle design is not involved, it is appropriate to utilize simplified models if they can be made to properly reflect the actual vehicle performance characteristics. It is also of great benefit to have available models that can be used interactively to study the impact of small changes in vehicle configuration or propulsion system design.

In what follows is described a set of simple algorithms devised for use in the present research program for the purposes outlined. The computer codes have evolved continuously throughout the study. The result is an integrated hypersonic vehicle performance package that has many applications beyond those originally envisioned.

II. Hypersonic Aerodynamic Performance Modeling

Simple hypersonic aerodynamic theory enables construction of practical and highly accurate representations of the performance characteristics of realistic hypersonic flight vehicles. In this section we review the basic theoretical approach and the implementation of this theory in the form of interactive computer software. The basic approach was to make the application of the model to a particular airframe conceptual design as simple as possible. Because of the interactive nature of the algorithms used, effects of even minor design modifications can be immediately assessed in terms of sensitivity parameters such as L/D ratio, overall vehicle drag coefficient, and trim moments.

The models developed have applications that range considerably beyond the ones addressed in this report. For example, they are a sufficiently accurate representation of the vehicle performance to allow assessment of off-design flight conditions as well as approximate stability and control studies. Although the emphasis in the following discussion is on the high-Mach number performance modeling, the computer program under development is being set up to cover the entire Mach number range from low subsonic to hypersonic speeds. The low speed aerodynamic performance models used are not as accurate as those in the hypersonic

range, but are sufficiently precise for use in simple performance modeling in which low speed flight affects such as the landing or takeoff flight phases are to be included.

In what follows is given a brief description of the operation of the computer program and the basic theory on which it is based. The methods used in applying the theory to a given vehicle configuration is reviewed for the benefit of readers unfamiliar with hypersonic aerodynamic modeling.

User Interface

The computer algorithms were designed to make their application to a given vehicle configuration as simple as possible. At present, limited access to actual flight vehicle configurations makes it necessary to work from rather sparse data sets. For example, the vehicle to be studied may be defined only by a simple three-view drawing. We have deliberately set out to make it possible to work effectively from such data. The configuration is entered into the program in a variety of ways. The simplest method allows input in the form of outlines of the wing planform, fuselage elevation and planform, body cross-section shapes, and tail surface configuration in the form of discrete points. It is not necessary that a large number of outline points be used. For example fuselage outline data can consist of as few as ten points in elevation and planform with acceptable accuracy. The program allows for variation in fuselage cross-section station by station along the axis of symmetry. It also allows for corners in the cross-section as often chosen in hypersonic vehicle layouts.

The configuration data can also be entered by scanning a three-view of the vehicle. Scaling is accomplished by selecting points at the nose and tail of the planform. The user then selects points interactively by means of a mouse or graphics table. Modifications in geometry can be directly implemented in the input process by altering position of control points. Wing and tail incidence, fin cant, control surface deflection , and other required information are entered in an interactive tabular input window. If insufficient data has been entered to properly define the complete configuration, the program warns the operator and indicates what additional information must be specified.

Interactive Program Mode

The computer program has been designed to take full advantage of modern computer graphical interface technology. Once a vehicle configuration has been implemented as described earlier, its attributes can be saved and modified later. At the discretion of the user, one or more attributes of the vehicle aerodynamic performance characteristics can be displayed simultaneously with the configuration input panel. For example, the lift coefficient vs angle of attack, lift/drag ratio, pitching moment vs lift coefficient or other information can be viewed at the same time changes in vehicle geometry such as wing area, incidence angle, airfoil shape, or

body cross-section shape are being input. This makes it very easy to determine the impact of design changes in a direct and graphically useful manner. When the program is linked to one of the postprocessing packages such as the one describing trajectory optimization discussed elsewhere in the report, it is possible to view effects of configuration modifications directly in terms of their impact on selected performance parameters.

Local Surface Inclination Theory with Blast Wave Corrections

Several decades of experience have shown that the simplest form of hypersonic flow field modeling yields a practical and accurate means for estimating vehicle performance. The Newtonian flow model gives an excellent representation for the pressure changes on the vehicle surfaces directly in terms of the inclination of the local surface to the freestream flow. Various modifications can also be applied to correct the pressure distribution for effects of strong shock formations at the leading edges of lifting surfaces and tail surfaces and on the nose of thefuselage. The blast wave theory is employed for this purpose.

Simple Newtonian impact theory shows that the pressure coefficient at any point on the windward vehicle surface is given by

$$C_p = 2\sin^2\theta \tag{B.1}$$

Thus all that is necessary to apply it to a three dimensional vehicle is to set up an algorithm that utilizes geometry information to determine whether a given element of the surface is on the windward side and to calculate the angle between the freestream velocity vector and the surface element. Samples of the computational method used in this program are discussed briefly in the following subsections.

Hypersonic Thin Airfoil Theory

In some situations, it is sufficiently accurate to represent hypersonic lifting surfaces as flat plates. However, in practical situations the need for adequate low-speed aerodynamic characteristics and surface structure dictates that a cambered airfoil of reasonable thickness be used. For example, the NASA vehicle designs used in our computations typically employed airfoils of of between 5 and 10% maximum thickness ratio. Thus it is useful to provide means for correcting the force calculations for camber and thickness effects. Figure B.1 defines the required geometry for a typical wing section.

On the windward side of the airfoil, the camber/thickness function is conveniently described as a functional relationship

$$y_\ell = F(x) \tag{B.2}$$

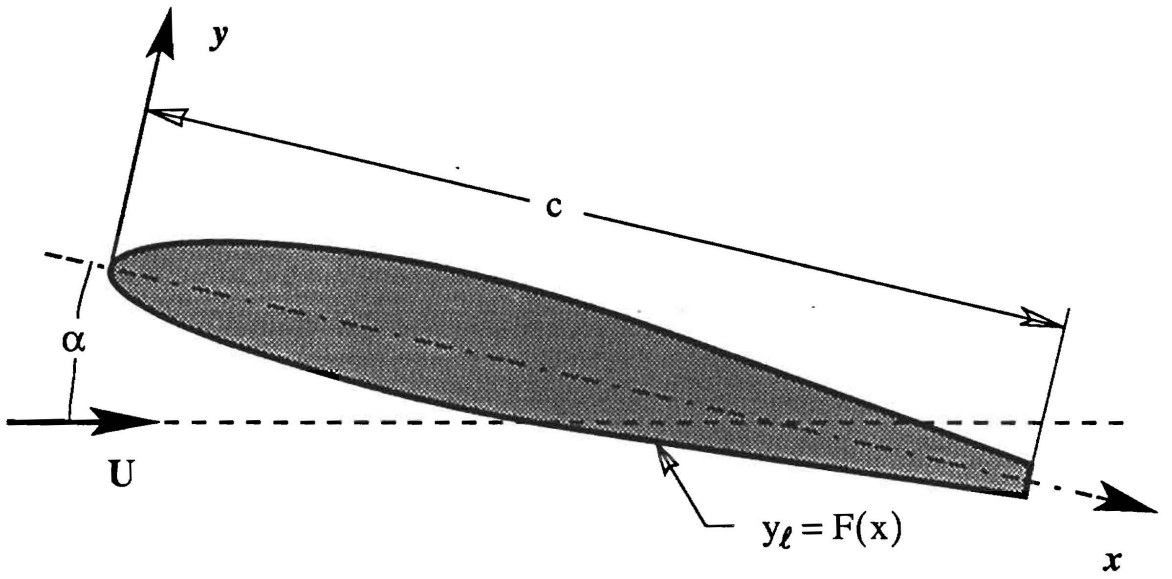

Figure B.1. Hypersonic Airfoil

This can be input in the computer program as a series of points taken from a scan of the airfoil or by inputing in tabular form. The program also allows the specification of the airfoil profile directly in analytical form. The program logic then determines the required calculation module from which to compute the wing characteristics. The program also contains provision for accounting for wing twist, although none of the vehicle models studied have employed twist. The local value of the pressure coefficient becomes

$$C_p = 2\sin^2\left(\alpha + \iota - \frac{dF}{dx}\right) \tag{B.3}$$

where α is the vehicle angle of attack measured between the fuselage reference plane (See Figure B.2), ι is the incidence angle between the wing chord line and the fuselage reference plane, and F is the airfoil envelope shape function as described above. This information is then used as the basis for determining the normal force coefficient for the airfoil. The result is

$$c_n = \frac{2}{c}\int_0^c \sin^2\left(\alpha + \iota - \frac{dF}{dx}\right) dx \tag{B.4}$$

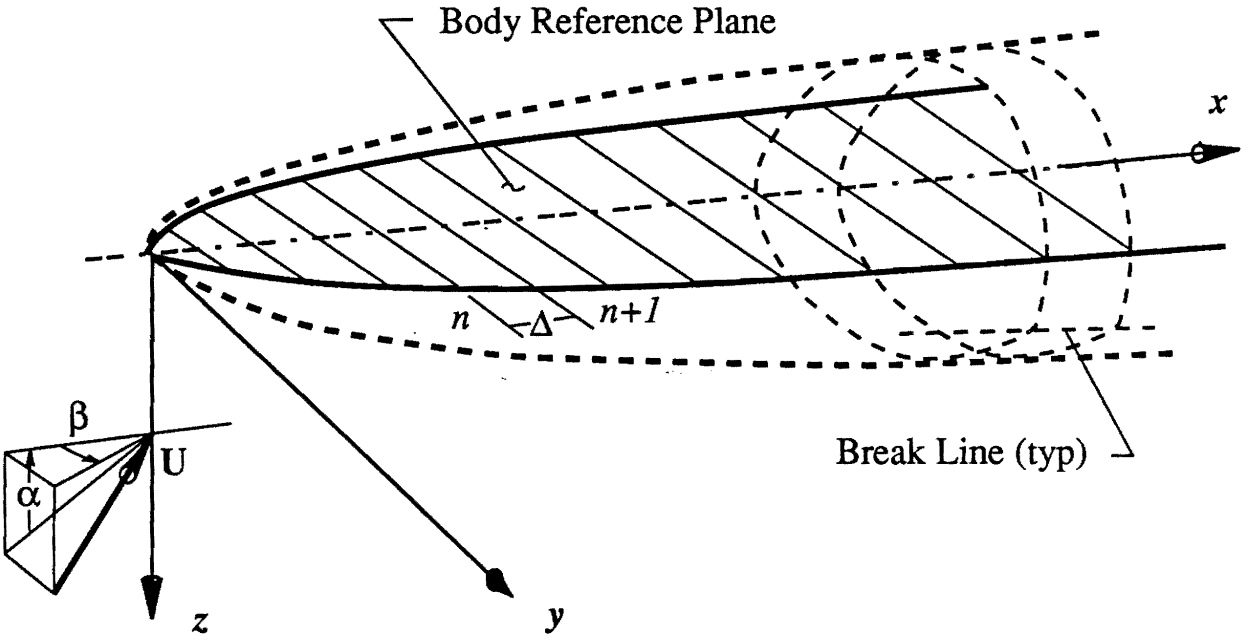

Figure B.2. Definition of Fuselage Reference Plane

and from this we find the section lift and drag coefficients.

$$\begin{cases} c_\ell = \dfrac{2\cos\alpha}{c}\displaystyle\int_0^c \sin^2\left(\alpha + \iota - \frac{dF}{dx}\right) dx & \text{(B.5)} \\ c_d = \dfrac{2\sin\alpha}{c}\displaystyle\int_0^c \sin^2\left(\alpha + \iota - \frac{dF}{dx}\right) dx & \text{(B.6)} \end{cases}$$

These coefficients are then used with the wing planform information giving the local values of chord length and incidence (for a twisted wing) to determine the force on the local wing section. The results for the entire wing are then accumulated. The program has provision for displaying the total lift and drag coefficients and the center of pressure location for the three-dimensional wing. It also determines contributions to the pitch, yaw, and roll moment coefficients.

Aileron, elevon or flaperon deflection effects are also computed. The user must input the desired control surface deflections. Differential elevon deflections are allowed. The program senses when the critical surface deflection angle (at which the freestream flow no longer impinges on the deflected surface) has been exceeded and properly adjusts the force system.

Hypersonic Lifting Body Theory

The integrated fuselage/propulsion system provides most of the lift of a typical hypersonic aircraft. Since the shapes may be somewhat complex, it is necessary to provide for an adequate geometrical representation. Figure B.2 shows the coordinate system used and defines the vehicle reference plane. This plane typically coincides with the body centerline as seen in the elevation drawing, but the program allows for arbitrary specification of this plane. For convenience, the origin of the coordinate system is located at the vehicle nose. The x-axis lies along the reference plane in the (assumed) normal plane of symmetry. The y-axis points to the left and the z-axis points downward.

Figure B.3 shows how the various profile curves defining the body shape are represented in the program. These curves may be determined by curve fitting of three-view drawings or may be input into the program as a table of points. It is not necessary to utilize a large number of points. Ten points per profile curve usually provide adequate accuracy unless the body shapes are exceptionally complex.

As shown in Figure B.3, the body cross-section profiles are not required to be continuous curves. Corners are allowed as represented by the break points shown in the drawings. The fuselage shape is specified in functional form as

$$\begin{cases} z = f(y) & \text{Cross Section Shape} \\ y = g(x) & \text{Planform Shape} \\ z = h(x) & \text{Fuselage Elevation} \end{cases} \tag{B.7}$$

These functions are determined in the program from the input coordinate points and are used to compute the unit vector normal to a point on the windward surface. The result is

$$\mathbf{n} = \sin\phi_1 \mathbf{i} + \sin\phi_2 \mathbf{j} + (\cos\phi_1 \cos\phi_2)\mathbf{k} \tag{B.8}$$

where

$$\phi_1 = \tan^{-1}\left(\frac{dh}{dx}\right) \tag{B.9}$$

$$\phi_2 = \tan^{-1}\left(\frac{df}{dy}\right) \tag{B.10}$$

An area element of the body surface at the same location can be written as

$$dS = \frac{\Delta}{\cos\phi_1 \cos\phi_2} dy \tag{B.11}$$

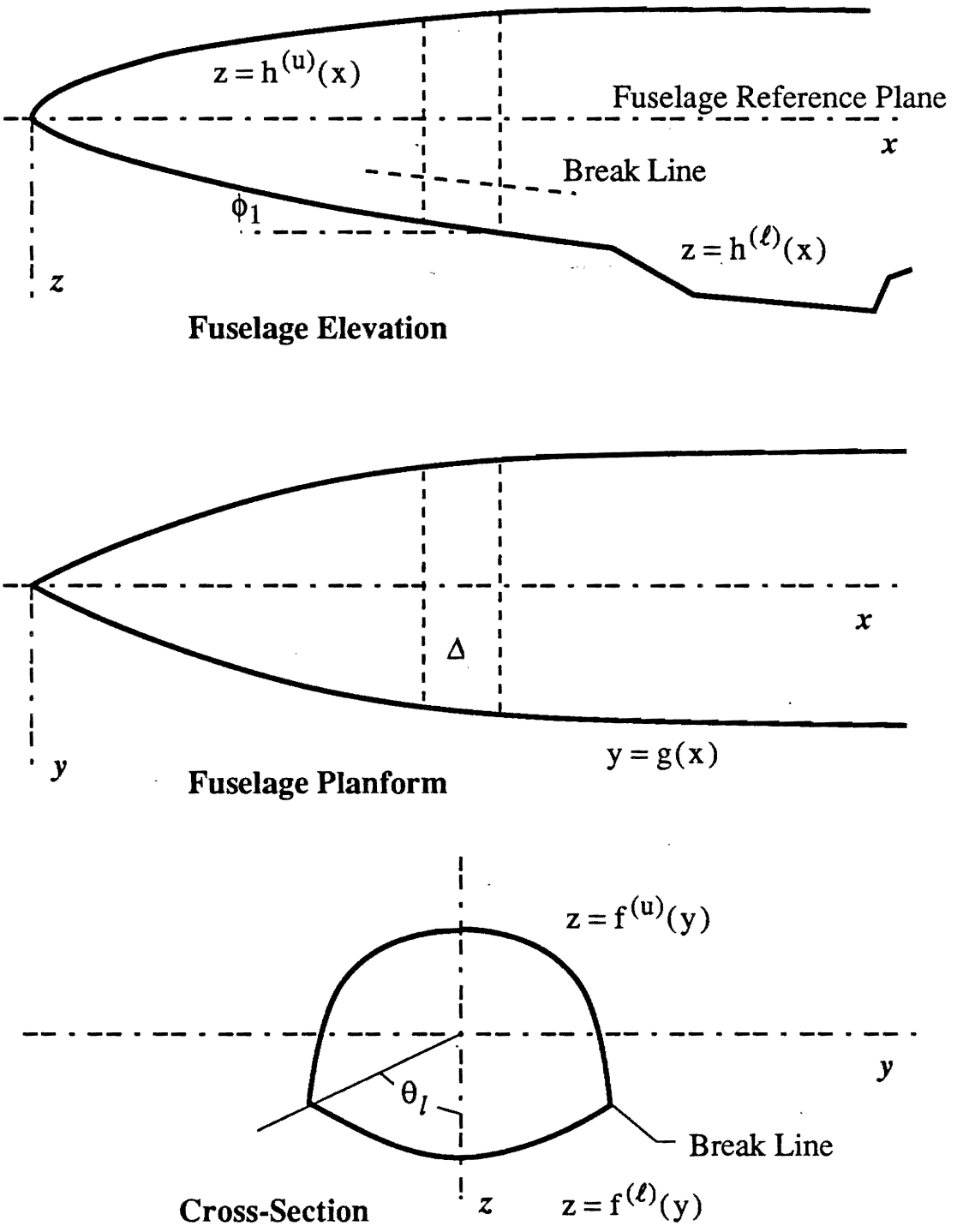

Figure B.3. Definition of Body Shape Functions

The projected width of the element in the reference plane is Δ as shown in Figure B.3. The inclination angle between the freestream velocity vector and the surface element is given by

$$\psi = \cos^{-1}\left(\frac{\mathbf{U}_\infty \cdot \mathbf{n}}{U_\infty}\right) - \frac{\pi}{2} \tag{B.12}$$

where the velocity vector is specified in body coordinates as

$$\mathbf{U}_\infty = U_\infty\left[(\cos\beta\cos\alpha)\mathbf{i} - (\sin\beta)\mathbf{j} - (\cos\beta\sin\alpha)\mathbf{k}\right] \tag{B.13}$$

The local pressure coefficient is

$$C_p = 2\sin^2[\psi] \tag{B.14}$$

The dimensionless normal force vector on the surface element is, in vector form

$$d\mathbf{F} = -2\sin^2[\psi]\, dS\, \mathbf{n} \tag{B.15}$$

Integration of this function across the width of the body gives the force vector on an axial element of the vehicle. The program then sums all contributions axially to determine the lift, drag, sideforce, and moment coefficients for the complete assembly.

The more detailed representation of the body geometry used in the present version of the program greatly improves the agreement between the predicted and measured aerodynamic performance. Earlier problems with the vehicle lift curve slope at zero angle of attack have been eliminated because the effects of body curvature and surface orientation are now properly accommodated in the calculations.

III. Scramjet Propulsion Model

Although the supersonic combustion ramjet concept has been known for over two decades, the lack of appropriate unclassified experimental data, cycle analyses, and combustion analyses requires that we use a simple conceptual model for the purposes of vehicle trajectory optimization. In what follows is a brief description of this model and the philosophy behind it.

Conceptually, the SCRAMJET is as simple an airbreathing combustion device as one could imagine. In the case of the new family of flight vehicles to use this propulsion concept,

the entire underside of the vehicle plays a role in the operation of the system. Figure 1 shows the basic configuration. Mechanically, the device can be thought of in terms of three elements. These are

1. Diffuser
2. Combustor
3. Expansion nozzle

Hypersonic vehicle designers attempt to utilize the forward fuselage, strakes, and wings to provide the majority of the diffusion. The lower part of the three-dimensional oblique shock formed at the leading edges is tailored to the shape of the combustor inlet so that air enters at approximately a Mach number of the order of 3 depending on the flight speed. Combustion of hydrogen fuel takes place in the duct at supersonic speeds in order to minimize energy losses due to dissociation, which would be enormous if the more conventional subsonic ramjet cycle were to be used in high speed flight. Liquid hydrogen is the fuel of choice not only because of its high energy content, but because it can be made to burn in a supersonic flow due to its wide flammability limits and high flame speed. Finally, the combustion products are expanded through a nozzle, which, like the diffuser is designed into the contour of the lower fuselage.

The propulsion system is mostly diffuser and nozzle. While these elements are fairly easy to model from the thermodynamic cycle point of view, the aerodynamics are quite complex, giving rise to a challenging design problem. Computational fluid dynamics (CFD) numerical techniques are being relied upon in conjunction with a new family of hypersonic test facilities to yield practical design solutions. Unfortunately, information on the current research is classified, so that realistic design data is not available for projects of the type reported here.

The computational model used here to represent the SCRAMJET propulsion system was deliberately designed to be readily updated as new information becomes available. It directly accesses a standard atmosphere model (also easily adjustable to provide non-standard operating conditions), which simplifies its incorporation into a trajectory optimization program. The diffuser and nozzle performance is determined either with standard thermodynamic models or by means of optimal design curve fits such as those proposed by Billig. Since information concerning recent progress in supersonic combustion was not available, a simple combustor model was incorporated. This is a straightforward Rayleigh line calculation. An iterative scheme is used to determine the nozzle entrance Mach number, by maintaining the mixture ratio at or below the stoichiometric value. No detailed combustion calculations with multi-species gases is attempted in the present version of the model although these could be readily incorporated as a more definitive model of practical SCRAMJET combustion comes into focus.

The propulsive drag estimate of Billig was incorporated to account in a simple way for some of the frictional losses. No attempt was made to incorporate vehicle integration effects in an interactive fashion. Experience with the aerodynamic simulation shows that very small vehicle attitude changes take place during equilibrium flight. Therefore in the present state of development, no vehicle attitude dependence has been included in the propulsion model. The flexibility of the algorithm will make such additions quite easy to incorporate as the need for them is established.

References

B.1. Billig, F. S., "Design Considerations of Supersonic Combustion Ramjets," AIAA-86-0159, AIAA 24th Aerospace Science Meeting, Jan 6-9, 1986.

B.2. Northam, G. B. and G. Y. Anderson, "Supersonic Combustion Ramjet Research at Langley," AIAA-86-0159, AIAA 24th Aerospace Science Meeting, Jan 6-9, 1986.

B.3. Avery, W. H. and Dugger, G. L., "Hypersonic Airbreathing Propulsion," Astronautics and Space Engineering, June 1964, pp 42-47.

L-16-656

Rapid Near-Optimal Aerospace Plane Trajectory Generation and Guidance

Progress Report
November, 1990

Reporting Period: 5/1/90 - 10/31/90

Research Supported by the NASA Langley Research Center
NASA Grant Number: NAG-1-922

Principal Investigators: A. J. Calise and G. A. Flandro
Research Assistants: J. E. Corban and N. Markopoulos
NASA Contract Monitor: D. D. Moerder

School of Aerospace Engineering
Georgia Institute of Technology
Atlanta, Georgia 30332

Table of Contents

I. Summary

This progress report covers the period from May 1st to October 31st, 1990. During this period, efforts were focused upon developing a general understanding of singularly perturbed systems subject to state-variable inequality constraints. Such constraints are common to a wide class of flight vehicles, but have received little attention in the literature for the case of singularly perturbed dynamic systems. In the last progress report, it was noted that singularly perturbed optimal control problems with state-variable inequality constraints can exhibit complex boundary layer phenomenon. In particular, the boundary layer transitions associated with such problems can be of finite time when the state constraint is first encountered at the end of the boundary layer transition. The lack of a general theory for treating such systems was identified as a significant research problem.

A cursory look at this problem was completed prior to submission of the 1989 final report. Since that time, considerable progress has been made. The results of this effort are detailed in a technical paper that was first presented in Portland, Oregon at the 1990 AIAA GN&C Conference. A revision of the paper is included as an appendix to this report, and has been submitted for publication in the AIAA *Journal of Guidance, Dynamics and Control*. The results are summarized as follows.

The established necessary conditions for optimality in nonlinear control problems that involve state-variable inequality constraints were applied to a class of singularly perturbed systems. The distinguishing feature of this class of two-time-scale systems is a transformation of the state-variable inequality constraint, present in the full order problem, to a constraint involving states and controls in the reduced problem. The existence of a nonsingular control solution was assumed. It was of particular interest to construct the zeroth order initial boundary layer solution, or at least and approximation to it, when the reduced solution lies on a state constrain boundary. In the absence of a state constraint, one can take advantage of the fact that the reduced solution serves as an equilibrium point for the boundary layer system. However, it was shown that, when a state constraint is active in the reduced problem, the boundary layer problem can be of finite time in the stretched time variable. Thus, the usual requirement for asymptotic stability of the boundary layer system is not applicable, and can not be used to construct approximate boundary layer solutions. Furthermore, an active state constraint introduced the possibility of discontinuous costate variables at the juncture between constrained and unconstrained arcs.

Various means for treating such problems were investigated. A simple linear example was constructed and used to show that a Valentine transformation can be used to regain smoothness, but with limited advantage. That is, Valentine's transformation can be used to avoid the problems associated with discontinuous costate time histories, but at the expense of introducing a singular arc and discontinuities in the transformed control variable. A second linear example was used to illustrate the exact analytic solution of a simple singularly perturbed problem involving a state variable inequality constraint. The solution includes a "fast" costate discontinuity and a finite-time initial boundary layer transition. A third, but nonlinear, example for which the boundary layer system could not be solved analytically was then constructed. This example was used to illustrate a general feedback strategy that was developed for synthesizing a near-optimal boundary layer transition onto a constrained arc. In this technique, the costate jumps that can occur and the boundary layer final time are used as free parameters in order to satisfy continuity conditions in the state variables at the end of the boundary layer response. The resulting approximation was compared directly with the numerically generated optimal solution. The method proved

quite satisfactory when used to construct an approximate solution for this relatively simple nonlinear example, at least for small perturbations away from the reduced solution.

Several research problems requiring further attention have been identified. For instance, numerical problems were sometimes encountered in the solution process for Example 3 as time-to-go approached zero (i.e. as the boundary layer transition nears completion). This difficulty did not prevent the generation of an accurate approximation of the optimal solution for the example problem, and further manipulation of Example 3 has lead to a completely analytic characterization of the solution. However, the possibility of approaching a singularity should be investigated in a generic setting.

The application of the developed technique to guidance of a generic aerospace vehicle is now underway. But, the approximation technique being employed depends upon a linearization of the boundary layer system about a non equilibrium point. It does not appear possible to characterize the stability of the approximation for a given set initial conditions. And though guidance along a constraint boundary will likely be subject to small perturbations only, linearization does introduce the likelihood of control saturation for sufficiently large perturbations. A multiple time scale approach, in which altitude and flight path angle dynamics are examined on separated time scales, could eliminate this dependence on linearization and should be investigated. There is also a question of applicability when atmospheric disturbances lead to a constraint violation. The activities planned for the next reporting period include an investigation of these matters while applying the methodology to guide a generic aerospace plane configuration in numerical simulations. A paper which reports on our progress is being planned for presentation at either the 1991 ACC or the AIAA GN&C Conference.

II. Progress this Reporting Period

This research project is focused upon various aspects of real-time trajectory generation and guidance for a generic aerospace plane configuration. Funding was initiated in July of 1987 and the research results obtained through 1989 have been documented in a series of reports and papers which are cited as references [1-8]. The results reported in [1-8] are summarized in a paper which has been submitted to the AIAA Journal of Guidance, Dynamics and Control entitled "Rapid Near-Optimal Aerospace Plane Trajectory Generation and Guidance" [9]. Climb paths generated using the derived near-optimal trajectory generation algorithm have since been compared with numerically generated optimal trajectories. One of these comparisons is documented in [10] and illustrates the excellent agreement obtained. There was a funding lag for the period from January to May of 1990 during which no research was conducted in this area. Funding resumed on the first of May.

This progress report covers the period from May 1st to October 31st, 1990. During this period, efforts were focused upon developing a general understanding of singularly perturbed systems subject to state-variable inequality constraints. Such constraints are common to a wide class of flight vehicles, but have received little attention in the literature for the case of singularly perturbed dynamic systems. In the last progress report, it was noted that singularly perturbed optimal control problems with state-variable inequality constraints can exhibit complex boundary layer phenomenon. In particular, the boundary layer transitions associated with such problems can be of finite time when the state constraint is first encountered at the end of the boundary layer transition. The lack of a general theory for treating such systems was identified as a significant research problem.

The results of our effort to date on state constrained singularly perturbed problems are are summarized in Section I, and detailed in a technical paper that was first presented in Portland, Oregon at the 1990 AIAA GN&C Conference [11]. A revision of the paper is attached as an appendix to this report, and the reader is referred to this appendix for a discussion of the technical details. This revision has been submitted for publication in the AIAA *Journal of Guidance, Dynamics and Control.*

Since the completion of [11] and Appendix A, a fully analytic solution to Example 3 has been obtained. In particular, the complete analytic solution of the system (78-81) of Appendix A was derived, where the unknowns are τ_f, θ, c and d. The solution proceeds as follows.

Solve (81) for the unknown value of d in terms of e and τ_f

$$d = \tau_f^2 + 2e\tau_f \tag{1}$$

Substitute (1) into (78) to obtain

$$5\tau_f^4 + 8e\tau_f^3 - 24b\tau_f - 12a = 0 \tag{2}$$

Substitute (1) into (79) to obtain

$$2\tau_f^3 + 3e\tau_f^2 - 6b = 0 \tag{3}$$

Solve (3) for $e\tau_f^2$

$$e\tau_f^2 = -2\tau_f^3/3 + 2b \tag{4}$$

Finally, substitute (4) into (2) to obtain

$$\tau_f^4 + 24b\tau_f + 36a = 0 \tag{5}$$

The complete analytic solution of the quartic polynomial (5) is available by standard handbook methods and yields four possible values of τ_f. Note that all allowable combinations of initial conditions fall into two general categories, those for which $a < 0$ and $b > 0$ and those for which $a < 0$ and $b < 0$. For either case, one can show that only one positive real solution for τ_f will occur.

The fact that three of the four unknowns in equations (78-81) enter linearly leads to the possibility of analytic solution. It appears that this will also be the case when considering altitude and flight path angle dynamics of an aerospace plane, though the eigen values will no longer be exactly zero. Thus, it may be possible to reduce the requirement for numerical solution of the corresponding set of four nonlinear algebraic equations to the solution of a single transcendental equation.

III. Plans for the Next Reporting Period

Several research problems requiring further attention have been identified. For instance, numerical problems were sometimes encountered in the solution process for Example 3 of [11] as time-to-go approached zero (i.e. as the boundary layer transition nears completion). This difficulty did not prevent the generation of an accurate approximation of the optimal solution for the example problem, and further manipulation of Example 3 has lead to a completely analytic characterization of the solution. However, the possibility of approaching a singularity should be investigated in a generic setting.

The application of the developed technique to guidance of a generic aerospace vehicle is now underway. But, the approximation technique being employed depends upon a linearization of the boundary layer system about a non equilibrium point. It does not appear possible to characterize the stability of the approximation for a given set initial conditions. And though guidance along a constraint boundary will likely be subject to small perturbations only, linearization does introduce the likelihood of control saturation for sufficiently large perturbations. A multiple time scale approach, in which altitude and flight path angle dynamics are examined on separate time scales, could eliminate this dependence on linearization and should be investigated. This technique has been applied to guidance of fighter aircraft when a state-constraint is inactive [12]. In such case a weighted penalty on flight path angle is included in the index of performance and the weighting adjusted so that for small perturbations, the response of the nonlinear feedback systems mimics (at least with respect to natural frequency) that of the boundary layer system when linearized about the reduced solution. Note however, that full nonlinearity of the boundary layer system is retained for implementation. This technique cannot be applied directly to the state constrained case since the reduced solution no longer serves as an equilibrium point for the boundary layer system. However, it is expected that a similar approach, perhaps based upon matching of the boundary final time with the linearized case, can be developed.

A more rigorous identification of multiple time scales than has been accomplished in the past is also of interest. In particular, a formal multiple scale analysis is proposed. Multiple scale analysis is a collection of general perturbation techniques that includes as special cases the concepts used both in the boundary layer method and the WKB method [13-14]. (The WKB method is named for Wentzel, Kramers, and Brilloun, who popularized it.) The multiple scale approach is based upon the introduction of several time scales and then the use of these time scales to eliminate the emergence of secular, resonance causing terms. The number of different time scales still have to be guessed a priori for any given problem, a weakness of the method. However, the method has the advantage of allowing for nonlinear time scales, that is, time scales for which the stretched time variable τ is related to the original time variable t via a nonlinear relation of the form

$$\tau = g(\varepsilon)\, t$$

Here $g(\varepsilon)$ is a general function of ε to be determined (usually $g(\varepsilon) = \varepsilon^n$).

There is also a question of feedback law applicability when atmospheric disturbances lead to a constraint violation. Consider, for instance, a constraint on maximum allowable dynamic pressure. The value of dynamic pressure is dependent on both atmospheric density and velocity relative to a stationary atmosphere. Neither of these quantities are fully deterministic, thus one cannot truly define a trajectory along which the vehicle will

experience a constant dynamic pressure. Furthermore, it is quite possible that the vehicle could experience a violation of the constraint, at least for a short period of time. The algorithm developed to date does not function properly in the case of a constraint violation. Hence, further development is required in this area.

During the next reporting period (11-1-90 to 3-30-91), an investigation of these matters will be conducted while applying the developed methodology to guidance of a generic aerospace plane configuration. A paper which reports on our progress is being planned for presentation at either the 1991 ACC or the AIAA GN&C Conference.

References

[1] Calise, A. J., J. E. Corban, and G. A. Flandro, "Trajectory Optimization and Guidance Law Development for National Aerospace Plane Applications," Proceedings of the 1988 ACC, Vol. 2, pp. 1406-1411, Atlanta, GA, June 15-17.

[2] Calise, A. J., J. E. Corban, and G. A. Flandro, "Trajectory Optimization and Guidance Law Development for National Aerospace Plane Applications," Final Report for Period July 1, 1987 to November 30, 1988, NASA Grant No. NAG-1-784, December 1988.

[3] Corban, J. E., Calise, A. J., and Flandro, G. A., "Trajectory Optimization and Guidance Law Development for Transatmospheric Vehicles," Proceeding of the 1989 IEEE International Conference on Control and Applications (ICCON), April 3-6, Jerusalem, Israel.

[4] Corban, J. E., A. J. Calise, and G. A. Flandro, "A Real-Time Guidance Algorithm for Aerospace Plane Optimal Ascent to Low Earth Orbit," Proceedings of the 1989 ACC, Vol. 3, June 21-23, Pittsburgh, PA, pp. 2475-2481.

[5] Corban, J. E., A. J. Calise, and G. A. Flandro, "Optimal Guidance and Propulsion Control for Transatmospheric Vehicles," Presented at the 1989 AIAA GN&C Conference, August 14-16, Boston, MA, available as AIAA Paper 89-3617.

[6] Calise, A. J., and J. E. Corban, "Optimal Control of Singularly Perturbed Nonlinear Systems with State Variable Inequality Constraints," Presented at the IFAC Workshop on Singular Perturbations and Asymptotic Methods in Systems and Control, Boston, MA, August 17-18, 1989.

[7] Corban, J. E., "Real-Time Guidance and Propulsion Control for Single-Stage-to-Orbit Airbreathing Vehicles," Ph.D. Dissertation, The Georgia Institute of Technology, December 1989.

[8] Corban, J. E., A. J. Calise, and G. A. Flandro, "Rapid Near-Optimal Trajectory Generation and Guidance Law Development for Single-Stage-to-Orbit Airbreathing Vehicles," Final Report for Period January 1 to December 31, 1989, NASA Grant No. NAG-1-922, January 1990.

[9] Corban, J. E., A. J. Calise, and G. A. Flandro, "Rapid Near-Optimal Aerospace Plane Trajectory Generation and Guidance," Submitted for Publication in the AIAA *Journal of Guidance, Dynamics and Control.*

[10] Van Buren, M. A., and K. D. Mease, "Aerospace Plane Guidance Using Geometric Control Theory," Proceedings of the 1990 ACC, San Diego, CA, May 23-25, Vol. 2, p. 1829-1838.

[11] Calise, A. J., and J. E. Corban, "Optimal Control of Singularly Perturbed Nonlinear Systems with State-Variable Inequality Constraints," Proceedings of the 1990 AIAA Guidance, Navigation and Control Conference, August 20-22, Portland, OR, also submitted for publication in the AIAA *Journal of Guidance, Dynamics and Control.*

[12] Calise, A. J., "Optimization of Aircraft and Flight-Path Angle Dynamics," Journal of Guidance, Dynamics and Control, Vol. 7, No. 1, Jan.-Feb. 1984, pp. 123-125.

[13] Bender and Orszag, "Advanced Mathematical Methods for Scientist and Engineers," McGraw-Hill, New York, NY, 1978.

[14] Cakmak, Botha and Gray, "Computational and Applied Mathematics for Engineering Analysis," Springer-Verlag, 1987.

Appendix A

Technical Supplement

Presented at the 1990 AIAA Guidance, Navigation and Control Conference, Portland, Oregon

Optimal Control of Singularly Perturbed Nonlinear Systems with State-Variable Inequality Constraints

A. J. Calise* and J. E. Corban†
The Georgia Institute of Technology, School of Aerospace Engineering, Atlanta, GA 30332

Abstract

The established necessary conditions for optimality in nonlinear control problems that involve state-variable inequality constraints are applied to a class of singularly perturbed systems. The distinguishing feature of this class of two-time-scale systems is a transformation of the state-variable inequality constraint, present in the full order problem, to a constraint involving states and controls in the reduced problem. It is shown that, when a state constraint is active in the reduced problem, the boundary layer problem can be of finite time in the stretched time variable. Thus, the usual requirement for asymptotic stability of the boundary layer system is not applicable, and can not be used to construct approximate boundary layer solutions. Several alternative solution methods are explored and illustrated with simple examples.

I. Introduction

State-variable inequality constraints are commonly encountered in the study of dynamic systems. The study of rigid body aircraft dynamics and control is certainly no exception. For instance, a maximum allowable value of dynamic pressure is usually prescribed for aircraft with supersonic capability. This limit is required to ensure that the vehicle's structural integrity is maintained. Given a typical state-space description of the vehicle dynamics, this limit constitutes an inequality constraint on vehicle state.

State inequality constraints have been studied extensively by researchers in the field of optimal control. First-order necessary conditions for optimality when general functions of state are constrained have been obtained.[1-3] However, the construction of solutions via this set of conditions proves difficult. Most practitioners seeking an open loop control solution rely on direct approaches to optimization that employ penalty functions for satisfaction of state inequality constraints.[4] As a rule, algorithms employing such methods are computationally intense and slow to converge. Consequently, they are not well suited for real-time implementation.

As discussed in the literature, the use of singular perturbation techniques in the study of aircraft trajectory optimization can, through order reduction, lead to both open and closed loop solutions that are computationally efficient. These methods can sometimes be used to circumvent difficulties associated with enforcing a state inequality constraint as well.[5] As an example consider the minimum time intercept problem of Ref. 6 which employs a model of the F-8 aircraft. A near-optimal feedback solution is obtained via singular perturbation theory that includes consideration of an inequality constraint on dynamic pressure. In the zero order reduced solution, algebraic constraints are obtained when the perturbation parameter, ε, which premultiplies the so called "fast" dynamic equations, is set to zero. These constraints can be used to eliminate the fast states (in this case altitude and flight path angle) from the reduced problem. One can choose, however, to retain one or more of the fast states and to eliminate instead a corresponding number of the original control variables. In such case, the retained fast state variables are treated as controls, and the original state constraint becomes a constraint involving both state and control. This transformation of the constraint function from one dependent only on state to one dependent on both state and control leads to considerable simplification when seeking a solution to the reduced problem. In subsequent analysis of boundary layers, altitude resumes its status as a state variable, and dynamic pressure once again becomes a function of state alone. However, because the reduced solution for the example F-8 aircraft does not lie on the constraint boundary during ascent, the inequality constraint on dynamic pressure does not have to be considered in the boundary layer analysis. The problem of treating a pure state constraint is thus avoided. Of note is the fact that modern supersonic fighter aircraft (such as the F-15) do ride the dynamic pressure constraint boundary during the ascent leg of the minimum time to intercept path.

In addition to the example cited above, dynamic pressure bounds are encountered during fuel-optimal climb for supersonic transports[7], for rocket powered launch vehicles such as the U.S. space shuttle[8], and for single-stage-to-orbit air-breathing launch vehicles[9]. If in applying singular perturbation methods when seeking a feedback solution to any of these problems, the reduced solution climb path lies directly on the dynamic pressure constraint boundary for a portion of the flight, then it is necessary to consider boundary layer transitions onto the constrained arc. This problem has not received attention in the literature.

In the absence of a state-variable inequality constraint (i.e. when it is inactive), the initial boundary layer solution for the class of systems being considered is an infinite time process. A solution is sought which asymtotically approaches the reduced solution. However, it will be shown that, when a state constraint is active in the reduced solution, the boundary layer problem can be of finite time in the stretched time variable. Thus, the usual requirement

---

* Professor, School of Aerospace Engineering. Associate Fellow AIAA.

† Post Doctoral Researcher. Member AIAA.

for asymptotic stability of the boundary layer system is not applicable, and can not be used to construct an approximate boundary layer solution.[10] The presence of an active state inequality constraint also introduces the possibility of discontinuous costate variables at the juncture between constrained and unconstrained arcs. A Valentine transformation can be used to convert the constrained problem to an equivalent unconstrained problem of increased dimension. Smoothness is regained in the process, but to little or no advantage when seeking a solution for real-time implementation. This point is discussed in greater depth later.

It is shown by example that one can analytically obtain a solution to a simple singularly perturbed example involving a state inequality constraint by dealing with the possible costate discontinuities directly. In addition, a general procedure for constructing a near-optimal boundary layer transition onto the constraint boundary is formulated for use when an exact analytic solution can not be obtained. The resulting approximation proves quite satisfactory when compared with the optimal solution, at least for small perturbations away from the reduced solution.

This paper proceeds as follows. Section II provides a brief review of the first order necessary conditions that have been obtained for state-variable inequality constrained problems in optimal control. Section III discusses the optimal control of singularly perturbed systems subject to state-variable inequality constraints in general, and in particular examines the features of state inequality constrained boundary layers when the reduced solution lies on the constraint boundary. Section IV presents the solutions to three example problems. The first two are linear and simply illustrate the problem features discussed in earlier sections. A nonlinear example is then used to illustrate a general feedback strategy for the construction of near-optimal boundary layer transitions onto a constrained arc. The approximate solution is then compared directly with the optimal solution. Section V completes the paper by providing some concluding remarks.

II. State-Variable Inequality Constrained Problems in Optimal Control

The introduction of a state-variable inequality constraint of the form

$$S(z,t) \le 0 \tag{1}$$

can lead to considerable difficulty when attempting to obtain an optimal control solution to a general nonlinear problem. In (1), the variable z denotes the system's state vector and t denotes time. One approach to incorporating state-variable inequality constraints in the formulation of first-order necessary conditions for optimality consists of constructing successive total time derivatives of S until explicit dependence on the control, u, appears. If p time derivatives are required then Eq. (1) is referred to as a p^{th} order state-variable inequality constraint. The relation $S^p(z,u,t) = 0$ is then adjoined to the Hamiltonian as a constraint to be enforced when $S = 0$. In this instance, the superscript p denotes the p^{th} total time derivative of S. This approach introduces additional "tangency" conditions that must be satisfied at points of entry onto and exit from a constrained arc. These conditions are given by

$$N(z,t) = \begin{bmatrix} S(z,t) \\ S^1(z,t) \\ \vdots \\ S^{p-1}(z,t) \end{bmatrix} = 0 \tag{2}$$

Eq. (2) constitutes a set of interior boundary conditions that must be met at each juncture between a constrained and unconstrained arc. In order to satisfy these interior boundary conditions one must allow for the possibility of discontinuities in the costate variables at the junctures.[1]

An alternative set of necessary conditions can be obtained by adjoining the constraint function (1), rather than its p^{th} derivative, to the Hamiltonian and then employing a separating hyperplane theorem.[2] The resulting necessary conditions prove simpler and "sharper" than those of Ref. 1, but the possibility for discontinuous costate variables remains. The relationship between the necessary conditions of Ref's. 1 and 2 is defined in Ref. 3. Other approaches to treating such problems include employing a transformation technique in which a slack variable is used to transform the state constrained problem into an equivalent unconstrained problem of higher dimension and various direct numerical methods of solution[4,11].

III. Optimization of Singularly Perturbed Systems Subject to State Inequality Constraints

Consider the singularly perturbed optimal control formulation:

$$dx/dt = f(x,y,u,t) \qquad x(t_o) = x_o \qquad x \in R^n \qquad u \in R^1 \tag{3}$$

$$\varepsilon\, dy/dt = g(x,y,u,t) \qquad y(t_o) = y_o \qquad y \in R^m \tag{4}$$

with an index of performance and scalar inequality constraint of the form

$$J = \phi[x(t_f), \varepsilon y(t_f)] \qquad S(x,y) \le 0 \tag{5}$$

where ε is a small parameter. It is further assumed that $g_u^T g_u > 0$, $S_y^T S_y > 0$ (the superscript T denotes transpose and the subscripts denote partial differentiation), and that the problem is regular so that the control is continuous at the juncture of unconstrained and constrained arcs. Zero-order necessary conditions for optimality of the associated reduced and boundary layer problems in the absence of state variable inequality constraints are readily available.[12] In addition to basic smoothness assumptions on both f and g, sufficient conditions for the existence of a boundary layer solution carry the requirement that there exist an isolated root of $g = 0$ along the reduced solution to serve as an

asymptotically stable equilibrium point for the boundary layer dynamics. Furthermore, the initial condition on y must lie in the domain of attraction of this root at the initial time, which amounts to a controllability requirement in this context. Similar requirements exist at the final time.

The extension of the necessary conditions for state constrained problems discussed in the previous section to include the singular perturbation formulation in (3-5) is as follows. Adjoining the constraint in (5) directly, the Hamiltonian is given by

$$H = \lambda_x f + \lambda_y g + \nu S \quad \text{where} \quad \nu(t) \geq 0 \tag{6}$$

The additional first order necessary conditions for optimality are:

$$d\lambda_x/dt = -H_x \qquad \lambda_x(t_f) = \phi_x(t_f) \qquad H_u = 0 \tag{7}$$

$$\varepsilon\, d\lambda_y/dt = -H_y \qquad \lambda_y(t_f) = \phi_y(t_f)/\varepsilon \tag{8}$$

with the jump conditions

$$\lambda_x(t_i^+) = \lambda_x(t_i^-) - \sigma(t_i, \varepsilon)S_x(t_i) \qquad H(t_i^+) = H(t_i^-) \tag{9}$$

$$\lambda_y(t_i^+) = \lambda_y(t_i^-) - \sigma(t_i, \varepsilon)S_y(t_i)/\varepsilon \tag{10}$$

The t_i represent the times at which a constrained and unconstrained arc meet. In (9,10) the scalar multiplier σ is $o(\varepsilon)$. Note that in the limit as ε goes to zero, there are no jumps in the slow costate variables. In contrast, the fast costates can exhibit finite jumps proportional to S_y. In order to arrive at the condition (10) it is important to note that the interpretation for λ_y in a singular perturbation formulation is different from that of a non-singular formulation, namely

$$\lambda_y(t_o) = [\partial J/\partial y(t_o)]\,/\varepsilon \tag{11}$$

The reduced problem and associated necessary conditions are obtained by setting $\varepsilon = 0$ in (3-10). The fast states act as control variables as a consequence of setting $\varepsilon = 0$ in Eq. (8). Hence, the constraint S can be viewed as a function of both states and controls, and the possibility of jumps in the slow costates is eliminated. The reduced solution necessary conditions are given by:

$$dx/dt = f(x,y,u,t) \qquad x(t_o) = x_o \qquad g(x,y,u,t) = 0 \tag{12}$$

$$H = \lambda_x f + \lambda_y g + \nu S \quad S(x,y) \leq 0 \quad \text{where} \quad \nu(t) \geq 0 \tag{13}$$

$$d\lambda_x/dt = -H_x \qquad \lambda_x(t_f) = \phi_x(t_f) \qquad H_y = H_u = 0 \tag{14}$$

The zero-order initial boundary layer solution associated with (3-5) is obtained by introducing the time stretching transformation $\tau = (t - t_o)/\varepsilon$ and again setting ε to zero. On this time scale the slow states and costates are essentially frozen at their reduced solution values. The initial boundary layer necessary conditions are given by:

$$dx/d\tau = 0 \Rightarrow x(\tau) = x^o \qquad d\lambda_x/d\tau = 0 \Rightarrow \lambda_x(\tau) = \lambda_x{}^o \tag{15}$$

$$dy/d\tau = g(x^o, y, u, \tau) \qquad d\lambda_y/d\tau = -H_y \tag{16}$$

$$H_{BL} = \lambda_x{}^o f + \lambda_y g + \nu S \quad \nu(t) \geq 0 \tag{17}$$

$$H_{BL_u} = 0 \qquad S(x,y) \leq 0 \tag{18}$$

where $[\,]^o$ denotes the reduced solution evaluated at $t = t_o$. When the reduced solution trajectory does not lie on the constraint boundary, the boundary layer solution, if it exists, is expected to be an infinite time process and to asymptotically approach the reduced solution. A local stability test, accomplished by linearizing the boundary layer necessary conditions about the reduced solution, is usually employed to test for the existence of a solution. Since the linearized dynamics [with the control eliminated using Eq. (18)] in general have eigenvalues symmetrically arranged about the origin, thus the sufficiency condition is reduced to the requirement that none of the resulting eigenvalues lie on the imaginary axis.[10] When this condition holds true, a feedback solution for small perturbations away from the reduced solution can be constructed by selecting the initial conditions on the perturbations in λ_y to lie in the subspace spanned by the eigenvectors associated with the stable eigenvalues.

When the reduced solution lies on the state constraint boundary, it may no longer act as an equilibrium point of the boundary layer dynamics. This feature is evident upon examination of (14) and (16). A critical requirement is that $d\lambda_y/d\tau$ approach zero as the reduced solution is approached. In the unconstrained case this is a natural consequence of the fact that $H_y = 0$ is satisfied by the reduced solution. However, when the reduced solution lies on a constraint boundary, the situation is considerably more complicated. It may happen that the state constraint is encountered before the end of the boundary layer transition, in which case the reduced solution would serve as an equilibrium point in a reduced state space associated with riding the constraint boundary. If on the other hand the state constraint is not encountered until the end of the boundary layer transition, then the reduced solution is very likely not an equilibrium point, which typically occurs when S is dependent on only one fast state variable. This is often the case in aircraft flight mechanics problems. As a consequence, $d\lambda_y/d\tau$ does not approach zero at the end of the boundary layer transition, but instead "jumps" to zero due to the jumps that occur in λ_y. This further implies that the boundary layer arc is of finite time in the τ time scale. In this case, the traditional asymptotic stability analysis and method of matched asymptotic expansions can not be used in constructing an approximate solution.

In this paper, several alternate means for constructing such an approximation are presented. In particular, the costate jumps that can occur and the boundary layer final time are used as free parameters in order to satisfy continuity conditions in the state variables at the end of the boundary layer response. Note that the continuity condition

on H in (9) is guaranteed if the problem is regular. Though not addressed in this paper, a similar finite time phenomenon has been observed when considering boundary layer transitions onto singular arcs.[13]

As mentioned earlier, one approach to treating these problems that avoids the difficulties associated with costate discontinuities consists of using a Valentine transformation to convert the constrained problem to an equivalent unconstrained one of higher dimension.[11] The inequality constraint in (5) is converted to an equality constraint by the introduction of a slack variable $\alpha(t)$ as follows

$$S(x,y,t) + 1/2\alpha^2(t) = 0 \qquad (19)$$

Differentiating (19) p times with respect to time, the following set of equations is obtained

$$S^1 + \alpha\alpha_1/\varepsilon = S_x f + S_y\, g/\varepsilon + S_t + \alpha\alpha_1/\varepsilon = 0 \qquad \varepsilon d\alpha/dt = \alpha_1$$

$$S^2(x,y,t) + \alpha_1^2/\varepsilon^2 + \alpha\alpha_2/\varepsilon^2 = 0 \qquad \varepsilon d\alpha_1/dt = \alpha_2$$

$$S^3(x,y,t) + 3\alpha_1\alpha_2/\varepsilon^3 + \alpha\alpha_3/\varepsilon^3 = 0 \qquad \varepsilon d\alpha_2/dt = \alpha_3$$

$$\vdots$$

$$S^p(x,y,u,t) + \{\text{terms involving } \alpha_{p-1},\ldots,\alpha_1,\varepsilon\} + \alpha\alpha_p/\varepsilon^p = 0$$

$$\varepsilon d\alpha_{p-1}/dt = \alpha_p \qquad (20)$$

where the presence of ε in (20) is representative of the fact that α and all the α_i must be fast variables in order to maintain the equality in (19). Using the p^{th} equation in (20), one can solve for the control u to obtain

$$u = G(x,y,\alpha_{p-1},\ldots,\alpha_1,\alpha\alpha_p,\varepsilon,t) \qquad (21)$$

Using (21) and treating $\alpha, \ldots, \alpha_{p-1}$ as additional fast state variables, the following unconstrained problem, with α_p as the new control variable is obtained

$$dx/dt = f(x,y,G,t)$$

$$\varepsilon\, dy/dt = g(x,y,G,t)$$

$$\varepsilon d\alpha/dt = \alpha_1$$

$$\varepsilon d\alpha_1/dt = \alpha_2$$

$$\vdots$$

$$\varepsilon d\alpha_{p-1}/dt = \alpha_p \qquad (22)$$

with the index of performance again given by

$$J = \phi[x(t_f), \varepsilon y(t_f)] \qquad (23)$$

Note that the dimension of (22) can be reduced using (19) and the first p–1 equalities in (20) to eliminate some of the original fast state variables. The initial conditions $\alpha(t_o)$, ..., $\alpha_{p-1}(t_o)$ are chosen to satisfy (19) and the first p–1 equations in the set (20):

$$\alpha(t_o) = \pm\,[-2S(x(t_o),y(t_o),t_o)]^{1/2}$$

$$\alpha_1(t_o) = -\,\varepsilon S^1(x(t_o),y(t_o),t_o)/\alpha(t_o)$$

$$\alpha_2(t_o) = -\,\varepsilon^2[S^2(x(t_o),y(t_o),t_o) + \alpha_1^2(t_o)]/\alpha(t_o)$$

$$\vdots \qquad (24)$$

With this choice of boundary conditions, (19-20) are satisfied for all time on the interval of interest for any control function α_p; that is, any function α_p will produce an admissible trajectory. Thus the original constrained problem (3-5) is replaced by a transformed unconstrained problem (22-24). In general, however, this technique simply trades one difficulty for another. Constrained arcs which occur in the reduced solution of the original problem correspond to singular arcs in the the transformed variables. Linearization of the boundary layer dynamics and exploitation of asymptotic stability properties again is not possible since the first variation with respect to α_p vanishes along the reduced solution, and α_p is in general discontinuous at the juncture of singular and non-singular arcs.

IV. Examples

Several simple examples are now presented. The first illustrates the use of the Valentine transformation and the finite time nature of the boundary layer solutions. The second example is solved without resorting to the Valentine transformation and illustrates the complete analytic solution to a singularly perturbed problem of optimal control involving a state-variable inequality constraint. A third nonlinear example is introduced for which a complete analytic solution is unavailable. In this case a feedback strategy is employed to construct an approximation to the boundary layer transition onto the constraint arc. This strategy is based on a Taylor's series expansion to first order about a non-equilibrium point. The costate jump that can occur and the boundary layer final time are used as free parameters in order to satisfy continuity conditions in the state variables at the end of the boundary layer response. The optimal solution of the third example was generated numerically for direct comparison to this feedback approximation.

Example 1

Consider the singularly perturbed dynamical system,

$$dx/dt = y - u^2 \qquad \varepsilon dy/dt = u \qquad S = y - 1 \le 0 \qquad (25)$$

with the initial conditions specified as $x(0) = y(0) = 0$. The final value $x(t_f) > 0$ is specified and the objective is to minimize the time required to reach this specified end condition. The state constraint in this case is first order. Introduction of a slack variable and transformation results in the equivalent unconstrained dynamics:

$$dx/dt = 1 - \alpha^2/2 - (\alpha\alpha_1)^2 \qquad x(0) = 0 \tag{26}$$

$$\varepsilon d\alpha/dt = \alpha_1 \qquad \alpha(0) = (2)^{1/2} \tag{27}$$

where y has been eliminated using (19).

Reduced solution: The reduced solution Hamiltonian is given by

$$H = \lambda_x [1 - \alpha^2/2 - (\alpha\alpha_1)^2] + \lambda_\alpha \alpha_1 + 1 = 0 \tag{28}$$

where $\alpha_1{}^o = 0$ as a consequence of setting $\varepsilon = 0$ in (27). Evaluation of first order necessary conditions for optimality results in the following:

$$H = 0 \text{ and } H_\alpha = 0 \Rightarrow \lambda_x{}^o = -1 \quad \alpha^o = 0 \tag{29}$$

$$H_{\alpha_1} = 0 \Rightarrow \lambda_\alpha{}^o = 0 \tag{30}$$

from which it is evident that

$$x^o(t) = t \qquad y^o(t) = 1 \qquad u^o = 0 \tag{31}$$

Boundary Layer Solution: Introducing the time scale transformation $\tau = t/\varepsilon$ and again setting ε to zero, the boundary layer dynamics become

$$d\alpha/d\tau = \alpha_1 \qquad \alpha(0) = (2)^{1/2} \tag{32}$$

The boundary layer Hamiltonian is given by

$$H_{BL} = \alpha^2/2 + (\alpha\alpha_1)^2 + \lambda_\alpha \alpha_1 = 0 \tag{33}$$

and the associated necessary conditions are:

$$d\lambda_\alpha/d\tau = -\alpha(1 + 2\alpha_1{}^2) \tag{34}$$

$$H_{\alpha_1} = 0 \Rightarrow \alpha_1 = -\lambda_\alpha/2\alpha^2 \tag{35}$$

$$H = 0 \Rightarrow \lambda_\alpha = -(2)^{1/2}\alpha^2 \tag{36}$$

Substituting (36) into (35) yields

$$\alpha_1(\tau) = -1/(2)^{1/2} \neq \alpha_1{}^o \qquad \alpha(\tau) = (2)^{1/2} - \tau/(2)^{1/2} \tag{37}$$

When the boundary layer trajectory reaches the constraint boundary, $\alpha(\tau_f) = 0$ and (37) yields $\tau_f = 2$. Transforming back, we obtain a feedback solution for u in terms of y,

$$u = [1 - y]^{1/2} \tag{38}$$

Integration of (25) on the τ time scale using (38) gives

$$y(\tau) = 1 - [1 - \tau/2]^2 \tag{39}$$

Note that while α_1 is discontinuous at $\tau = \tau_f$, the original control is continuous.

Example 2

Now consider a third-order version of the preceding example.

$$dx/dt = y_1 - u^2 \qquad \varepsilon dy_1/dt = y_2 \qquad \varepsilon dy_2/dt = u \tag{40}$$

$$S = y_1 - 1 \leq 0 \tag{41}$$

with initial conditions $x(t_o)$, $y_1(t_o) < 1$, and $y_2(t_o)$ given. As before, the final condition on x is prescribed and greater than $x(t_o)$, the final conditions on y_1 and y_2 are free, and the objective is to minimize the final time. In this case, the state constraint is of order two. In contrast to Example 1, the solution to this problem is carried out in terms of the original variables.

Reduced Solution: The reduced solution Hamiltonian is given by

$$H = \lambda_x(y_1 - u^2) + \lambda_{y_1} y_2 + \lambda_{y_2} u + \nu(y_1 - 1) + 1 = 0 \tag{42}$$

where $y_2{}^o(t)$ and $u^o(t)$ are zero as a consequence of setting $\varepsilon = 0$ in (41). Evaluation of first order necessary conditions for optimality results in the following:

$$H = H_{y_1} = 0 \Rightarrow \nu^o(t) = 1 \quad y_1{}^o(t) = 1 \quad \lambda_x{}^o(t) = -1$$

$$H_{y_2} = 0 \Rightarrow \lambda_{y_1}{}^o(t) = 0$$

$$H_u = 0 \Rightarrow \lambda_{y_2}{}^o(t) = 0 \tag{43}$$

Thus all the variables except x are constant, the control is maintained at zero, the initial conditions on y_1 and y_2 cannot be met, y_1 remains on the constraint boundary, and x is propagated to its specified final value according to the relation

$$x^o(t) = x(t_o) + t \tag{44}$$

Boundary Layer Solution: Introducing the time scale transformation $\tau = t - t_o/\varepsilon$ and again setting ε to zero, the boundary layer dynamics become:

$$dy_1/d\tau = y_2 \qquad y_1(\tau_f) = y_1{}^o(t_o) = 1 \tag{45}$$

$$dy_2/d\tau = u \qquad y_2(\tau_f) = y_2{}^o(t_o) = 0 \tag{46}$$

where the terminal conditions on the fast states are chosen to match their reduced solution values. The boundary layer Hamiltonian is given by

$$H = \lambda_x^{\,o}\,(y_1 - u^2) + \lambda_{y_1}\,y_2 + \lambda_{y_2}\,u + \nu(y_1 - 1) + 1 = 0 \tag{47}$$

and the associated necessary conditions are:

$$d\lambda_{y_1}/d\tau = 1 \qquad \lambda_{y_1}(\tau_f) = \sigma \ \text{(i.e. free)} \tag{48}$$

$$d\lambda_{y_2}/d\tau = -\lambda_{y_1} \qquad \lambda_{y_2}(\tau_f) = \lambda_{y_2}^{\,o}(t_o) = 0 \tag{49}$$

$$H_u = -2\lambda_x^{\,o}u + \lambda_{y_2} = 0 \quad \Rightarrow \quad u = -\lambda_{y_2}(\tau)/2 \tag{50}$$

Note that when the boundary layer solution reaches the constraint boundary, it has also reached the reduced solution, i.e. it is not possible for the boundary layer system to ride the constraint boundary before reaching the reduced solution. Thus the initial boundary layer problem can be viewed as an unconstrained two-point-boundary-value problem in which the terminal conditions must match the state and costate conditions just prior to entering onto the constrained arc. Integration of the state and costate dynamic equations following elimination of the control u using (50) and assuming t_o=0 yields:

$$y_1(\tau) = \tau^4/48 + \lambda_{y_1}(0)\tau^3/12 - \lambda_{y_2}(0)\tau^2/4 + y_2(0)\,\tau + y_1(0) \tag{51}$$

$$y_2(\tau) = \tau^3/12 + \lambda_{y_1}(0)\,\tau^2/4 - \lambda_{y_2}(0)\,\tau/2 + y_2(0) \tag{52}$$

$$\lambda_{y_1}(\tau) = \lambda_{y_2}(0) + \tau \tag{53}$$

$$\lambda_{y_2}(\tau) = -\tau^2/2 - \lambda_{y_1}(0)\,\tau + \lambda_{y_2}(0) \tag{54}$$

Evaluating (51-54) at τ_f results in four algebraic equations in four unknowns: $\lambda_{y_1}(0)$, $\lambda_{y_2}(0)$, $\lambda_{y_1}(\tau_f)$, and τ_f. The solution to this system is obtained as follows

$$\lambda_{y_1}(\tau_f) = \lambda_{y_2}(0) + \tau_f \tag{55}$$

$$\lambda_{y_2}(0) = \tau_f^2/2 + \lambda_{y_1}(0)\,\tau_f \tag{56}$$

where

$$\lambda_{y_1}(0) = [y_2(0) - t_f^3/6]4/t_f^2 \tag{57}$$

and

$$\tau_f^4 + 48\,y_2(0)\,\tau_f + 144\,[y_1(0) - 1] = 0 \tag{58}$$

Equation (58) must in general be solved numerically and will yield at most one real positive solution for the final time, τ_f. For the particular choice of initial conditions of $x(t_o) = y_1(t_o) = y_2(t_o) = 0$, (58) can be solved directly yielding

$$\tau_f = 2(3)^{1/2} = 3.464$$

$$\lambda_{y_1}(0) = -2\tau_f/3 = -2.309 \qquad \lambda_{y_2}(0) = -\tau_f^2/6 = -2.000$$

The costate λ_{y_1} is discontinuous at the juncture between the unconstrained (boundary layer) and constrained (reduced solution) arcs as evidenced by its finite value at τ_f.

$$\lambda_{y_1}(\tau_f) = 2(3)^{1/2}/3 = 1.155$$

In essence, the time τ_f corresponds to a juncture time t_i in (10). Note that

1. The control solution in (50) can be put in feedback form by solving the boundary layer problem for an arbitrary initial condition and evaluating at τ=0.

2. The control solutions in (38) and (50) are exact in the sense that they satisfy the necessary conditions for the full order problems. Thus all of the higher-order correction terms are zero. This is a consequence of the fact that both the dynamics and the constraints in these examples are independent of the slow state variable.[14]

Solutions to the system of equations (55-58) for a number of different initial conditions are presented in Table 1. Representative state, costate, and control histories are presented in Figures 1-4. Note that x simply propagates to its specified final value according to (44) after the solution for y_1 reaches the constraint boundary. The x trajectories achieve large negative values initially for cases 4 and 5 and are not shown. Cases in which $x(t_f)$ is reached before y_1 reaches the constraint boundary indicate that the singular perturbation approximation is inappropriate. In general, for $\varepsilon = 1$ it is possible to nondimensionalize the dynamics so that $\varepsilon = 1/x(t_f)$.

Example 3

Consider the addition of a nonlinear term in the dynamic system of Example 2 as follows

$$dx/dt = y_1 - u^2 \quad \varepsilon dy_1/dt = y_2 + y_1y_2 \quad \varepsilon dy_2/dt = u \tag{59}$$

$$S = y_1 - 1 \le 0 \tag{60}$$

As in Example 2, the state constraint is of order two.

Reduced Solution: The reduced solution Hamiltonian is given by

$$H = \lambda_x(y_1 - u^2) + \lambda_{y_1}(y_2 + y_1y_2) + \lambda_{y_2}u + \nu S + 1 = 0 \tag{61}$$

where $y_2^{\,o}(t)$ and $u^o(t)$ are again zero as a consequence of setting $\varepsilon = 0$ in (59). The reduced solution is identical to that of Example 2. All the variables except x are constant and the control is maintained at zero.

Boundary Layer Solution: Introducing the time scale transformation $\tau = t - t_o/\varepsilon$ and again setting ε to zero, the boundary layer dynamics become:

$$dy_1/d\tau = y_2 + y_1 y_2 \qquad y_1(\tau_f) = 1 \tag{62}$$

$$dy_2/d\tau = u \qquad y_2(\tau_f) = 0 \tag{63}$$

where the terminal conditions on the fast states are chosen to match their reduced solution values. The boundary layer Hamiltonian is given by

$$H = \lambda_x{}^o(y_1 - u^2) + \lambda_{y_1}(y_2 + y_1 y_2) + \lambda_{y_2} u + \nu S + 1 = 0 \tag{64}$$

and the associated necessary conditions are:

$$d\lambda_{y_1}/d\tau = 1 - \lambda_{y_1} y_2 \qquad \lambda_{y_1}(\tau_f) = \sigma \text{ (i.e. free)} \tag{65}$$

$$d\lambda_{y_2}/d\tau = -\lambda_{y_1}(1 + y_1) \qquad \lambda_{y_2}(\tau_f) = y_2{}^o = 0 \tag{66}$$

$$H_u = -2\lambda_x{}^o u + \lambda_{y_2} = 0 \quad \Rightarrow \quad u = -\lambda_{y_2}(\tau)/2 \tag{67}$$

Because an analytical solution for the state and costate dynamic equations (following elimination of the control) could not be found, we must resort to numerical methods of solution or seek approximations to the optimal solution.

As discussed earlier, the reduced solution does not act as an equilibrium point for the boundary layer system. However, one can write a Taylor's series expansion for the boundary layer system about a non-equilibrium point. We choose as such a point the state and costate conditions just prior to the juncture of the unconstrained boundary layer trajectory and the reduced solution which lies on the constraint boundary. The corresponding time is denoted as τ_f which is representative of the time t_i^- in (10). All the conditions at this point are known except for the value of $\lambda_{y1}(\tau_f)$, which is free to jump from a finite value to its reduced solution value of zero at the end of the boundary layer transition. To first order, the perturbation dynamics are described by

$$d\delta z/dt \equiv f[z(\tau_f)] + \partial f/\partial z\Big|_{z(\tau_f)} \delta z \tag{68}$$

where the vector z is composed of the boundary layer states and costates and the vector f represents the right-hand sides of their corresponding differential equations given by (62,63,65,66). The perturbations are defined as follows:

$$\delta y_1 = y_1(\tau) - 1.0 \tag{69}$$

$$\delta y_2 = y_2(\tau) \tag{70}$$

$$\delta\lambda_{y_1} = \lambda_{y_1}(\tau) - \lambda_{y_1}(\tau_f) \tag{71}$$

$$\delta\lambda_{y_2} = \lambda_{y_2}(\tau) \tag{72}$$

The relation (68) is of the general form

$$d\delta z/d\tau = A\delta z + B \tag{73}$$

where

$$A = \begin{bmatrix} 0 & 2 & 0 & 0 \\ 0 & 0 & 0 & -1/2 \\ 0 & -\theta & 0 & 0 \\ -\theta & 0 & -2 & 0 \end{bmatrix} \tag{74}$$

$$B^T = [0 \quad 0 \quad 1 \quad -2\theta] \tag{75}$$

and

$$\theta \equiv \lambda_{y_1}(\tau_f) \tag{76}$$

The solution to (73) is well known to be of the form

$$\delta z(\tau) = e^{A(\tau - \tau_o)}\,\delta z(\tau_o) + \int_{\tau_o}^{\tau} e^{A(\tau - \zeta)}\,B\,d\zeta \tag{77}$$

Note that the eigenvalues of A in this case are all zero. The state transition matrix is obtained analytically, and the response of the perturbation equations given an arbitrary set of initial condition can be written as:

$$\delta y_1 = \tau^4/12 + e\tau^3/3 - d\tau^2/2 + 2b\tau + a \tag{78}$$

$$\delta y_2 = \tau^3/6 + e\tau^2/2 - d\tau/2 + b \tag{79}$$

$$\delta\lambda_{y_1} = -\theta\tau^4/24 - e\theta\tau^3/6 + d\theta\tau^2/4 + (1 - \theta b)\tau + c \tag{80}$$

$$\delta\lambda_{y_2} = -\tau^2 - 2e\tau + d \tag{81}$$

where for convenience

$$a \equiv \delta y_1(t_o) \qquad b \equiv y_2(t_o) \tag{82}$$

$$c \equiv \lambda_{y_1}(t_o) \qquad d \equiv \lambda_{y_2}(t_o) \tag{83}$$

and

$$e \equiv \theta(1 + a/2) + c \tag{84}$$

We wish to drive these perturbations to zero at $\tau = \tau_f$. Thus, the left-hand sides of (78-81) are set to zero. The initial conditions $y_1(t_o)$ and $y_2(t_o)$ are known. It is left to determine the corresponding final time τ_f (i.e. time t_i^-), θ as defined in (76), and the costate initial conditions. A Newton method was used to numerically obtain the solution.

The initial costate values determined in this way can be used to approximate the initial costates for the nonlinear boundary layer system. By periodically updating these estimates while numerically integrating the nonlinear boundary layer dynamics forward in time, one can generate an approximate solution to the boundary layer problem. As for Examples 1 and 2, the control solution (67) is exact in the sense that it satisfies the necessary conditions for the full order problem. Thus all of the higher-order correction terms are zero.

Table 2 presents the solution to (78-81) at time τ_f for various combinations of initial conditions. The feedback

strategy described above was employed to generate approximations to the optimal boundary layer transitions. Representative state, costate, and control time histories are depicted in Figures 5–8 for the case where $x(t_o) = y_1(t_o) = y_2(t_o) = 0$. For comparison, the optimal solution was generated numerically using a multiple shooting algorithm. The full-order dynamic system was considered and the associated unconstrained two-point-boundary value problem solved for the case when $t_o = 0$, $x(t_o) = y_1(t_o) = y_2(t_o) = 0$, t_f free, $y_1(t_f) = 1$, $y_2(t_f) = 0$ and $x(t_f)$ free. The optimal state, costate, and control time histories are superimposed over the approximations presented in Figures 5–8. In the optimal case, y_1 reaches the constraint boundary in 2.767 seconds. At that time x has a value of 1.117 and λ_{y_1} is 0.856. In contrast, at 2.8 seconds the approximated boundary layer transition has not quite reached the reduced solution. The value of x is 1.139, y_1 is .999, y_2 is .010 and the time-to-go is estimated as 0.18 seconds. Using linear interpolation, the value of x at 2.767 seconds is 1.107, thus the x approximation is slightly less than the optimal value of x as it should be. An open loop simulation of the nonlinear dynamic system starting with the approximation obtained via (78-81) is also depicted in Figures 5-8. These trajectories clearly illustrate the need to regularly update the approximate solution.

V. Conclusions

Singularly perturbed optimal control problems with state-variable inequality constraints can exhibit complex boundary layer phenomenon. In particular, the boundary layer transitions associated with such problems can be of finite time when the state constraint is first encountered at the end of the boundary layer transition. Valentine's transformation can be used to avoid the problems associated with discontinuous costate time histories, but at the expense of introducing a singular arc and discontinuities in the transformed control variable. Because of the finite time nature of the boundary layer solutions, the traditional asymptotic stability analysis and method of matched asymptotic expansions can not be used in constructing an approximate solution. Instead, the costate jumps that can occur and the boundary layer final time can be used as free parameters in order to satisfy continuity conditions in the state variables at the end of the boundary layer response. This technique has proved quite satisfactory when used to construct an approximate solution for a relatively simple nonlinear example, at least for small perturbations away from the reduced solution.

Acknowledgement

This research was support by the NASA Langley Research Center under Grant Number NAG-1-922.

References

[1]Bryson, A. E., Jr., and Ho, Yu-Chi, *Applied Optimal Control*, Hemisphere Publishing Corp., New York, 1975.

[2]Jacobson, D. H., M. M. Lele, and J. L. Speyer, "New Necessary Conditions of Optimality for Control Problems with State-Variable Inequality Constraints," Journal of Mathematical Analysis and Applications, 35, pp. 255-284, 1971.

[3]Kreindler, E., "Additional Necessary Conditions for Optimal Control with State-Variable Inequality Constraints," Journal of Optimization Theory and Applications," Vol. 30, No. 2, Oct. 1982, pp. 241-251.

[4]Boykin, W. H., Jr., and T. E. Bullock, "State Constraints and Singular Solutions to Penalty Function Optimization Problems," AIAA Journal, Vol. 10, No. 2, Feb. 1972, pp. 137-141.

[5]Calise, A. J., "On the Use of Singular Perturbation Methods in the Solution of Variational Problems," Proceedings of the Joint Automatic Controls Conference, Columbus, Ohio, 1973, pp. 184-192.

[6]Calise, A.J., Moerder, D.D., "Singular Perturbation Techniques for Real Time Aircraft Trajectory Optimization and Control," NASA Contractor Report 3597, August, 1982.

[7]Falco, M. and H. J. Kelly, "Aircraft Symmetric Flight Optimization," Control and Dynamic Systems, Advances in Theory and Applications, Vol. 10, Academic Press, New York, NY, 1973. (see Figure 14 on page 114)

[8]McHenry, R. L., T. J. Brand, A. D. Long, B. F. Cockrell, and J. R. Thibodeau III, "Space Shuttle Ascent Guidance, Navigation, and Control," *The Journal of the Astronautical Sciences*, Vol. XXVII, No. 1, pp. 1-38, January-March, 1979.

[9]Hargraves, C. R., and S. W. Paris, "Direct Trajectory Optimization Using Nonlinear Programming and Collocation," *Journal of Guidance*, Vol. 10, No. 4, July-August 1987, pp. 338-342.

[10]Ardema, M. D., "Linearization of the Boundary Layer Equations of the Minimum Time to Climb Problem," Journal Guidance and Control, Vol. 2, No. 5, pp. 434-436.

[11]Jacobson, D. H. and M. M. Lele, "A Transformation Technique for Optimal Control Problems with a State Variable Inequality Constraint," *IEEE Transactions on Automatic Control*, Vol. AC-14, No. 5, Oct. 1969, pp. 457-464.

[12]Ardema, M. D., "Singular Perturbations in Flight Mechanics," NASA TM X-62, 380, Aug. 1974; Revised July 1977.

[13]Ardema, M. D., "Nonlinear Singularly Perturbed Optimal Control Problems with Singular Arc," *Automatica*, Vol. 16, No. 1, Jan. 1980, pp. 99-104.

[14]Calise, A. J., "A New Boundary Layer Matching Procedure for Singularly Perturbed Systems," *IEEE Transactions on Automatic Control*, Vol. AC-23, No. 3, June 1978, pp. 434-438.

Table 1.

Representative solutions of Equations (55-58) in Example 2

Case	$y_1(0)$	$y_2(0)$	$\lambda_{y_1}(0)$	$\lambda_{y_2}(0)$	$\lambda_{y_1}(\tau_f)$	τ_f
1	0.00	0.00	-2.309	-2.000	1.155	3.464
2	0.80	0.20	-0.982	-0.121	0.849	1.830
3	0.99	0.01	-0.620	-0.123	0.371	0.991
4	-5.00	-5.00	-5.143	-11.260	1.980	7.122
5	0.80	-5.00	-4.681	-9.717	1.573	6.254

Table 2.

Representative solutions of the linearized boundary layer system (78-81) in Example 3 at time τ_f

Case	$y_1(0)$	$y_2(0)$	$\lambda_{y_1}(0)$	$\lambda_{y_2}(0)$	$\lambda_{y_1}(\tau_f)$	τ_f
1	0.00	0.00	-2.041	-2.000	0.817	2.449
2	0.80	0.20	-1.075	-0.264	0.687	1.144
3	0.99	0.01	-0.667	-0.089	0.268	0.668
4	-5.00	-5.00	-1.019	-13.500	1.469	5.427
5	0.80	-5.00	-4.828	-12.210	1.243	4.952

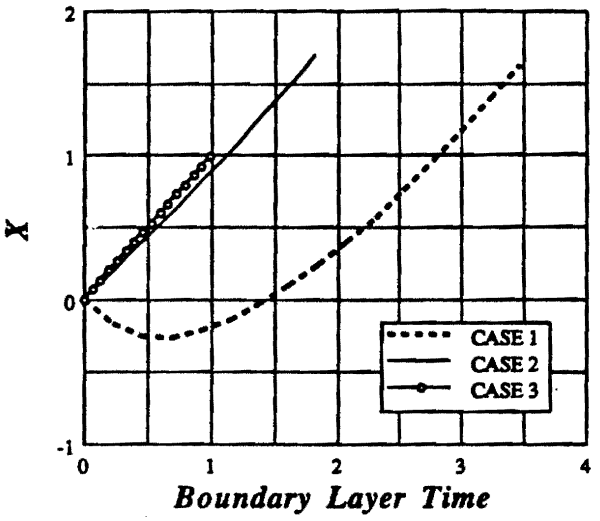

Figure 1. Example 2: x versus τ for several different sets of initial conditions (see Table 1).

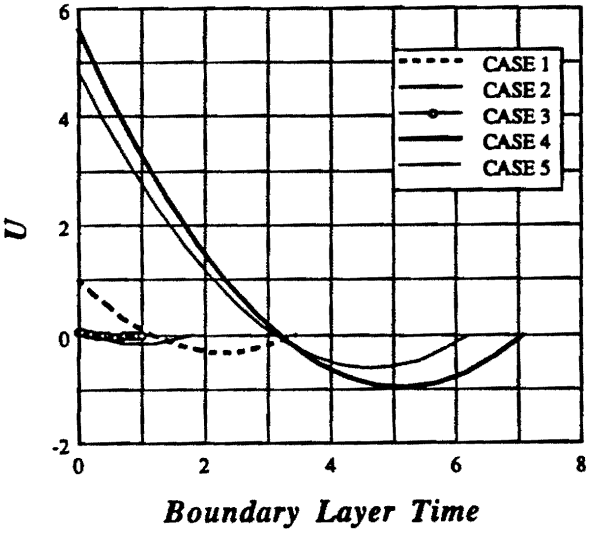

Figure 3. Example 2: u versus τ for several different sets of initial conditions (see Table 1).

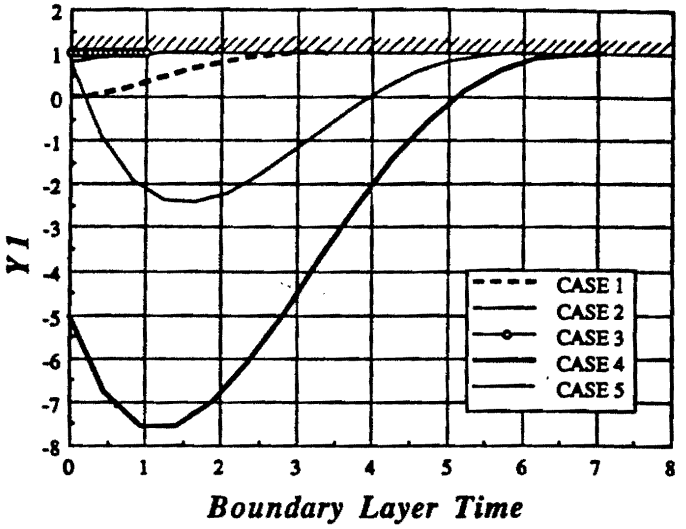

Figure 2. Example 2: y_1 versus τ for several different sets of initial conditions (see Table 1).

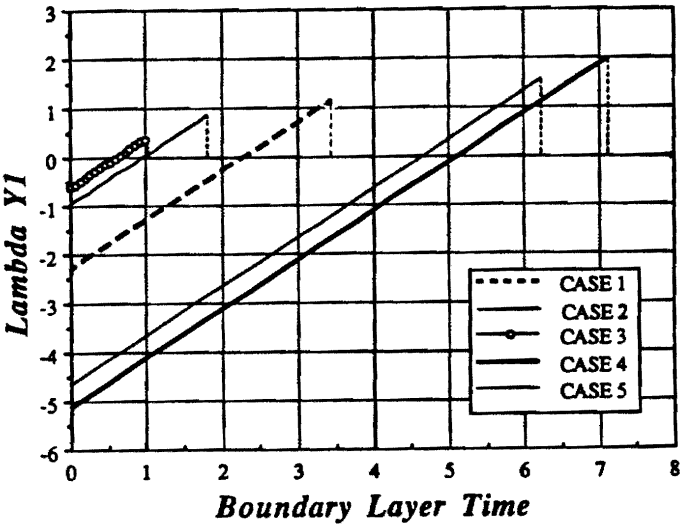

Figure 4. Example 2: λ_{y_1} versus τ for several different sets of initial conditions (see Table 1).

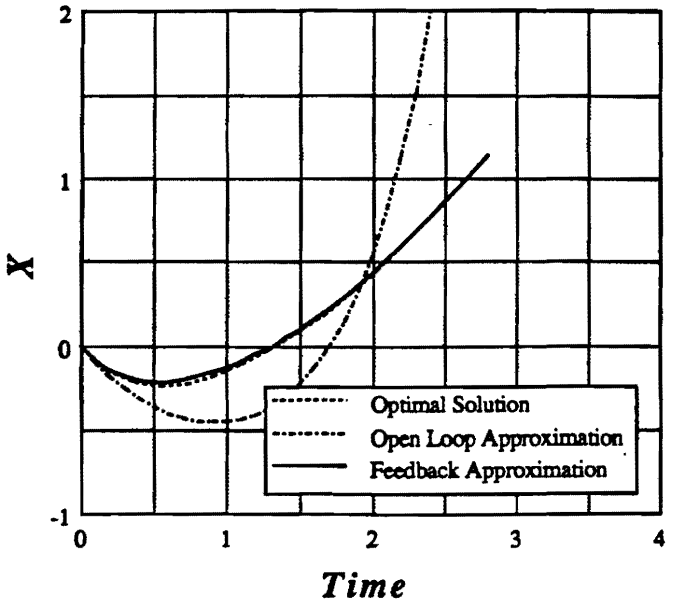

Figure 5. Example 3: Optimal and approximate x versus t when $x(0) = y_1(0) = y_2(0) = 0$.

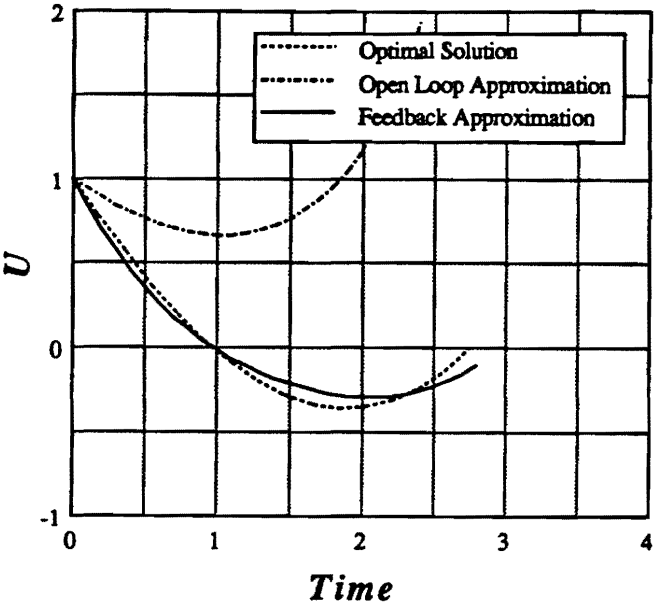

Figure 7. Example 3: Optimal and approximate u versus t when $x(0) = y_1(0) = y_2(0) = 0$.

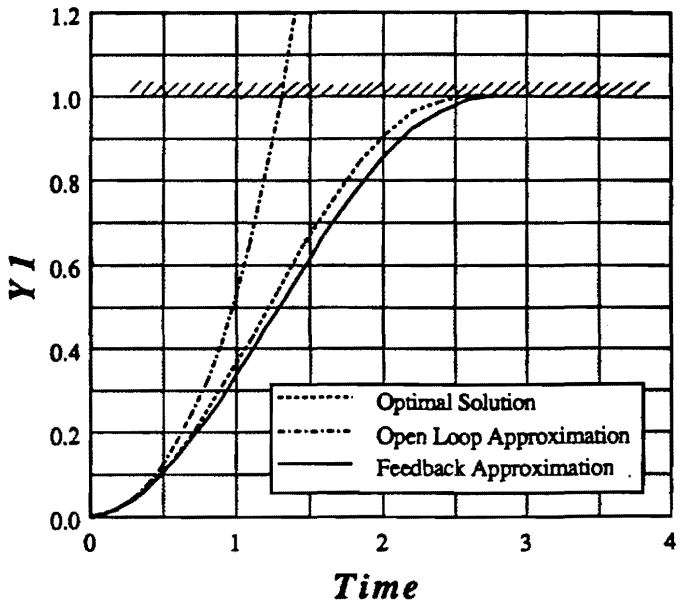

Figure 6. Example 3: Optimal and approximate y_1 versus t when $x(0) = y_1(0) = y_2(0) = 0$.

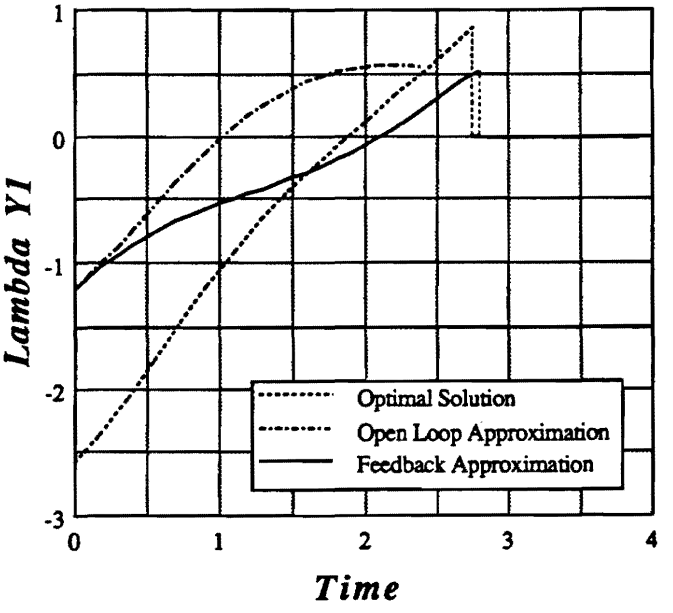

Figure 8. Example 3: Optimal and approximate λ_{y_1} versus t when $x(0) = y_1(0) = y_2(0) = 0$.

Rapid Near-Optimal Aerospace Plane Trajectory Generation and Guidance

Final Report
November, 1991

Reporting Period: 12/1/88 - 8/31/91

Research Supported by the NASA Langley Research Center
NASA Grant Number: NAG-1-922

Principal Investigators: A. J. Calise
Research Assistants: J. E. Corban and N. Markopoulos
NASA Contract Monitor: D. D. Moerder

School of Aerospace Engineering
Georgia Institute of Technology
Atlanta, Georgia 30332

Table of Contents

List of Figures

List of Tables

I. Summary from previous reporting periods

This is the final progress report covering the complete period from December 1, 1988 to August 31, 1991, funded under the NASA Contract NAG-1-922. The research effort was directed toward the problems of real-time trajectory optimization and guidance law development for National Aerospace Plane applications. In particular, singular perturbation methods were used to develop guidance algorithms suitable for on board, real-time implementation.

The bulk of the work completed during the period is summarized in three previous reports, listed as references [1]-[3]. Reference [4] cites the final progress report from the previous project (funded under the NASA Contract NAG-1-784).

The work completed during the period from December 1, 1988 to June 30, 1989 (See Ref. [1]) consisted primarily of extensions to the analysis reported in reference [4] to include a number of important considerations. In particular, the vehicle model was extended to include angle of attack effects, the thrust vector component normal to the velocity vector, and flight in the subsonic and supersonic regimes. A multi-mode propulsion system consisting of turbojet, ramjet, scramjet and rocket engines was assumed and simple models for thrust generation and fuel consumption were adopted for each engine cycle. The state-space was further constrained by considering a maximum allowable heating rate. Singular perturbation methods were applied to this more realistic model, leading to a simple algorithm suitable for generating a nearly-fuel-optimal altitude profile in real time. A simple iterative algorithm was derived that approximates the optimal engine transition points and the regions of cycle overlap. Feedback linearization was employed to derive an angle of attack controller which can be used to guide the vehicle along the nearly-fuel-optimal altitude profile in simulations of flight within the atmosphere. A computer subroutine based on the space shuttle explicit guidance algorithm was written to handle the exoatmospheric phase of ascent guidance which allows for the simulation of insertion into orbit. The resulting software was employed to examine the influence of the added model complexity on the fuel-optimal ascent trajectories and the performance of the guidance algorithms.

During the second reporting period, up to December 31, 1989 (See Ref. [2]) general problems associated with on-board trajectory optimization, propulsion system cycle selection, and with the synthesis of guidance laws were addressed for ascent to low-Earth-orbit of an air-breathing, single-stage-to-orbit vehicle. The work built directly upon the analytical results of reference [1]. A good portion of the work focused on making improvements to the vehicle models employed. The NASA "Generic Hypersonic Aerodynamic Model Example" and the "Langley Accelerator" aerodynamic data sets were acquired and implemented. Work pertaining to the development of purely analytic aerodynamic models also continued at a low level. A generic model of a multi-mode propulsion system was developed that includes turbojet, ramjet, scramjet, and rocket engine cycles. Provisions were made in the dynamic model for a component of thrust normal to the flight path. Computational results, which characterize the nonlinear sensitivity of scramjet performance to changes in vehicle angle of attack, were obtained and incorporated into the engine model. Additional trajectory constraints were also introduced. The constraints treated were: maximum dynamic pressure, maximum aerodynamic heating rate per unit area, angle of attack and lift limits, and limits on acceleration both along and normal to the flight path.

The remainder of the research effort during the second period focused, for the most part, on required modifications to the previously derived algorithm when the model complexity

cited above was added. In particular, analytic switching conditions were derived which, under appropriate assumptions, govern optimal transition from one propulsion mode to another for two cases: the case in which engine cycle operations can overlap, and the case in which engine cycle operations are mutually exclusive. The resulting guidance algorithm was implemented in software and exercised extensively. It was found that the approximations associated with the assumed time scale separation employed in this work are reasonable except over the Mach range from roughly 5 to 8. This phenomenon is due to the very large thrust capability of scramjets in this Mach regime when sized to meet the requirement for ascent to orbit. Very little mass penalty is induced by the resulting inaccuracies in the trajectory over this region because it is traversed rapidly. However, the reduced solution climb paths prove to be unfeasible within this Mach range when subject to the full model dynamics and active trajectory constraints. These difficulties were successfully overcome by accounting for flight path angle and flight path angle rate in construction of the flight path over this Mach range. The resulting algorithm provides the means for rapid near-optimal trajectory generation and propulsion cycle selection over the entire Mach range from take-off to orbit given a realistic nonlinear vehicle model and all pertinent trajectory constraints.

A significant problem area encountered was the lack of a general theory for singularly perturbed systems that are subject to state-variable inequality constraints (Ref. [2]). Such constraints are common to a wide class of flight vehicles but have received little attention in the literature when the dynamic system is singularly perturbed. A study was initiated in this area and it was found that, when the reduced solution lies on a state-variable inequality constraint boundary, the boundary layer trajectories are of finite time in the stretched time scale. The possibility of costate discontinuities at the juncture between constrained and unconstrained arcs makes direct application of existing theory difficult at best. A transformation technique was identified that eliminates some of these difficulties, but at the cost of possibly increased system order and the introduction of singular arcs. Much work remains to be done in this area.

Work on the development of simple, efficient algorithms for prediction of vehicle aerodynamic and propulsive performance continued during the second phase of the program (Ref. [2]). Improvements in the modeling of the hypersonic lifting body module eliminated previous discrepancies between measured and predicted aerodynamic behavior. Several modes of data entry can now be implemented making assessment of a given vehicle configuration very simple. An interactive program mode was devised that makes possible direct and immediate assessment of configuration changes on selected vehicle performance parameters. The algorithms developed in this program are of potential use in applications beyond those originally envisioned.

The first two reporting periods resulted in four conference papers (Ref. [5]-[8]) which discuss most of the results of this research effort. A Ph.D. Dissertation that details the entire effort to date was published in December of 1989 (Ref. [9]). A full-length paper entitled "Rapid Near-Optimal Trajectory Generation for Single-Stage-to-Orbit Airbreathing Vehicles" has also been submitted and accepted for publication in the AIAA Journal of Guidance, Control and Dynamics (Ref. [10]).

There was a funding lag for the period from January to May of 1990 during which no research was conducted. Funding resumed on the first of May.

During the next reporting period, from May 1 to October 31, 1990 efforts were primarily focused upon developing a general understanding of singularly perturbed systems subject to state-variable inequality constraints and also upon developing criteria for the applicability of singular perturbation techniques to flight mechanics problems and in particular to aircraft

energy climbs (Ref. [3]). As noted in reference [2], singularly perturbed optimal control problems with state-variable inequality constraints can exhibit complex boundary layer phenomena. In particular, the boundary layer transitions associated with such problems can be of finite time when the state constraint is first encountered at the end of the boundary layer transition. The lack of a general theory for treating such systems was identified as a significant research problem.

A cursory look at the problem was completed prior to the submission of the 1989 final report (Ref. [2]). Since that time, considerable progress was made. The results of the effort are detailed in a technical paper that was first presented at the 1990 AIAA GN&C Conference (Ref. [11]). A revision of the paper has also been accepted for publication in the AIAA *Journal of Guidance, Dynamics and Control.* The results are summarized as follows.

The established necessary conditions for optimality in nonlinear control problems that involve state-variable inequality constraints were applied to a class of singularly perturbed systems. The distinguishing feature of this class of two-time-scale systems is a transformation of the state-variable inequality constraint, present in the full order problem, to a constraint involving states and controls in the reduced problem. The existence of a nonsingular control solution was assumed. It was of particular interest to construct the zeroth order initial boundary layer solution, or at least and approximation to it, when the reduced solution lies on a state constrain boundary. In the absence of a state constraint, one can take advantage of the fact that the reduced solution serves as an equilibrium point for the boundary layer system. However, it was shown that, when a state constraint is active in the reduced problem, the boundary layer problem can be of finite time in the stretched time variable. Thus, the usual requirement for asymptotic stability of the boundary layer system is not applicable, and can not be used to construct approximate boundary layer solutions. Furthermore, an active state constraint introduced the possibility of discontinuous costate variables at the juncture between constrained and unconstrained arcs.

Various means for treating such problems were investigated. A simple linear example was constructed and used to show that a Valentine transformation can be used to regain smoothness, but with limited advantage. That is, Valentine's transformation can be used to avoid the problems associated with discontinuous costate time histories, but at the expense of introducing a singular arc and discontinuities in the transformed control variable. A second linear example was used to illustrate the exact analytic solution of a simple singularly perturbed problem involving a state variable inequality constraint. The solution includes a "fast" costate discontinuity and a finite-time initial boundary layer transition. A third, but nonlinear, example for which the boundary layer system could not be solved analytically was then constructed. This example was used to illustrate a general feedback strategy that was developed for synthesizing a near-optimal boundary layer transition onto a constrained arc. In this technique, the costate jumps that can occur and the boundary layer final time are used as free parameters in order to satisfy continuity conditions in the state variables at the end of the boundary layer response. The resulting approximation was compared directly with the numerically generated optimal solution. The method proved quite satisfactory when used to construct an approximate solution for this relatively simple nonlinear example, at least for small perturbations away from the reduced solution.

Several problems requiring further attention were identified. For instance, numerical problems were sometimes encountered in the solution process for Example 3 (See Ref. [11]) as time-to-go approached zero (i.e. as the boundary layer transition nears completion). This difficulty did not prevent the generation of an accurate approximation of the optimal solution for the example problem, and further manipulation of Example 3 has

lead to a completely analytic characterization of the solution. However, the possibility of approaching a singularity should be investigated in a generic setting. The approximation technique being employed depends upon a linearization of the boundary layer system about a non equilibrium point. It does not appear possible to characterize the stability of the approximation for a given set of initial conditions. And though guidance along a constraint boundary will likely be subject to small perturbations only, linearization does introduce the likelihood of control saturation for sufficiently large perturbations. A multiple time scale approach, in which altitude and flight path angle dynamics are examined on separate time scales, could eliminate this dependence on linearization. There is also a question of applicability when atmospheric disturbances lead to a constraint violation.

II. Progress this reporting period

During the last reporting period, from November 1, 1990 to August 31, 1991 efforts were again focused upon developing a general understanding of singularly perturbed systems subject to state-variable inequality constraints and also upon developing more stringent criteria for the applicability of singular perturbation techniques to flight mechanics problems and in particular to aircraft energy climbs. Specifically, a systematic approach was devised for naturally identifying the perturbation parameter ε in a singular perturbation analysis of aircraft optimal guidance and expressing it in terms of original physical problem parameters. The approach, which is based on a nondimensionalization of the equations of motion, can be used to evaluate the appropriateness of forced singular perturbation formulations used in the past for transport and fighter aircraft, and to assess the applicability of energy state approximations and singular perturbation analyses for airbreathing transatmospheric vehicles with hypersonic cruise and orbital capabilities. Furthermore, the approach can easily be extended to asses the possibility of treating the same problems by assuming multiple (more than two) time scale behavior.

The lack of strict criteria for the applicability of singular perturbation techniques to flight mechanics problems served as an incentive for our efforts during the last reporting period. The methods of matched asymptotic analysis in singular perturbation theory are based on the presence of small parameters in the differential equations of motion which give rise to multiple time scale behavior. It has been noted by numerous authors (Ref. [13],[14]) that, in spite of a wide number of papers attesting to the applicability of singular perturbation methods to optimization problems in aircraft flight mechanics, few have been successful in first casting the equations of motion in a singular perturbation form. A few notable exceptions are Refs. [13]-[16]. In Ref. [13] two methods for time scale separation analysis are proposed to identify the proper assignment of state variables to various time scales. These methods are based on forming an estimate of the state variable speeds. In Ref. [14] a rescaling to nondimensional variables is recommended. However, it is noted that the proper scaling transformation is not obvious, even if the time scale separation of the variables is well known from analysis or experience. Both of these papers (and in particular Ref. [13]) provide extensive references to earlier studies which employ so-called forced singular perturbation formulations, in which the perturbation parameter (say ε), nominally equal to 1, is artificially introduced as a book keeping parameter in a formal expansion of the solution about $\varepsilon = 0$. In particular, there exists a large number of publications on the optimization of aircraft energy climbs (see for example Refs. [17]-[20]), none of which make any attempt to identify an appropriate perturbation parameter in terms of the original problem parameters. This is particularly disturbing considering the number of years that have passed since such analysis techniques were first introduced in the flight mechanics literature. In any singular perturbation analysis, every attempt should be made to identify

the perturbation parameter in terms of the original problem parameters (which in general include the boundary conditions) so that the physical process that gives rise to the two time scale behavior is clearly understood. Then, the range of parameter values for which the perturbation analysis is valid can be easily identified. Knowledge of time scale separability present in the system dynamics, and success in exploiting this characteristic to obtain approximate solutions, is not, in itself justification for artificially introducing ε. That is, within the framework of our system of logic it is always possible to have conclusions that are *true*, which follow from assumptions that are *wrong*.

Our work has partially rectified this situation by presenting a systematic (albeit still ad-hoc) approach to nondimensionalize variables in nonlinear optimization problems in flight mechanics. Most of the considerations that were presented apply in other fields as well. Our main motivation for collecting and stating these considerations was to define the thought process by which it is possible to arrive at a suitable scaling of the aircraft energy climb problem. Of particular interest was the assessment of the applicability of energy state approximations and singular perturbation analyses for airbreathing transatmospheric vehicles with hypersonic cruise and orbital capabilities.

The major result of our effort was the demonstration that for energy climbs that take place on a vertical plane the singular perturbation parameter ε is always equal to the maximum longitudinal loading factor of the vehicle. Two time scale behavior is suggested according to whether ε is less than one or not. Based on this result it is straightforward to see why singular perturbation methods applied to aircraft performance optimization have worked so well in the past. The maximum longitudinal loading factors associated with the majority of conventional aircraft are either less than one because the aircraft lack very high thrusting capabilities, or because they are restricted to be so for other reasons (structural, comforting, etc.). A few notable exceptions do occur for some modern fighters. This directly suggests that most conventional aircraft can be expected to exhibit two-time-scale behavior for almost any energy climb that they are allowed to perform. This then appears to be the reason for the past success of so many singular perturbation treatments of aircraft energy climbs. The implication for transatmospheric vehicles is rather direct. If we consider such a vehicle as a passenger transport, then, in order to assure passenger comfort it is only natural to *impose* as a constraint a maximum longitudinal loading factor for the vehicle that is less than one. Our work suggests that such a constraint would imply two-time-scale behavior for any type of energy climb that such a vehicle would be allowed to perform. Therefore, singular perturbation formulations of such maneuvers still appear to be promising, even with all the added complexities that the flight regimes of such vehicles can involve. A paper which reports on our progress has been presented at the 1991 AIAA GN&C Conference. A copy of the paper is included as an Appendix.

References

[1] Calise, A. J., J. E. Corban, and G. A. Flandro, "Trajectory Optimization and Guidance Law Development for National Aerospace Plane Applications," Progress Report for Period December 1, 1988 to June 30, 1989, NASA Grant No. NAG-1-922, July 1989.

[2] Corban, J. E., A. J. Calise, and G. A. Flandro, "Rapid Near-Optimal Trajectory Generation and Guidance Law Development for Single-Stage-to-Orbit Airbreathing Vehicles," Progress Report for Period January 1 to December 31, 1989, NASA Grant No. NAG-1-922, January 1990.

[3] Calise, A. J., J. E. Corban, G. A. Flandro, and N. Markopoulos, "Rapid Near-Optimal Aerospace Plane Trajectory Generation and Guidance," Progress Report for Period May 1 to October 31, 1990, NASA Grant No. NAG-1-922, November 1990.

[4] Calise, A. J., J. E. Corban, and G. A. Flandro, "Trajectory Optimization and Guidance Law Development for National Aerospace Plane Applications," Final Report for Period July 1, 1987 to November 30, 1988, NASA Grant No. NAG-1-784, December 1988.

[5] Calise, A. J., J. E. Corban, and G. A. Flandro, "Trajectory Optimization and Guidance Law Development for National Aerospace Plane Applications," Proceedings of the 1988 ACC, Vol. 2, pp. 1406-1411, Atlanta, GA, June 15-17.

[6] Corban, J. E., Calise, A. J., and Flandro, G. A., "Trajectory Optimization and Guidance Law Development for Transatmospheric Vehicles," Proceeding of the 1989 IEEE International Conference on Control and Applications (ICCON), April 3-6, Jerusalem, Israel.

[7] Corban, J. E., A. J. Calise, and G. A. Flandro, "A Real-Time Guidance Algorithm for Aerospace Plane Optimal Ascent to Low Earth Orbit," Proceedings of the 1989 ACC, Vol. 3, June 21-23, Pittsburgh, PA, pp. 2475-2481.

[8] Corban, J. E., A. J. Calise, and G. A. Flandro, "Optimal Guidance and Propulsion Control for Transatmospheric Vehicles," Presented at the 1989 AIAA GN&C Conference, August 14-16, Boston, MA, available as AIAA Paper 89-3617.

[8a] Calise, A. J., and J. E. Corban, "Optimal Control of Singularly Perturbed Nonlinear Systems with State Variable Inequality Constraints," Presented at the IFAC Workshop on Singular Perturbations and Asymptotic Methods in Systems and Control, Boston, MA, August 17-18, 1989.

[9] Corban, J. E., "Real-Time Guidance and Propulsion Control for Single-Stage-to-Orbit Airbreathing Vehicles," Ph.D. Dissertation, The Georgia Institute of Technology, December 1989.

[10] Corban, J. E., A. J. Calise, and G. A. Flandro, "Rapid Near-Optimal Aerospace Plane Trajectory Generation and Guidance," Accepted for Publication in the AIAA *Journal of Guidance, Dynamics and Control.*

[11] Calise, A. J., and J. E. Corban, "Optimal Control of Singularly Perturbed Nonlinear Systems with State-Variable Inequality Constraints," Proceedings of the 1990 AIAA Guidance, Navigation and Control Conference, August 20-22, Portland, OR, also accepted for publication in the AIAA *Journal of Guidance, Dynamics and Control.*

[12] Calise A. J., N. Markopoulos, and J. E. Corban, "Nondimensional Forms for Singular Perturbation Analyses of Aircraft Energy Climbs," Presented at the 1991 AIAA GN&C Conference, August 11-14, New Orleans, LA, available as AIAA Paper 91-2640.

[13] Ardema, M. D., "Separation of Time Scales in Aircraft Trajectory Optimization," AIAA Journal of Guidance and Control, Vol. 8, No. 2, March-April 1985.

[14] Shinar, J., "On Applications of Singular Perturbation Techniques in Nonlinear Optimal Control," *Automatica*, Vol. 19, No. 2, 1983.

[15] Breakwell, J. V., "Optimal Flight-Path Angle Transitions in Minimum-Time Airplane Climbs," Journal of Aircraft, Vol. 14, August 1977.

[16] Calise, A. J., "Optimal Thrust Control with Proportional Navigation Guidance," AIAA Journal of Guidance and Control, Vol. 3, No. 4, July-August 1980.

[17] Kelley, H. J. and Edelbaum, T. N., "Energy Climbs, Energy Turns, and Asymptotic Expansions," Journal of Aircraft, Vol. 7, Jan-Feb 1970.

[18] Ardema, M. D., "Solution of the Minimum Time-to-Climb Problem by Matched Asymptotic Expansions," AIAA Journal, Vol. 14, No. 7, July 1976.

[19] Calise, A. J., "Extended Energy Management Methods for Flight Performance Optimization," AIAA Journal, Vol. 15, No. 3, March 1977.

[20] Calise, A. J., "Singular Perturbation Techniques for On-Line Optimal Flight-Path Control," AIAA Journal of Guidance and Control, Vol. 4, No. 4, July-August 1981.

[21] Corban, J. E., Calise, A. J., and Flandro, G. A., "Rapid Near-Optimal Trajectory Generation for Single-Stage-to-Orbit Airbreathing Vehicles," To appear in the *AIAA Journal of Guidance, Control and Dynamics.*

Appendix

Nondimensional Forms for Singular Perturbation Analysis of Aircraft Energy Climbs

NONDIMENSIONAL FORMS FOR SINGULAR PERTURBATION ANALYSES OF AIRCRAFT ENERGY CLIMBS

A. J. Calise, N. Markopoulos and J. E. Corban

Aerospace Engineering Department
Georgia Institute of Technology, Atlanta, Georgia

Presented at the AIAA Guidance, Navigation and Control Conference
New Orleans, Luisiana, August 12-14, 1991

Abstract

This paper proposes a systematic approach for identifying the perturbation parameter in singular perturbation analysis of aircraft optimal guidance, and in particular considers a family of problems related to aircraft energy climbs. It is first shown that for energy climbs that take place on a vertical plane the singular perturbation parameter can always be taken to be the maximum allowed longitudinal loading factor of the vehicle. Two time scale behavior is suggested according to whether this parameter is sufficiently less than one. The approach, which is based on a nondimensionalization of the equations of motion, is then used to evaluate the appropriateness of forced singular perturbation formulations used in the past for transport and fighter aircraft, and to assess the applicability of energy state approximations and singular perturbation analysis for airbreathing transatmospheric vehicles with hypersonic cruise and orbital capabilities.

Introduction

The methods of matched asymptotic analysis in singular perturbation theory are based on the presence of small parameters in the differential equations of motion which give rise to multiple time scale behavior. It has been noted by several authors[1,2] that, in spite of a wide number of papers attesting to the applicability of singular perturbation methods to optimization problems in aircraft flight mechanics, few have been successful in first casting the equations of motion in a singular perturbation form. A few notable exceptions are Refs. 1-4. In Ref. 1 two methods for time scale separation analysis are proposed to identify the proper assignment of state variables to various time scales. These methods are based on forming an estimate of the state variable speeds. In Ref. 2 a rescaling to nondimensional variables is recommended. However, it is noted that the proper scaling transformation is not obvious, even if the time scale separation of the variables is well known from analysis or experience. Both of these papers (and in particular Ref. 1) provide extensive references to earlier studies which employ so-called forced singular perturbation formulations, in which the perturbation parameter (say ε), nominally equal to 1, is artificially introduced as a book keeping parameter in a formal expansion of the solution about $\varepsilon = 0$. In particular, there exists a large number of publications on the optimization of aircraft energy climbs (see

for example References 5-8), none of which make any attempt to identify an appropriate perturbation parameter in terms of the original problem parameters. This is particularly disturbing considering the number of years that have passed since such analysis techniques were first introduced in the flight mechanics literature. In any singular perturbation analysis, every attempt should be made to identify the perturbation parameter in terms of the original problem parameters (which in general include the boundary conditions) so that the physical process that gives rise to the two time scale behavior is clearly understood. Then, the range of parameter values for which the perturbation analysis is valid can be easily identified. Knowledge of time scale separability present in the system dynamics, and success in exploiting this characteristic to obtain approximate solutions, is not, in itself justification for artificially introducing ϵ. That is, within the framework of our system of logic it is always possible to have conclusions that are *true*, which follow from assumptions that are *wrong*.

In this note we attempt to partially rectify this situation by presenting a systematic (albeit still ad-hoc) approach to nondimensionalize variables in nonlinear optimization problems in flight mechanics. Most of the considerations that are presented apply in other fields as well. Our main motivation for collecting and stating these considerations is to define the thought process by which it is possible to arrive at a suitable scaling of the aircraft energy climb problem. Of particular interest is an assessment of the applicability of energy state approximations and singular perturbation analysis for airbreathing transatmospheric vehicles with hypersonic cruise and orbital capabilities.

Subsonic-Supersonic Regimes, Flat Earth Approximation

Consider atmospheric flight of a conventional aircraft, viewed as a point mass, in a vertical plane over a flat Earth. The equations governing such flight can be reduced to a three-state model in: mass specific energy E, flight path angle γ, and altitude h. The vehicle mass, m, is assumed to be constant. The equations are:

$$\frac{dE}{dt} = \frac{V(T - D)}{m} \tag{1}$$

$$\frac{d\gamma}{dt} = \left(\frac{L}{mV}\right) - \left(\frac{g \cos \gamma}{V}\right) \tag{2}$$

$$\frac{dh}{dt} = V \sin\gamma \tag{3}$$

where L, D and g denote the lift, the drag and the (constant) gravitational acceleration. It is assumed that the atmosphere is stationary, and that the thrust, T, is directed along the flight path. The specific energy (mechanical energy per unit mass of the vehicle) E and the speed V are related by

$$E = \frac{V^2}{2} + gh \tag{4}$$

and E rather than V has been employed as a state variable.

In many of the earlier singular perturbation studies the traditional way of writing down Eqs. (2) and (3) was:

$$\varepsilon\frac{d\gamma}{dt} = \left(\frac{L}{mV}\right) - \left(\frac{g\cos\gamma}{V}\right) \tag{5}$$

$$\varepsilon\frac{dh}{dt} = V \sin\gamma \tag{6}$$

that is, by artificially introducing a parameter ε and then stating that its nominal value was equal to 1. Since our main purpose in the present paper is to avoid such an artificial introduction at the outset, Eqs. (5) and (6) will serve only as a guide for the natural introduction of ε.

Nondimensional form

The first step is to put Eqs. (1) through (3) in nondimensional form. To this end we define the set S

$$S \equiv \{t_0, E_0, h_0, V_0, T_0, D_0, L_0\} \tag{7}$$

The elements of the set S are at this point *arbitrary positive quantities*, and the only restriction that we impose upon them is that:

t_0 has dimensions of time

E_0 has dimensions of energy per unit mass

h_0 has dimensions of lenght

V_0 has dimensions of speed

T_0, D_0, and L_0 have dimensions of force

Using the elements of S to define the nondimensional quantities:

$$t = \frac{t}{t_0} \; ; \; E = \frac{E}{E_0} \; ; \; h = \frac{h}{h_0} \; ; \; V = \frac{V}{V_0} \tag{8}$$

$$T = \frac{T}{T_0} \; ; \; D = \frac{D}{D_0} \; ; \; L = \frac{L}{L_0} \tag{9}$$

Eqs. (1) through (3) can be put into the following nondimensional form:

$$\frac{dE}{dt} = V(TT_0 - DD_0)\left(\frac{t_0 V_0}{E_0 m}\right) \tag{10}$$

$$\frac{d\gamma}{dt} = \left(\frac{L}{V}\right)\left(\frac{L_0 t_0}{m V_0}\right) - \left(\frac{\cos\gamma}{V}\right)\left(\frac{g\, t_0}{V_0}\right) \tag{11}$$

$$\frac{dh}{dt} = \left(\frac{V_0 t_0}{h_0}\right) V \sin\gamma \tag{12}$$

The goal is now to put Eqs. (10) through (12) in the traditional singular perturbation format. We thus multiply both sides of Eqs. (11) and (12) by $(h_0 / V_0 t_0)$. This results in:

$$\left(\frac{h_0}{V_0 t_0}\right)\frac{d\gamma}{dt} = \left(\frac{L}{V}\right)\left(\frac{L_0 h_0}{m V_0^2}\right) - \left(\frac{\cos\gamma}{V}\right)\left(\frac{g\, h_0}{V_0^2}\right) \tag{13}$$

$$\left(\frac{h_0}{V_0 t_0}\right)\frac{dh}{dt} = V \sin\gamma \tag{14}$$

Comparing the set of Eqs. (10), (13) and (14) with the set (1), (5) and (6), it is evident that we can make the two sets similar by imposing the following *four* conditions on the elements of the set S:

$$T_0 = D_0 \tag{15}$$

$$\frac{T_0 t_0 V_0}{E_0 m} = 1 \tag{16}$$

$$\frac{L_0 h_0}{m V_0^2} = 1 \tag{17}$$

$$\frac{g h_0}{V_0^2} = 1 \tag{18}$$

If we *define* ε as

$$\varepsilon \equiv \frac{h_0}{V_0 t_0} \tag{19}$$

then, Eqs. (10), (13) and (14) assume the form:

$$\frac{dE}{dt} = V(T - D) \tag{20}$$

$$\varepsilon \frac{d\gamma}{dt} = \left(\frac{L - \cos\gamma}{V}\right) \tag{21}$$

$$\varepsilon \frac{dh}{dt} = V \sin\gamma \tag{22}$$

To summarize, it was shown in the present section that it is possible to introduce a parameter ε naturally into the equations of motion (Eqs. (1) - (3)) by first introducing a set of arbitrary positive quantities S (see Eq. (7)) to scale the variables of interest, and then by imposing *four* conditions (Eqs. (15) - (18)) on these quantities so that the resulting nondimensional equations assume the traditional singular perturbation form (Eqs. (20) - (22)). Note that only one of the arbitrary quantities in S is uniquely determined at this point. Combining Eqs. (17) and (18) it follows that

$$L_0 = m g \tag{23}$$

Specifying a particular nondimensional form

As shown in the previous section, only *four* conditions are imposed on the *seven* elements of the set S in transforming the equations of motion to the traditional singular perturbation format. This means that we can specify three of the elements of S to fit our convenience and then determine the remaining four using Eqs. (15)-(18). The first conclusion therefore is that in general the value of ε is *quite arbitrary*. For example, by choosing h_0 , V_0 and t_0 in two different ways ε can be made arbitrarily small or large. The separability of the time scales on the other hand is a property of the system and not of the particular nondimensional form of the equations of motion that is chosen. We therefore expect that if the

system does indeed have this property it will exhibit it no matter what the actual value of ε is. This is precisely the reason for the success of so many singular perturbation treatments of the past in which ε was introduced artificially and its nominal value was said to be fixed at one.

Although there is no unique way of specifying a particular nondimensional form of the equations of motion, we will now argue that there is one that results in additional physical insight. First, in order to maintain the relationship in Eq. (4) in the transformed variables, a *fifth* condition is introduced

$$E_0 = g h_0 \tag{24}$$

which together with Eq. (18) gives

$$E = \frac{V^2}{2} + h \tag{25}$$

Using Eqs. (16) and (24) in Eq. (19) it follows that

$$\varepsilon = \frac{T_0}{m g} \tag{26}$$

It is now evident that only *two* among the *seven* elements of the set S need to be specified. Then, the five conditions, Eqs. (15) - (18) and (24), uniquely determine the remaining elements.

Eq. (26) implies that ε depends *only* on T_0 and is independent of the value of the remaining elements of S. The question therefore arises naturally as to whether there is a particular choice of T_0 for which the resulting value of ε can be used as a strict criterion for the applicability of a singular perturbation analysis to Eqs. (20)-(22). The answer to this question is negative because, in a given time interval, it is the *relative magnitudes* of the three quantities

$$\frac{dE}{dt}, \quad \frac{d\gamma}{dt}, \quad \frac{dh}{dt}$$

and the *boundary conditions* of interest that determine the validity of a singular perturbation analysis. Specifically, for an aircraft to exhibit the well-known two-time-scale behavior in a given time interval, it is necessary that:

$$\frac{dE}{dt} \ll \frac{d\gamma}{dt} \tag{27}$$

$$\frac{dE}{dt} \ll \frac{dh}{dt} \tag{28}$$

in that interval, and that the required change in E is sufficiently large to permit the boundary layer responses in h and γ to reach their equilibrium values. Hence, the very question is whether or not the net change in E during the boundary layer response is sufficiently small to permit approximating E as a constant (to zero order in ε) in the boundary layer analysis. In addition, we are interested in knowing if this two-time-scale property is a consequence of the inherent dynamics of the aircraft, and not a consequence of using a high gain control solution for L. Therefore, we assume that the L resulting from the boundary layer analysis is of order one in Eq. (21).

Under the above assumptions, there is a choice for T_0 for which the value of ε can be used as a measure for the *existence* of time intervals in which two-time-scale behavior is exhibited. If the choice of T_0 is such that dE/dt is at most of the same order of magnitude as $\varepsilon d\gamma/dt$ and $\varepsilon dh/dt$, then, a value of ε sufficiently less than one indicates the possible existence of such intervals. By suitably choosing V_0 we can restrict V to be of order one. Then, for the choice

$$T_0 = (T - D)_{max} \tag{29}$$

dE/dt is of order one, and both $d\gamma/dt$ and dh/dt are of order $1/\varepsilon$. For this choice of T_0 , ε is given by

$$\varepsilon = \frac{(T - D)_{max}}{m\,g} \tag{30}$$

and is equal to the maximum longitudinal loading factor of the vehicle.

Note that Eq. (30) actually represents an *upper bound* for ε since it is obtained by selecting the flight condition where the difference between thrust and drag, T-D, reaches a maximum. The logical choice for V_0 is the speed at this flight condition. One can also adopt the viewpoint of evaluating ε along the energy climb path that results from a reduced solution. The value of ε as a function of E can then be used as a measure to distinguish energy levels where a singular perturbation analysis may be appropriate from other levels where it may not be valid.

It is interesting to note that a good deal can be anticipated from Eq. (30) for conventional aircraft without exact numerical evaluation: $(T\text{-}D)_{max}$ divided by mg is approximately equal to $\sin\gamma_{max}$ where

γ_{max} is the maximum climb angle that can be maintained at a given energy level without loss of airspeed. It follows therefore that $\varepsilon<1$ for all such aircraft types. For transport aircraft $\sin\gamma_{max}$ is approximately 0.1, while for fighter aircraft $\sin\gamma_{max}$ is approximately 0.8. This suggests that the forced singular perturbation analysis used in the past studies of optimal aircraft trajectories is valid for most conventional subsonic and supersonic aircraft.

Eq. (30) can also be used to estimate ε in terms of the quantities $(T/mg)_{max}$ and $(L/D)_{max}$ for a given aircraft. Since L is less than or equal to mg along the energy climb path, it follows that a second *upper bound* for ε is given by

$$\varepsilon < \varepsilon_{UB} \tag{31}$$

where ε_{UB} is defined as

$$\varepsilon_{UB} \equiv \left[(T/mg)_{max} - 1/(L/D)_{max}\right] \tag{32}$$

Estimates of ε_{UB} are given in Table 1.

Table 1

Estimation of ε_{UB} based on Eq. (32)

Parameter	Transports	Fighters
$(T/mg)_{max}$	0.25	0.90
$(L/D)_{max}$	13 – 15	4 – 7
ε_{UB}	0.17 – 0.18	0.65 – 0.76

Hypersonic Regime

Consider the flight of a hypersonic and possibly transatmospheric vehicle, viewed as a point mass, in a vertical plane over a *spherical non-rotating* Earth. The equations governing such flight can be reduced to a four-state model in E, m, γ and radial distance from the center of the Earth, r. The equations are:

$$\frac{dE}{dt} = \frac{V(\eta T - D)}{m} \tag{33}$$

$$\frac{dm}{dt} = -f(r, V, \eta) \tag{34}$$

$$\frac{d\gamma}{dt} = \left(\frac{L}{mV}\right) - \left(\frac{\mu \cos \gamma}{Vr^2}\right) + \left(\frac{V \cos \gamma}{r}\right) \tag{35}$$

$$\frac{dr}{dt} = V \sin \gamma \tag{36}$$

where T is the maximum available thrust at a given speed and altitude. The control variables are L and η, where $0<\eta<1$ is introduced as a nondimensional throttling variable. E and V are now related by

$$E = \frac{V^2}{2} - \frac{\mu}{r} \tag{37}$$

Note again that in earlier singular perturbation studies[9], the traditional way of writing down Eqs. (35) and (36) was:

$$\varepsilon \frac{d\gamma}{dt} = \left(\frac{L}{mV}\right) - \left(\frac{\mu \cos \gamma}{Vr^2}\right) + \left(\frac{V \cos \gamma}{r}\right) \tag{38}$$

$$\varepsilon \frac{dr}{dt} = V \sin \gamma \tag{39}$$

that is, by artificially introducing a parameter ε and then stating that its nominal value was equal to 1. Again, in order to avoid this artificial introduction, Eqs. (38) and (39) will serve only as a guide for the natural introduction of ε.

Nondimensional Form

In order to put Eqs. (33) through (36) in nondimensional form we now define the set of *arbitrary positive quantities*

$$S \equiv \{t_0, E_0, m_0, r_0, V_0, f_0, T_0, D_0, L_0\} \tag{40}$$

and impose the restrictions that:

t_0 has dimensions of time

E_0 has dimensions of energy per unit mass

m_0 has dimensions of mass

r_0 has dimensions of lenght

V_0 has dimensions of speed

f_0 has dimensions of mass per unit time

T_0, D_0, and L_0 have dimensions of force

Using the elements of S to define the nondimensional quantities:

$$t = \frac{t}{t_0} \; ; \; E = \frac{E}{E_0} \; ; \; m = \frac{m}{m_0} \; ; \; r = \frac{r}{r_0} \; ; \; V = \frac{V}{V_0} \tag{41}$$

$$f = \frac{f}{f_0} \; ; \; T = \frac{T}{T_0} \; ; \; D = \frac{D}{D_0} \; ; \; L = \frac{L}{L_0} \tag{42}$$

Eqs. (33) through (36) can be put into the following nondimensional form:

$$\frac{dE}{dt} = \frac{V(\eta T T_0 - D D_0)}{m}\left(\frac{t_0 V_0}{E_0 m_0}\right) \tag{43}$$

$$\frac{dm}{dt} = -\left(\frac{f_0 t_0}{m_0}\right) f(r, V, \eta) \tag{44}$$

$$\frac{d\gamma}{dt} = \left(\frac{L}{mV}\right)\left(\frac{L_0 t_0}{m_0 V_0}\right) - \left(\frac{\cos\gamma}{Vr^2}\right)\left(\frac{\mu t_0}{V_0 r_0^2}\right) + \left(\frac{V\cos\gamma}{r}\right)\left(\frac{V_0 t_0}{r_0}\right) \tag{45}$$

$$\frac{dr}{dt} = \left(\frac{V_0 t_0}{r_0}\right) V \sin\gamma \tag{46}$$

In order to put Eqs. (43) through (46) in the traditional singular perturbation format, we multiply both sides of Eqs. (45) and (46) by $(r_0 / V_0 t_0)$. This results in:

$$\left(\frac{r_0}{V_0 t_0}\right)\frac{d\gamma}{dt} = \left(\frac{L}{mV}\right)\left(\frac{L_0 r_0}{m_0 V_0^2}\right) - \left(\frac{\cos\gamma}{Vr^2}\right)\left(\frac{\mu}{V_0^2 r_0}\right) + \left(\frac{V\cos\gamma}{r}\right) \tag{47}$$

$$\left(\frac{r_0}{V_0 t_0}\right)\frac{dr}{dt} = V \sin\gamma \tag{48}$$

Comparing the set of Eqs. (43), (44), (47) and (48) with the set (33), (34), (38) and (39) results in the following *five* conditions on the elements of the set S:

$$T_0 = D_0 \tag{49}$$

$$\frac{T_0 t_0 V_0}{E_0 m_0} = 1 \tag{50}$$

$$\frac{f_0 t_0}{m_0} = 1 \tag{51}$$

$$\frac{L_0 r_0}{m_0 V_0^2} = 1 \tag{52}$$

$$\frac{\mu}{V_0^2 r_0} = 1 \tag{53}$$

By defining

$$\varepsilon \equiv \frac{r_0}{V_0 t_0} \tag{54}$$

Eqs. (43), (44), (47) and (48) assume the traditional singular perturbation form:

$$\frac{dE}{dt} = \frac{V(\eta T - D)}{m} \tag{55}$$

$$\frac{dm}{dt} = - f(r, V, \eta) \tag{56}$$

$$\varepsilon \frac{d\gamma}{dt} = \left(\frac{L}{mV}\right) - \left(\frac{\cos \gamma}{Vr^2}\right) + \left(\frac{V \cos \gamma}{r}\right) \tag{57}$$

$$\varepsilon \frac{dr}{dt} = V \sin \gamma \tag{58}$$

Specifying a particular nondimensional form

For the hypersonic case only *five* conditions on the *nine* elements of the set S are needed in order to put the equations of motion in the traditional singular perturbation format. Thus, we can specify four of the elements of S to fit our convenience and then determine the remaining five using Eqs. (49) - (53).

Again, in order to maintain the relationship in Eq. (37) in the transformed variables, a *sixth* condition is introduced

$$E_0 = \frac{\mu}{r_0} \tag{59}$$

which together with Eq. (53) gives

$$E = \frac{V^2}{2} - \frac{1}{r} \tag{60}$$

If we think of r_0 as a radial distance, then Eq. (53) restricts V_0 to be the circular orbital speed at r_0. Similarly, Eq. (52) restricts L_0 to be the centrifugal force that a point mass m_0 would experience in a circular orbit at r_0. Using Eqs. (50), (53), and (59) we have

$$\varepsilon = \frac{T_0 r_0^2}{\mu m_0} \tag{61}$$

Hence, by picking *three* among the *nine* elements of the set S arbitrarily, the six conditions Eqs. (49) - (53), and (59) uniquely determine the remaining elements.

The question arises again as to whether there is a particular choice for these three elements for which the resulting value of ε can be used as a measure for the applicability of a singular perturbation analysis to Eqs. (55)-(58). The right-hand-side of Eqs. (55) and (58) can be made of the same order of magnitude by choosing the ratio T_0/m_0 as

$$\frac{T_0}{m_0} = \left(\frac{\eta T - D}{m}\right)_{max} \tag{62}$$

Choosing r_0 as the sea level radius r_{SL}, r and V are of order one. Also, for these choices of T_0/m_0 and r_0, dE/dt is of order one, and both $d\gamma/dt$ and dr/dt are of order $1/\varepsilon$. By choosing f_0 as the value of f at the flight condition where the ratio $(\eta T - D)/m$ is a maximum, dm/dt can also be made of order one. With the above choices of T_0/m_0, r_0, and f_0

$$\varepsilon = \left(\frac{r_{SL}^2}{\mu}\right)\left(\frac{\eta T - D}{m}\right)_{max} \tag{63}$$

The right-hand-side of Eq. (63) is the maximum longitudinal loading factor of the vehicle in units of sea-level g's, and actually represents an *upper bound* for ε since it is obtained by selecting the flight condition where $(\eta T - D)/m$ reaches a maximum. One can again adopt the viewpoint of evaluating ε along the energy climb path that results from the reduced solution. The value of ε as a function of E can then be

used as a measure to distinguish energy levels where a singular perturbation analysis may be appropriate, from other levels where it may not be valid.

A hypersonic flight vehicle employing an airbreathing propulsion system and sized for acceleration to orbital velocity necessarily employs a multimode propulsion system. An example might include turbojet, ramjet, scramjet, and rocket modes. Each mode of propulsion can be characterized by a corresponding ε. Current models of this vehicle type exhibit large values of excess thrust at low hypersonic Mach numbers. In fact, Eq. (63) will produce an ε that is greater than one over such flight phases. Experience with hypersonic vehicle dynamics reported in Ref. 10 indeed suggests that the assumed time scale separation is not valid in these phases. However, over the majority of the trajectory, Eq. (63) results in an ε that is less than one just as in the Flat Earth, Subsonic-Supersonic case.

Numerical validation

It was shown in the preceding sections that for aircraft energy climbs that take place in a vertical plane, the singular perturbation parameter ε can always be identified as the maximum longitudinal loading factor of the vehicle, measured in units of sea-level g's. In order to further explore the implications of this result, numerical evaluations of ε will be presented in this section for several types of vehicles.

The idea that the authors would like to introduce at this point is that in general, for a given aircraft, it may be sufficient to evaluate an *upper bound* for ε, valid for the entire envelope, in order to get a hint for the possible two-time-scale behavior of the aircraft in question. If the resulting value of this upper bound is less than one, then, two-time-scale behavior is implied for any energy climb that the aircraft is allowed to perform. If however the resulting value of the upper bound turns out to be greater than one, then no conclusion can be drawn. The way to proceed in this latter case would be to evaluate a less conservative upper bound for ε and apply the same reasoning. As it turns out, the less conservative the upper bound, the more work one has to perform in order to evaluate it. If all the upper bounds for ε, evaluated for the entire envelope fail to yield any conclusions, the reasonable thing to do next is to evaluate ε as a function of the energy E using all the assumptions made in the evaluation of reduced

solutions in aircraft energy climbs (γ=0,L=mg etc.). By evaluating in this sense, and at each energy level the absolute maximum value of the longitudinal loading factor we obtain a curve C on the ε-E plane. The interesting properties of this curve are that for a given aircraft it need only be constructed once and that it lies above all other curves that may be evaluated similarly, but along the reduced solutions corresponding to *specific* problems. In other words, points on curve C represent *upper bounds* for ε at the corresponding energy levels. The portions therefore of curve C where ε is less than one immediately show the energy levels where two-time-scale behavior (boundary layer transitions along constant E) can be expected. If there are any portions of curve C where ε is greater than one, then no conclusions can be drawn as to the possible two-time-scale behavior at the corresponding energy levels. In the latter case one has again to evaluate a less conservative upper bound for ε at these energy levels. Such less and less conservative upper bounds would of course eventually lead to the maximum value of the longitudinal loading factor evaluated as a function of E along the reduced solution corresponding to a *specific* problem.

It should be clear now that if we are interested in the possible two-time-scale behavior of a vehicle along a particular trajectory (corresponding to a specific problem) then the *least* conservative upper bound for ε would be the maximum longitudinal loading factor encountered along that (exact) trajectory. Calculating this upper bound would not be very useful since it would require the actual computation of the trajectory first. The idea presented above suggests that there may be a hope of avoiding this by starting with a more conservative upper bound, and proceeding with less and less conservative upper bounds.

In order to demonstrate the above ideas in practice, numerical evaluations of ε are presented in Figs. 1-8 for four types of vehicles. For each type there is one plot showing the variation of the *maximum* longitudinal loading factor of the vehicle with energy E, and one or more plots showing the variation of the longitudinal loading factor with E along the reduced solution corresponding to a specific optimization problem.

Figs. 1 and 2 show the results for an F-8 fighter[10]. The two optimization problems considered for this case were minimum time to a specified energy and minimum time to a specified downrange position.

The reduced solutions corresponding to these problems are obtained by maximizing (with respect to V) at each energy level the quantities (T-D)V for the former and $[(T-D)V]/(V_0-V)$ for the latter, where V_0 is the maximum possible cruising speed of the aircraft and D is calculated at L=mg. Fig. 1 shows the actual paths in the envelope corresponding to these reduced solutions and to the maximum longitudinal loading factor of F-8. Fig. 2 shows the results for ε evaluated along these climb paths. Since the maximum longitudinal loading factor of F-8 stays always below one in Fig. 2, it is reasonable to assume that for a any optimization problem, if the required energy gain is sufficient, the transitions to the reduced solution will take place at nearly constant E, exhibiting the well known boundary layer structure.

Figs. 3 and 4 show similar results for an F-15 fighter[11]. The two optimization problems considered in this case were again minimum time to a specified energy and minimum time to a specified downrange position. A maximum dynamic pressure constraint of 1500 lbf per square feet is imposed on the climb paths for this case. Due to the large thrust to weight ratio of F-15, the ε levels in Fig. 4 are much higher than the ones corresponding to F-8 (compare with Fig. 2). In particular there is a small region at low energy where ε exceeds one, implying that two time scale separation at these energy levels may not be appropriate for the above two optimization problems.

Figs. 5 and 6 show the results for a conventional transport[12]. In this case however, the two optimization problems considered were minimum fuel to a specified energy and minimum fuel to a specified downrange position. The reduced solutions corresponding to these problems are obtained by maximizing (with respect to V and η) at each energy level the quantities $[(T-D)V]/f$ for the former and $[(T-D)V]/(fV_0-f_0V)$ for the latter, where V_0 is the most fuel efficient cruising speed of the aircraft and f_0 is the fuel consumption rate at this cruising flight condition[7]. It is interesting to note the very low levels of ε in Fig. 6 (compare with Figs. 2 and 4), suggesting two time scale behavior for the entire envelope.

Finally, Figs. 7 and 8 show the results for a hypersonic vehicle model, used by NASA and called "the Langley Accelerator"[13]. The only optimization problem considered in this case was minimum fuel to a specified energy, the reduced solution corresponding to which is obtained by maximizing the quantity $[(\eta T-D)V]/(mf)$ at each energy level (mass is not constant in this case). A maximum dynamic pressure constraint of 2000 lbf per square feet is imposed on the climb paths for this case. This particular vehicle

model employs a multimode propulsion system, sized for acceleration to orbital velocity and consisting of turbojet, ramjet, scramjet, and rocket cycles. Note that Figs. 7 and 8 correspond to a nonoptimal switching between the different propulsion cycles. Specifically, we first assume allowable operating ranges for the different propulsion cycles (expressed as bounds on the Mach number), and then, at each energy level we pick the cycle that maximizes $[(\eta T-D)V]/(mf)$ and $(\eta T-D)/m$. The switching therefore from one cycle of propulsion to the other is abrupt, with no overlap. The actual points of cycle transitions are also shown in the figures. Note also that in Fig. 8 ε is plotted against the speeds at which the constant energy contours intersect the zero altitude axis. The reason for this is that E is negative in this case. The actual value of ε is likely to be much lower if a practical method for cycle transition is employed. Note finally that as the energy levels get higher and higher we approach the boundary of the envelope and ε goes to zero. This is basically a characteristic of all aircraft (see also Figs. 2, 4, and 6) suggesting that the transitions to the reduced solution can be treated as boundary layers more succesfully at high energy levels than at low ones. The physical explanation for this comes from the behavior of the difference between the thrust T and the drag D. At low energy levels both the speed and altitude are low, implying that the thrust is high and the drag is low, so that T-D is high and can be used to change the energy during a transition. At high energy levels on the other hand either the speed or the altitude or both are high, implying that the difference T-D is low. Thus, transitions to the reduced solution at high energy levels can be expected to occur more or less by interchanging kinetic for potential energy (or vice versa), with the total energy staying nearly constant.

Conclusions

For both the conventional (subsonic-supersonic, flat Earth) and the transatmospheric (hypersonic, spherical Earth) flight regimes a systematic procedure was introduced to identify naturally a singular perturbation parameter ε in the differential equations of motion. The procedure consists of using a set of arbitrary scaling constants to nondimensionalize all the variables of interest and then applying a set of conditions on these constants to put the resulting nondimensional equations of motion in the traditional singular perturbation format. Because the number of conditions is less than the number of constants, the

scaling constants cannot be uniquely specified. Thus, the resulting expression for ε is in general quite arbitrary. There is, however, a particular choice of the scaling constants for which the values of the resulting ε can serve as a hint for a possible two-time-scale behavior of the aircraft in question. The primary result of the paper is the demonstration that for this "useful" choice of the scaling constants the resulting ε is always equal to the maximum longitudinal loading factor of the vehicle, measured in units of g's. Two time scale behavior is suggested according to whether ε is less than one or not. Based on this result it is straightforward to see why singular perturbation methods applied to aircraft performance optimization problems have worked so well in the past. The maximum longitudinal loading factors associated with the majority of conventional aircraft are either less than one because the aircraft lack very high thrusting capabilities, or because they are restricted to be so for other reasons (structural, comforting, etc.). A few notable exceptions do occur for some modern fighters. This directly suggests that most conventional aircraft can be expected to exhibit two-time-scale behavior for almost any energy climb that they are *allowed* to perform. This then appears to be the reason for the past success of so many singular perturbation treatments of aircraft energy climbs. The implication for transatmospheric vehicles is rather direct. If we consider such a vehicle as a passenger transport, then, in order to assure passenger comfort it is only natural to *impose* as a constraint a maximum longitudinal loading factor for the vehicle that is less than one. Our work suggests that such a constraint would imply two-time-scale behavior for any type of energy climb that such a vehicle would be allowed to perform. Therefore, singular perturbation formulations of such maneuvers still appear to be promising, even with all the added complexities that the flight regimes of such vehicles can entail.

Acknowledgement

This research was supported by NASA Langley Research Center under Grant No. NAG-1-922. The NASA technical monitor is Dr. Dan Moerder.

References

1. Ardema, M. D., "Separation of Time Scales in Aircraft Trajectory Optimization," AIAA Journal of Guidance and Control, Vol. 8, No. 2, March-April 1985.

2. Shinar, J., "On Applications of Singular Perturbation Techniques in Nonlinear Optimal Control," *Automatica*, Vol. 19, No. 2, 1983.

3. Breakwell, J. V., "Optimal Flight-Path Angle Transitions in Minimum-Time Airplane Climbs," Journal of Aircraft, Vol. 14, August 1977.

4. Calise, A. J., "Optimal Thrust Control with Proportional Navigation Guidance," AIAA Journal of Guidance and Control, Vol. 3, No. 4, July-August 1980.

5. Kelley, H. J. and Edelbaum, T. N., "Energy Climbs, Energy Turns, and Asymptotic Expansions," Journal of Aircraft, Vol. 7, Jan-Feb 1970.

6. Ardema, M. D., "Solution of the Minimum Time-to-Climb Problem by Matched Asymptotic Expansions," AIAA Journal, Vol. 14, No. 7, July 1976.

7. Calise, A. J., "Extended Energy Management Methods for Flight Performance Optimization," AIAA Journal, Vol. 15, No. 3, March 1977.

8. Calise, A. J., "Singular Perturbation Techniques for On-Line Optimal Flight-Path Control," AIAA Journal of Guidance and Control, Vol. 4, No. 4, July-August 1981.

9. Corban, J. E., Calise, A. J., and Flandro, G. A., "Rapid Near-Optimal Trajectory Generation for Single-Stage-to-Orbit Airbreathing Vehicles," To appear in the *AIAA Journal of Guidance, Control and Dynamics*.

10. Calise, A. J., and Moerder, D. D., "Singular Perturbation Techniques for Real Time Aircraft Trajectory Optimization and Control," NASA CR-3597, August 1982.

11. Calise, A. J., and Pettengil, J. B., "A Comparison of Time-Optimal Intercept Trajectories for the F-8 and F-15 - Final Report," NASA Grant No. NCC 2-506, January 1990.

12. Barman, J. F., and Erzberger, H., "Fixed-Range Optimum Trajectories for Short-Haul Aircraft," Journal of Aircraft, Vol. 13, No. 10, October 1976.

13. Corban, J. E., "Real-Time Guidance and Propulsion Control for Single-Stage-to-Orbit Airbreathing Vehicles," Ph.D. Dissertation, The Georgia Institute of Technology, December 1989.

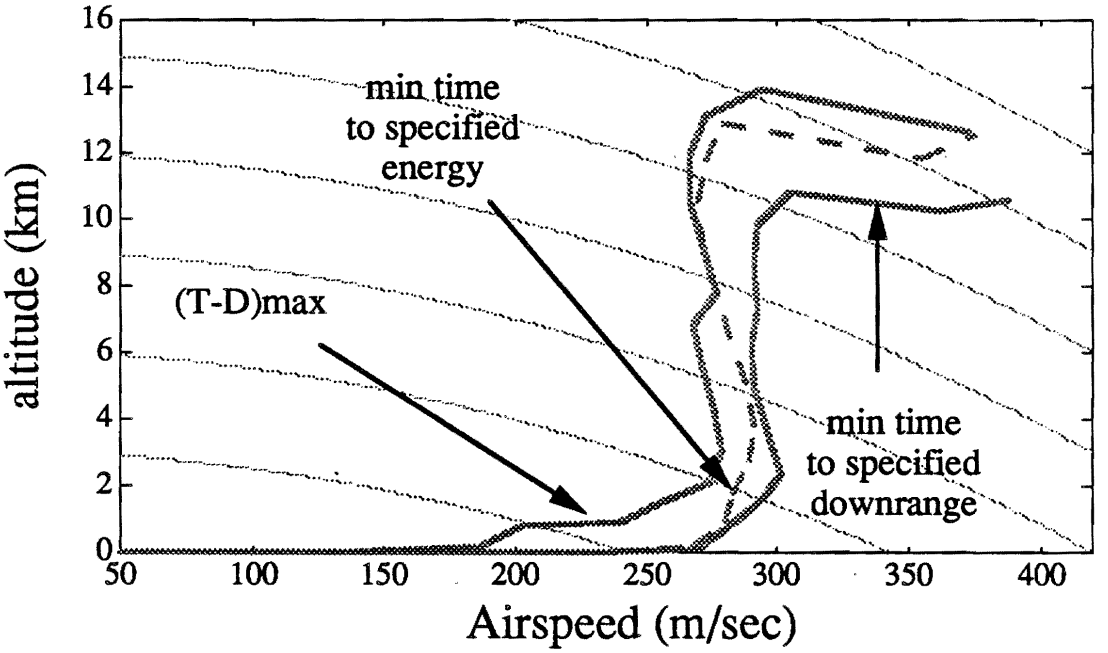

Fig. 1 Energy climb paths for an F-8 aircraft

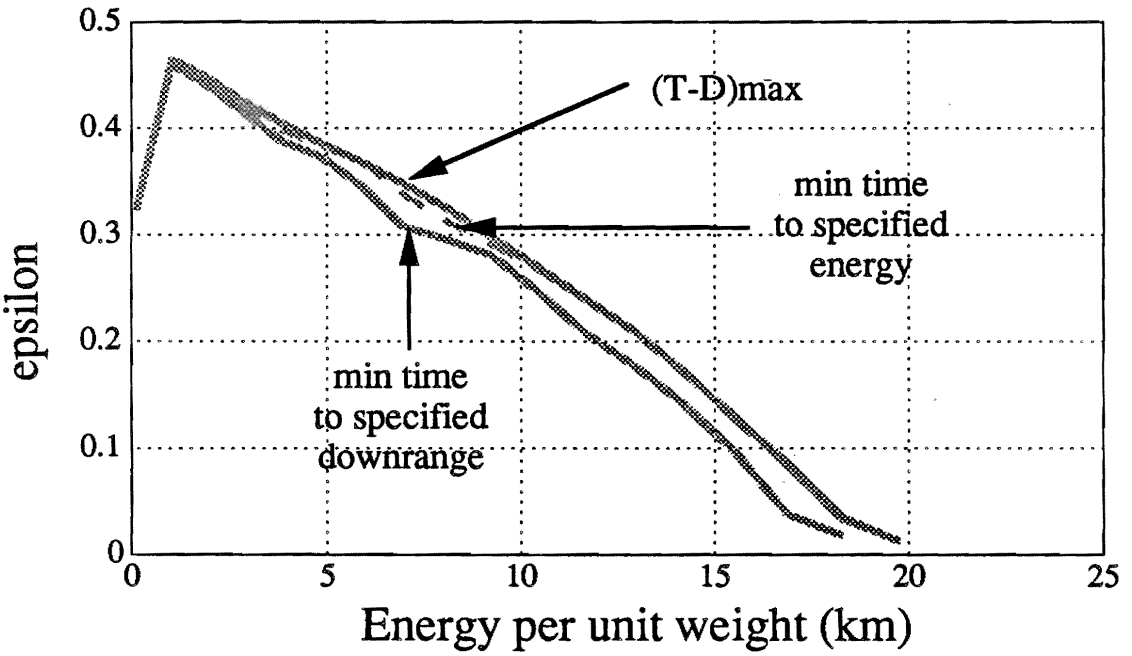

Fig. 2 Evaluation of ε(E) for an F-8 aircraft

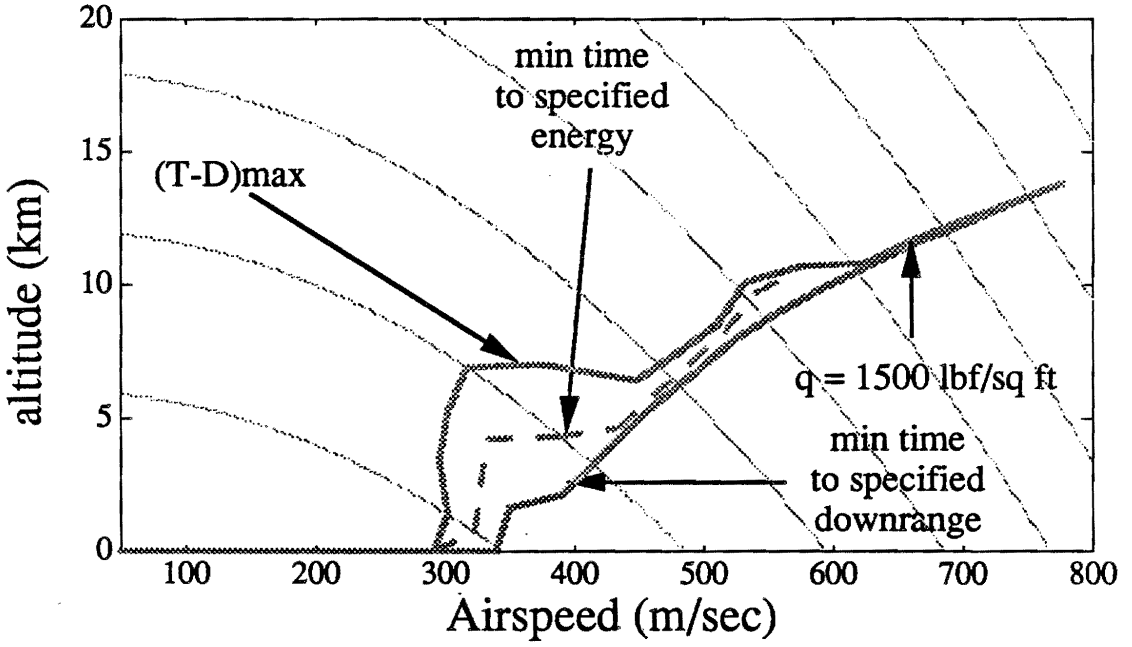

Fig. 3 Energy climb paths for an F-15 aircraft

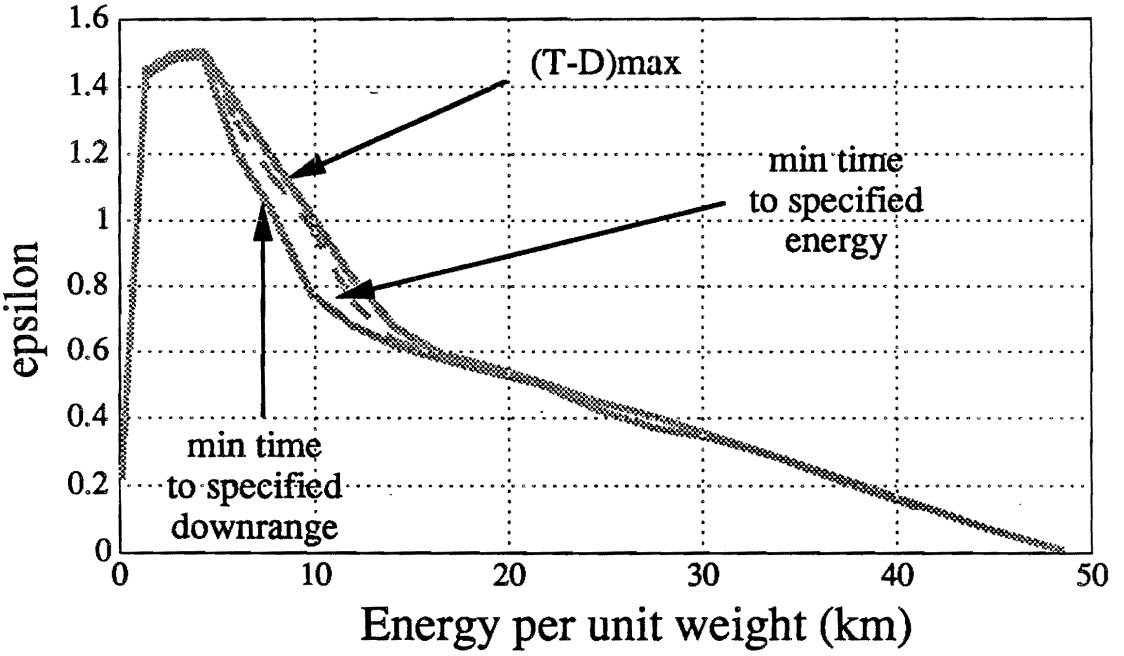

Fig. 4 Evaluation of ε(E) for an F-15 aircraft

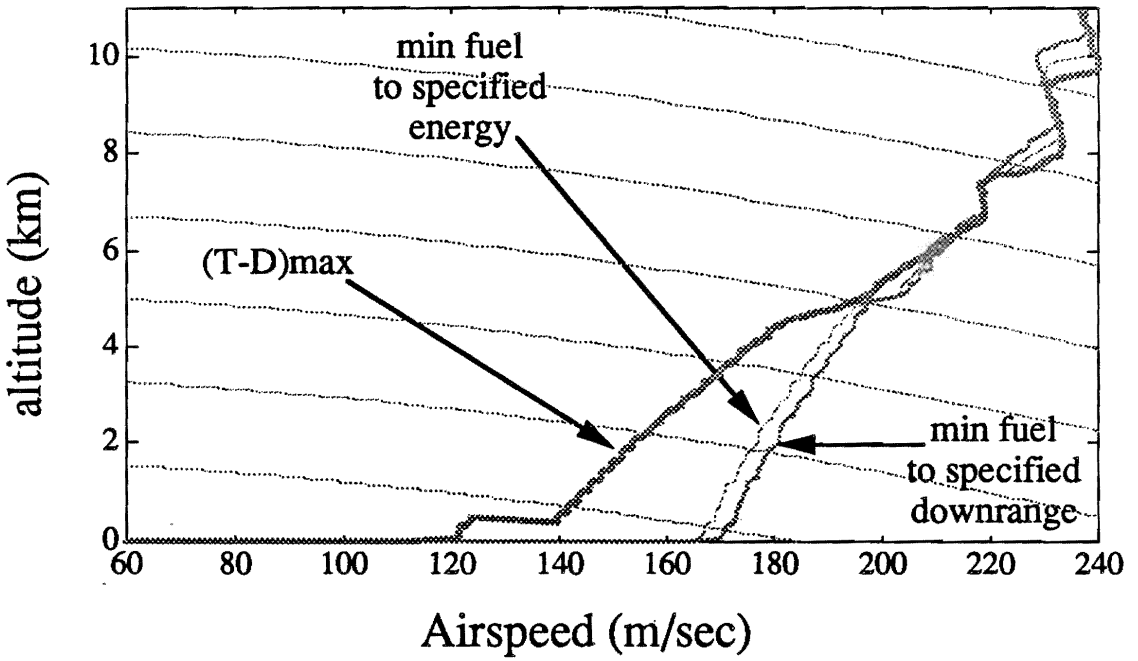

Fig. 5 Energy climb paths for a short-haul transport aircraft

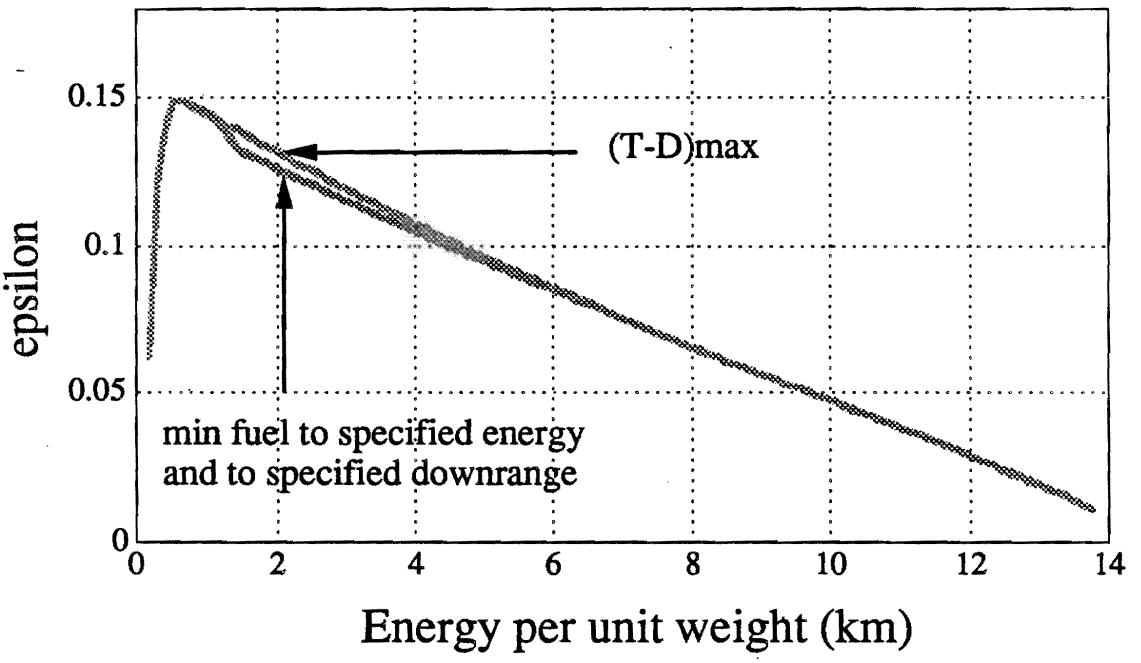

Fig. 6 Evaluation of ε(E) for a short-haul transport aircraft

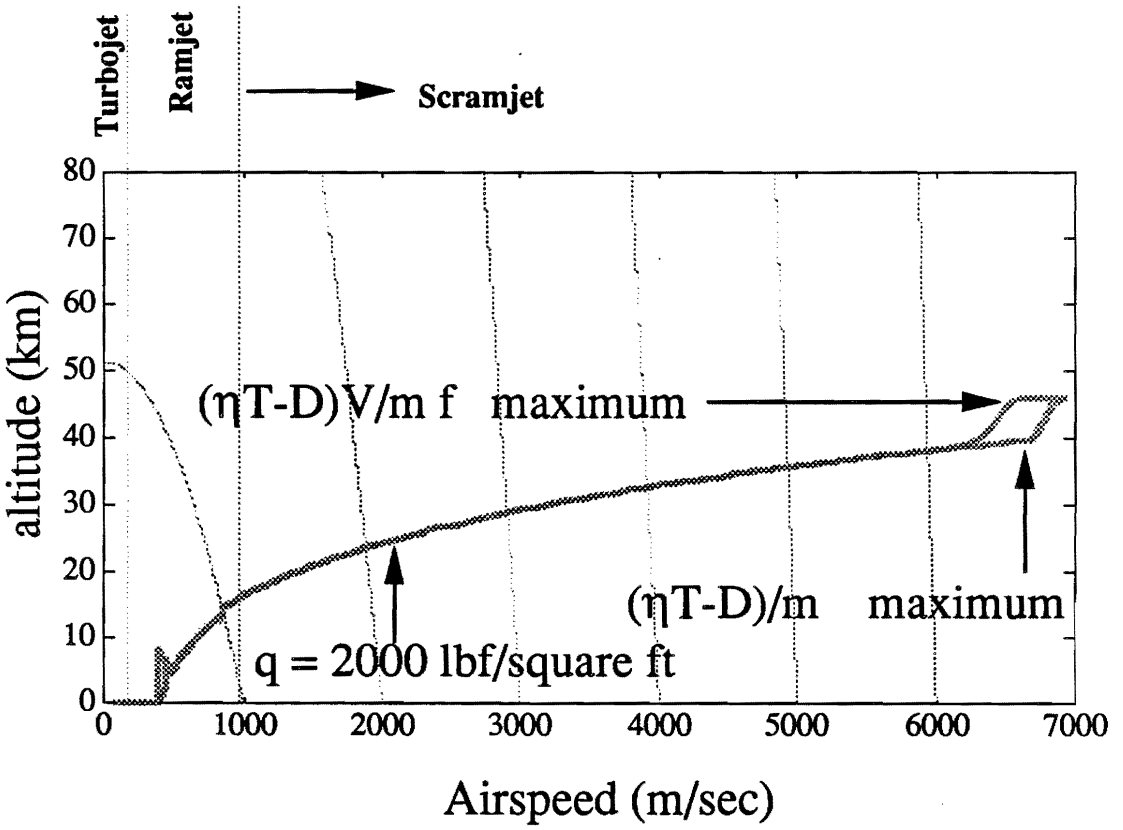

Fig. 7 Energy climb paths for a generic hypersonic vehicle

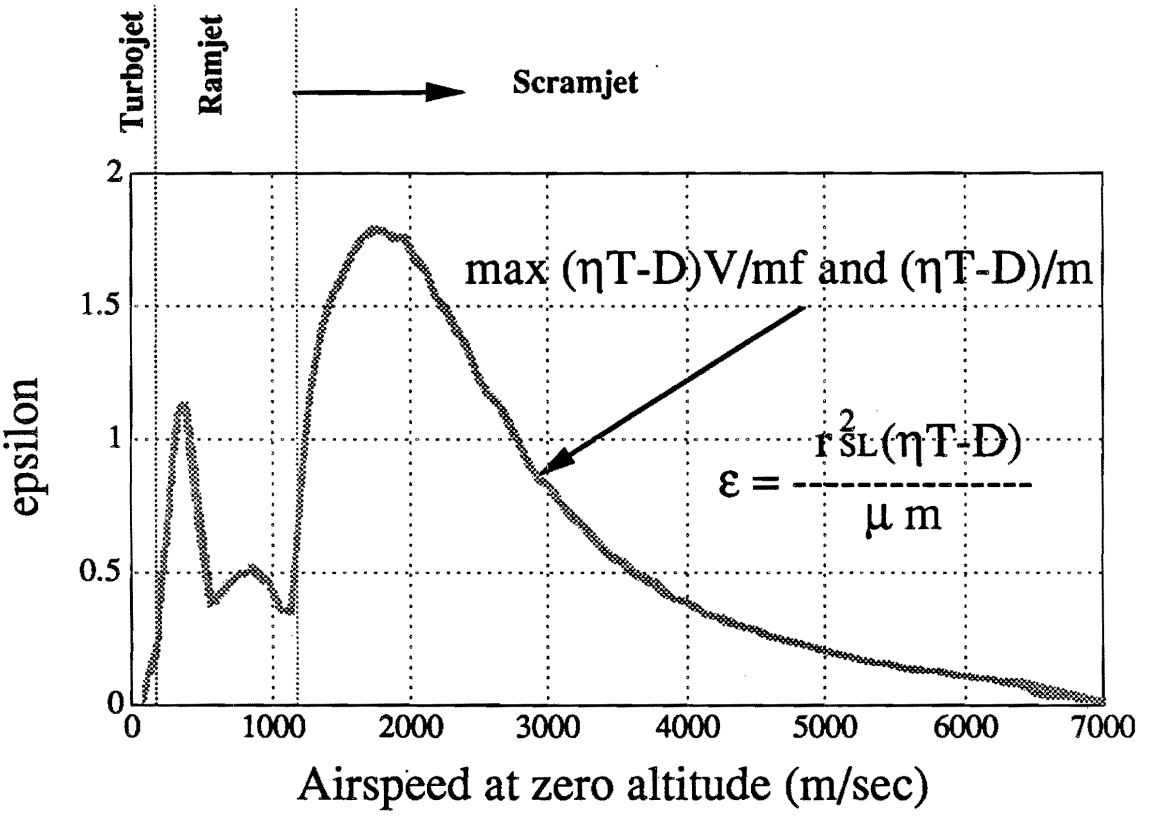

Fig. 8 Evaluation of ε(E) for a generic hypersonic vehicle